EDGEWOOD

CHEMICAL BIOLOGICAL CENTER

U.S. ARMY RESEARCH, DEVELOPMENT AND ENGINEERING COMMAND

ECBC-CR-076

VALIDATION AND SUPPORT OF A QUANTITATIVE INFRARED INSTRUMENT FACILITY AND GENERATION OF A LIBRARY OF CHEMICAL WARFARE AND RELATED MATERIALS BY FOURIER TRANSFORM INFRARED SPECTROSCOPY

Barry R. Williams
Melissa S. Hulet

EAI CORPORATION
Abingdon, MD 21009

Avishai Ben-David
Ronald W. Miles
Alan C. Samuels

RESEARCH AND TECHNOLOGY DIRECTORATE

Chiang-Jiang Zhu

BATTELLE MEMORIAL INSTITUTE
Columbus, OH 20590

Norman Green

SCIENCE AND TECHNOLOGY CORPORATION
Hampton, VA 23666

November 2006

ABERDEEN PROVING GROUND, MD 21010-5424

DISCLAIMER

The findings in this report are not to be construed as an official Department of the Army position unless so designated by other authorizing documents.

REPORT DOCUMENTATION PAGE

Form Approved

OMB No. 0704-0188

1. REPORT DATE *(DD-MM-YYYY)*	2. REPORT TYPE	3. DATES COVERED *(From - To)*
XX-11-2006	Final	Nov 2003 - Dec 2004

4. TITLE AND SUBTITLE

Validation and Support of a Quantitative Infrared Instrument Facility and Generation of a Library of Chemical Warfare and Related Materials by Fourier Transform Infrared Spectroscopy

5a. CONTRACT NUMBER

DAAD13-03-D-0017

5b. GRANT NUMBER

5c. PROGRAM ELEMENT NUMBER

6. AUTHOR(S)

Williams, Barry R.; Hulet, Melissa S. (EAI Corporation); Ben-David, Avishai; Miles, Ronald W.; Samuels, Alan C. (ECBC); Zhu, Chiang-Jiang (Battelle Memorial Institute); and Green, Norman (STC)

5d. PROJECT NUMBER

5e. TASK NUMBER

5f. WORK UNIT NUMBER

7. PERFORMING ORGANIZATION NAME(S) AND ADDRESS(ES)

EAI Corporation, 1308 Continental Drive, Suite J, Abingdon, MD 21009
Battelle Memorial Institute, 505 King Avenue, Columbus, OH 20590
Science and Technology Corporation (STE), 10 Basil Sawyer Drive, Hampton, VA 23666

8. PERFORMING ORGANIZATION REPORT NUMBER

ECBC-CR-076

9. SPONSORING / MONITORING AGENCY NAME(S) AND ADDRESS(ES)

DIR, ECBC, ATTN: AMSRD-ECB-RT, APG, MD 21010-5424

10. SPONSOR/MONITOR'S ACRONYM(S)

11. SPONSOR/MONITOR'S REPORT NUMBER(S)

12. DISTRIBUTION / AVAILABILITY STATEMENT

Approved for public release; distribution is unlimited.

13. SUPPLEMENTARY NOTES

14. ABSTRACT

This report summarizes the effort to generate a library of quantitative infrared spectra of chemical warfare agents and related materials and biosimulants. The results of tests to validate the equipment and procedures to be used in the laboratory are discussed.

15. SUBJECT TERMS

FTIR, Infrared, Diffuse reflectance, Bio, Liquid, Degradant, Vapor-phase, CW agent, Simulant, Condensed-phase, BG, Bacillus, Pellet

16. SECURITY CLASSIFICATION OF:			17. LIMITATION OF ABSTRACT	18. NUMBER OF PAGES	19a. NAME OF RESPONSIBLE PERSON
a. REPORT	b. ABSTRACT	c. THIS PAGE			Sandra J. Johnson
U	U	U	UL	96	19b. TELEPHONE NUMBER *(include area code)* (410) 436-2914

Blank

PREFACE

The work described in this report was authorized under Contract No. DAAD13-03-D-0017. This work was started in November 2003 and completed in December 2004.

The use of either trade or manufacturers' names in this report does not constitute an official endorsement of any commercial products. This report may not be cited for purposes of advertisement.

The text of this contractor report is published as received and was not edited by the Technical Releases Office, U.S. Army Edgewood Chemical Biological Center.

This report has been approved for public release. Registered users should request additional copies from the Defense Technical Information Center; unregistered users should direct such requests to the National Technical Information Service.

Blank

CONTENTS

FIGURES

TABLES

VALIDATION AND SUPPORT OF A QUANTITATIVE INFRARED INSTRUMENT FACILITY AND GENERATION OF A LIBRARY OF CHEMICAL WARFARE AND RELATED MATERIALS BY FOURIER TRANSFORM INFRARED SPECTROSCOPY

1. INTRODUCTION

1.1 Background

The work performed under this task continued an effort started under contract DAAD13-02-P-0075.[1] This is a multi-year effort to develop FTIR laboratory capabilities.

Infrared (IR) spectroscopy has been used for many decades in chemistry as an analytical tool. It is based upon the principle that the different parts of an organic molecule absorb individual wavelengths of infrared light selectively. When the IR absorption is plotted against wavelength, the result is a spectrum that is characteristic of the functional groups within the molecule. For this reason, the primary use of IR spectroscopy in the past was qualitative, i.e., to aid in the identification of unknown materials.

The development of Fourier Transform Infrared spectrometers and the increasing speed of computers to reduce and store the large data files has enabled the rapid acquisition of high resolution spectra at high signal to noise ratios. These changes, combined with the miniaturization of components, have led to the development of mobile open-path FTIR systems for use in environmental monitoring and military applications. Such systems have been used to detect materials present in the atmosphere as either vapors or aerosols. Compounds present as vapors require reference spectra in the vapor-phase. If the data are to be used for quantification, the reference spectra need to be quantitative. The currently available spectra of CW compounds by the Edgewood Chemical and Biological Center (ECBC) are limited and were, for the most part, acquired more than thirty years ago on grating spectrophotometers. The need for more current data prompted the development of a laboratory to acquire an updated library. An additional effort begun represents investigation of a laboratory technique to acquire reference spectra of compounds for standoff detection and quantitation of aerosols.

Diffuse reflectance (DR) has been used since the early 1980's to detect and quantitate organic and inorganic compounds in a number of matrices, including agricultural samples and in the pharmaceutical industry. More recently, the Edgewood Chemical and Biological Center has undertaken laboratory efforts to investigate the potential use of the technique for development of a system for detection and quantitation of chemical warfare agents (CWA).

Both biological and chemical agents may be disseminated as aerosols. For this reason, absorptivity coefficients of these materials in the condensed-phase (both liquids and solids) are necessary.

1.2 Summary of Work Performed

The work performed under the contract continued an effort started under contract DAAD13-02-P-0075, and represents the continuation of a multi-year effort to develop laboratory capabilities in FTIR. The work described in this report represents a collaborative effort between EAI and ECBC personnel.

Tasks completed toward development of the quantitative FTIR capability included:

- Absorptivity coefficients of benzene in the vapor phase.
- Analysis of NIST prepared benzene standards to validate the vapor-phase laboratory capability.
- Wavelength calibration of the Bruker IFS66V FTIR spectrometer.
- Experiments to verify the pathlength settings of the Schott variable-pathlength gas cell.
- Publication and approval of CR8-OSP137, Generation of Quantitative Diffuse Reflectance Infrared Fourier Transform (DRIFT) Spectra.*
- Publication and approval of CR8-OSP141, Generation of Quantitative Diffuse Reflectance Infrared Fourier Transform (DRIFT) Spectra in KBr Powder.*
- Publication and approval of CR8-ONP142, Generation of Quantitative Agent Transmission Spectra Through Potassium Bromide Pellets.*
- Development of algorithms to calculate absorptivity coefficients and statistical errors from quantitative spectra of materials measured in condensed and vapor-phase.
- Investigation of mathematical adjustments to the Kubelka-Munk transformation of diffuse reflectance spectra to correct the effects of baseline shifts on the intensities of bands.*
- Quantitative measurements of dimethyl methylphosphonate in liquid-phase.
- Quantitative measurements of bacillus atrophaeus (bacillus globigii, BG) in KBr pellets.
- Diffuse reflectance measurements of various species on silver membrane filters.*
- Publication and presentation of data at scientific conferences*.[1,2]

2. VAPOR-PHASE ABSORPTIVITY COEFFICIENTS OF BENZENE

Benzene had been selected during the design phase of the quantitative FTIR laboratory as a compound to be used to validate the laboratory capabilities because of

---

* Published separately.

the availability of high quality reference spectra from two other independent laboratories, the National Institute of Standards and Technology (NIST) and Pacific Northwest National Laboratory (PNNL). The absorptivity coefficients of benzene referenced in the earlier report was obtained prior to the installation of the environmental box. The box, (Figure 1) with its associated feedback loop mechanisms, significantly reduces the temperature fluctuations experienced by both the Bruker IFS66V FTIR spectrometer and the gas cell (Figure 2). For this reason, the decision was made to repeat the earlier study to obtain updated quantitative spectra of the compound, using the saturator cell technique developed for the earlier tests.

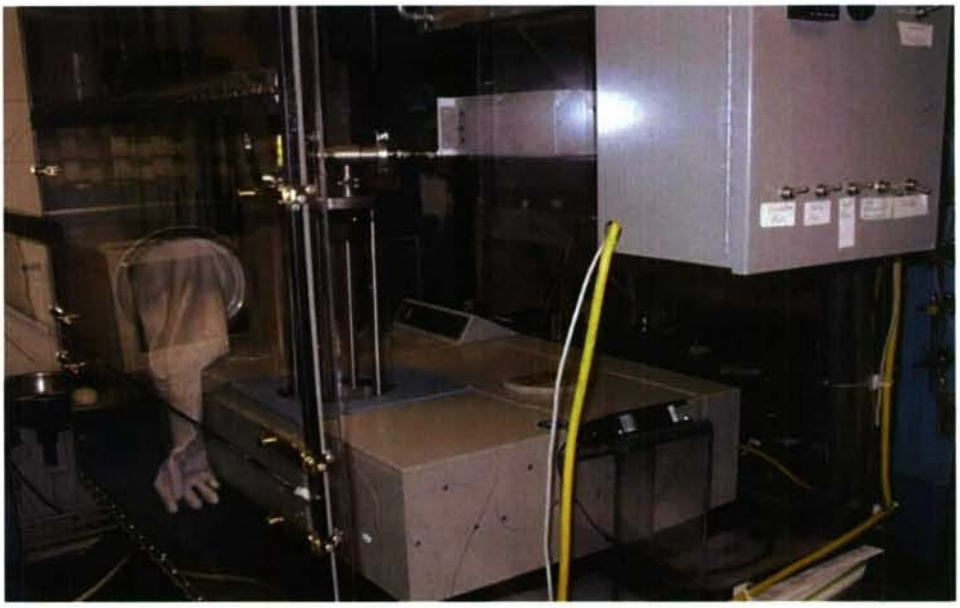

Figure 1. Environmental Box with Bruker FTIR Spectrometer Installed

Six separate trials (defined as filling and weighing the saturator cell with benzene, establishing a carrier gas flow rate for a period of 1-2 days, and reweighing to determine the mass rate) were run, resulting in the collection of a total of 15 spectra of benzene. Temperature and pressure data, as recorded by the Instrunet® system, along with the pathlengths set into the variable path gas cell, were used to normalize the resulting spectra to 760 Torr (101.32 KPa) and 296.15 K, using the ideal gas law.

According to the Beer-Lambert Law, at a wavelength, λ,

$$A=\alpha CL,$$

where A is equal to absorbance, α is equal to the absorptivity coefficient, C is equal to concentration, and L is equal to the pathlength. By rearranging the above equation, it is possible to calculate the absorptivity coefficient from a spectrum of known concentration-pathlength by rearranging the above equation thus: $\alpha=A/CL$. The resulting approximation can be improved by using a series of spectra at different

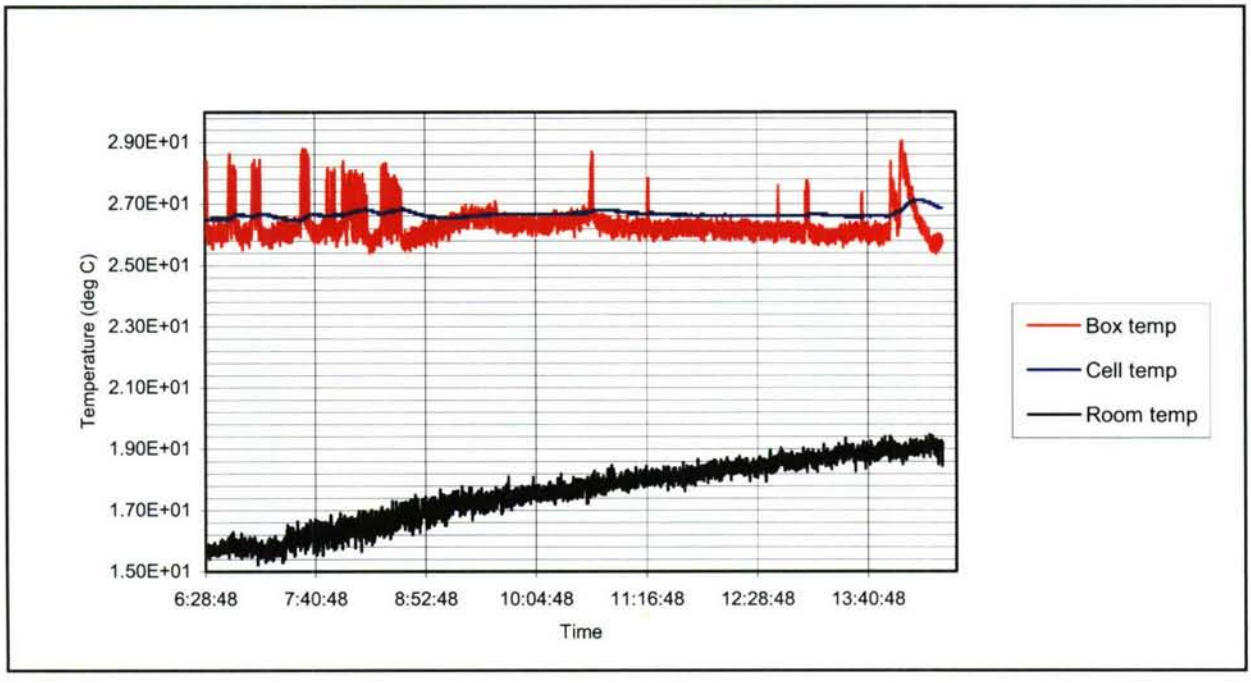

Figure 2. Temperature Stability Study Showing Relationship between Temperatures of Environmental Box, Gas Cell, and Laboratory Room

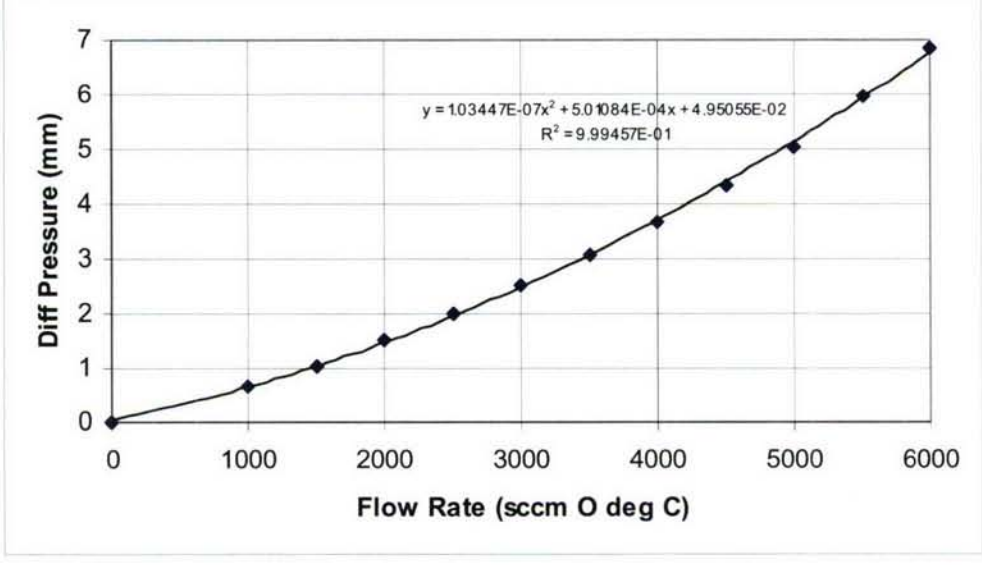

Figure 3. Differential Pressure in Schott Variable Path White Cell

concentrations and pathlengths and averaging the data statistically, for example, with classical least squares.

Mass loss data for the six trials are shown in Table 1. The standard deviation of the benzene mass rate from the expected (in mg per minute based upon the vapor

pressure and carrier gas flow rate) is 1.6%, probably a good estimate of the uncertainty of the saturator cell method for generating vapor streams of benzene given that the compound is frozen at the temperature of the constant temperature bath (-12° C). Row 4 refers to the fractional part of day(s) the saturator cell was operated prior to reweighing. Carrier gas flows are in standard cubic centimeters per minute (referenced to 273.15 K). Table 2 uses the temperature and pressure data, along with the pathlength, to obtain the concentration-pathlength products of the 15 individual spectra. The dynamic measurement system results in a differential pressure in the gas cell versus the recorded barometric pressure. The differential pressure is a function of the flow rate through the cell as shown in Figure 3. The corrected pressure, taking this flow-induced differential pressure was used to calculate the concentration of the analyte.

Table 1. Mass Rate Calculations for Saturator Cell Benzene Trials

	3/2/2004 14:51	3/10/04 15:52	3/16/04 5:51	3/17/04 6:33	4/7/04 6:26	
	3/3/2004 14:23	3/11/04 12:53	3/16/04 13:08	3/17/04 13:43	4/7/04 15:19	
	0.980555556	0.875694444	0.303472222	0.298611111	0.370138889	
min	1412	1261	437	430	533	
Start wt.	182.8865	182.9105	182.9600	182.9701	183.0198	
End wt.	181.6355	182.0226	181.9667	182.0333	182.4272	
mass loss	1.251	0.8879	0.9933	0.9368	0.5926	
sccm	20	16	50	50	25	
mg/min	0.8860	0.7041	2.2730	2.1786	1.1118	
Expected	0.885	0.708	2.210	2.210	1.105	Std Dev
Difference	0.11%	-0.55%	2.85%	-1.42%	0.62%	0.016061042

Instrumental parameters for the FTIR were as follows:

- Resolution: 0.112 cm^{-1}
- Scanner speed: 60 KHz
- Zerofill: 2x
- Aperture: 2 mm
- Detector HgCdTe
- Folding limits 0-17598 cm^{-1}
- Phase resolution: 4 cm^{-1}
- Phase correction: Mertz
- FFT limits: 550-6,500 cm^{-1}

512 scans of the reference and sample were averaged to obtain each of the 15 spectra used in the final calculations. The instrument's nonlinearity correction was applied prior to the Fourier transform, and boxcar apodization was used.

The instrumental resolution over the spectral range, coupled with the additional zerofilling factor, results in spectra with 98,722 lines. Obtaining the absorptivity coefficients of such a large number of lines requires extensive mathematical calculations. Further manipulation of the data is needed to obtain the statistical

uncertainties associated with the plot of the coefficients. MatLab®, which will run on a desktop computer, was selected as the software to be used for this purpose, and an algorithm was written to perform the necessary calculations. A system of spectral file names was specified which included both a compound identifier and the concentration-pathlength product: analytename_xeyz_i.spc, where xeyz is the coded concentration-pathlength (See Appendix A, the full MatLab code, for examples).

Table 2. Concentration-Pathlength Products of Benzene Spectra from Tests of Saturator Cell Method of Generating Continuous Vapor Streams

File	04030801	04030901	04030902	04030903	04031001	04031002	04031101	04031102	04031201	04031202	04031601	04031602	04031603	04031604	04031701.0
deg C	26.71	2.68E+01	2.68E+01	2.65E+01	2.67E+01	2.67E+01	2.68E+01	2.67E+01	2.68E+01	2.67E+01	2.67E+01	2.67E+01	2.67E+01	2.68E+01	2.68E+01
K	299.86	299.94	299.91	299.62	299.87	299.88	299.91	299.90	299.93	299.80	299.87	299.86	299.88	299.94	299.91
Amb press (mm)	757.2	762.7	763.0	763.0	768.1	768.1	764.5	763.6	759.8	760.1	763.3	762.9	762.3	759.4	760.3
Flow rate (sccm)	5010	4010	5010	3510	5025	4025	5016	4016	5025	5025	2050	2050	2550	5050	2550
Press corr (mm)*	762.4	766.5	768.1	766.1	773.3	771.8	769.7	767.3	765.0	765.3	764.8	764.4	764.3	764.6	762.3
Path (m)	1.32	1.32	1.32	1.32	1.32	1.32	1.32	1.32	2.64	3.96	10.56	7.92	7.92	5.28	5.28
Mass rate (mg/min)	0.4519	0.4519	0.4519	0.4519	1.1330	1.1330	0.7041	0.7041	1.0541	1.0541	2.2730	2.2730	2.2730	2.2730	2.1786
Mass rate (umol/min)**	5.785	5.785	5.785	5.785	14.505	14.505	9.015	9.015	13.496	13.496	29.100	29.100	29.100	29.100	27.891
CL umol/mol***	34.14	42.65	34.14	48.73	85.33	106.53	53.13	66.36	158.79	238.19	3357.17	2517.87	2024.17	681.41	1293.41
CL normalized#	33.80	42.45	34.05	48.52	85.71	106.79	53.10	66.12	157.74	236.81	3334.59	2499.96	2009.27	676.57	1280.37

* ambient pressure corrected for dynamically induced differential pressure using the equation in Figure 3

** μmol per minute of benzene

*** in the gas cell

normalized to 296.15K and 101.32 KPa

sequence in the case of spectra having the same CL. The output is a series of arrays containing wavelength data, absorptivity coefficients, zero intercepts, and type A statistical uncertainties. The m-file portion of the code is available in Appendix A.

Benzene is a challenging compound. This results first from the fact that benzene is frozen at the temperature of the bath used in the experiments, –12°C. The vapor is produced, therefore, through sublimation of the crystals formed on the surfaces of the wick and sides of the glass in the saturator cell. Second, in the vapor-phase, the infrared spectrum is dominated by an intense and very narrow series of bands that include much rotational fine structure, centered around cm^{-1} and arising from aromatic C-H wag. The absorptivity of the bands in this region are approximately 60 times greater than the second strongest bands, those just above 3000 cm^{-1} from aromatic C-H stretch.

Maximum diameter of the aperture (Jaquinot stop) of an FTIR spectrometer needed for a desired optical resolution ($\Delta\sigma$) can be determined from the equation:

$$d = 2\sqrt{2} * f * \sqrt{\Delta\sigma / \sigma \max},$$

where f is equal to the focal length (153.7-mm for the IFS66V). To achieve the desired resolution of 0.1125 cm^{-1} at the shortest wavelength of the data acquired during the benzene experiments (6500 cm^{-1}), the above equation indicates an aperture of ≤1.8-mm is needed, slightly smaller than the 2-mm setting used during acquisition of the benzene spectra. At 4000 cm^{-1}, however, an aperture of 2-mm is adequate. The larger setting was chosen for several reasons. First, the throughput is higher, improving the signal to noise ratio in the spectra. Furthermore, features in the region above 4000 cm^{-1} are generally very weak and broad overtone and combination bands, and the reduction in optical resolution may not have had a measurable effect upon the spectra, at least within the experimental conditions. Finally, the larger diameter probably aided in the elimination of aperture-induced artifacts (double modulation and warm aperture) from the spectra, problems researched extensively by Johnson, *et al.*[4] This was considered desirable even though such effects are generally less apparent with a multipass gas cell, as used in these experiments.

Reduction of the data from the benzene experiments resulted in the absorptivity coefficients depicted in Figure 4. The fractional uncertainties (type A, expanded to 2σ) are shown graphically as a function of aborptivity coefficient in Figure 5. These do not exceed 6% within the range of 0.00001 $(\mu mol/mol)^{-1}m^{-1}$ to the highest absorptivities measured and are generally 1-3% for absorptivities within the range of 0.00002-0.009 $(\mu mol/mol)^{-1}m^{-1}$. Type A and B and combined uncertainties are shown in Table 3. The expanded combined uncertainty of 4% applies to the more limited range of absorptivities shown above, with a maximum combined uncertainty of 7% for absorptivity coefficients >0.00001. Table 4 compares the integrated peak areas of the 674 and 3000 cm^{-1} regions of the ECBC data with that obtained by NIST[5] and PNNL[6]. The differences in the values obtained within the two regions are within the combined

uncertainties of the measurement process, even if the uncertainties of the measurements by the other two laboratories are ignored.

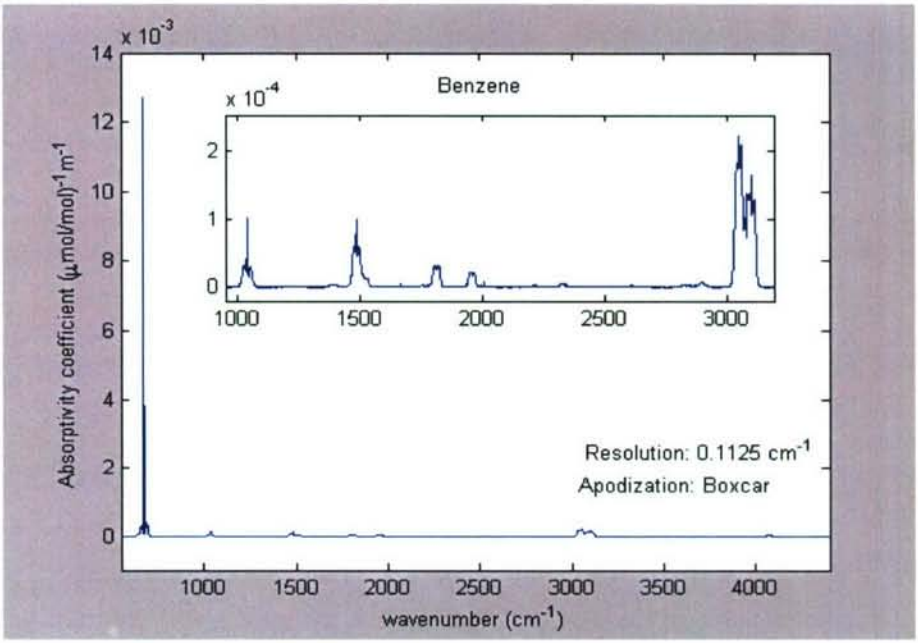

Figure 4. Vapor-Phase Absorptivity Coefficients of Benzene Obtained at ECBC Using Saturator Cell System

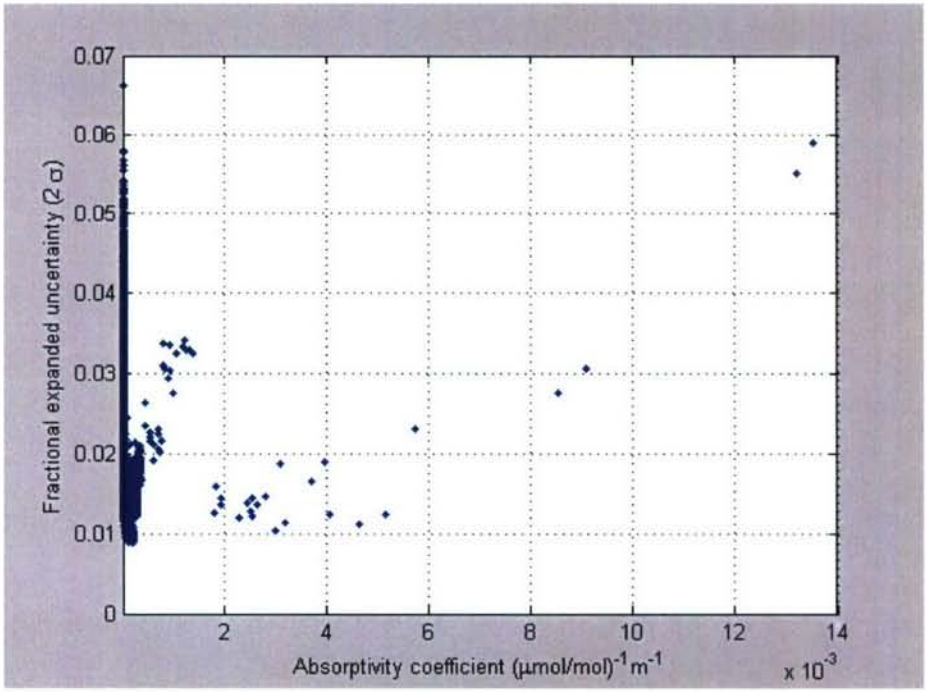

Figure 5. Fractional Type A Uncertainties (2σ) of Absorptivity Coefficients of Benzene Obtained during Testing at ECBC

Table 3. Uncertainties for Benzene Absorptivity Coefficient Experiments

Symbol	Value (fractional)	Source
ΔL	0.005	Optical path length
ΔT	0.0007	Temperature in white cell
ΔP	0.00046	Pressure in white cell
$\Delta FTIR$	0.0005 (from PNNL/NIST data)	Drift in spectrometer
ΔNL	0.005 (from PNNL data)	Detector non-linearity
ΔMR	0.016	Benzene mass rate
ΔD	0.01 (per manufacturer's specs.)	Dilution flow rate
Δ_B	0.039	Combined Type B (2σ)
Δ_A	0.005-0.03	Statistical Type A
Δ_{A+B}	0.04-0.07	Combined Type A + B (2σ)

Table 4. Comparison of Absorptivity Coefficients of Benzene Data Obtained at NIST, PNNL, and ECBC

	Integration Area	NIST	PNNL	ECBC	(NIST-PNNL)/ NIST	NIST-ECBC/NIST	PNNL-ECBC/ PNNL
Peak Area	630-720	0.018774	0.018527	0.017857	1.3%	4.89%	3.6%
Peak Area	3000-3140	0.0132	0.01305	0.012695	1.1%	3.83%	2.7%

3. WAVELENGTH CALIBRATION OF BRUKER IFS66V

The wavelength calibration routine of the Bruker Opus® software AT, instrument test macro, measures the position of a water vapor line at 1553.353 cm^{-1} to set the frequency of the laser wavenumber, nominally at 15,798 cm^{-1}. Because the macro uses only a few scans, with the deuterated trigycine sulfide (DTGS) detector at 1 cm^{-1} resolution, this was found to be unsatisfactory, resulting in large shifts in the setpoint each time the macro ran. When the positions of multiple water vapor lines were checked against the High Resolution Transmission (HITRAN) database, the resulting instrumental response also showed similar large shifts.

In order to improve upon the results obtained with the Bruker macro, an alternative approach was developed. First, an iterative process was used to set the laser wavenumber. A reference spectrum was taken with the sample chamber evacuated and then a spectrum with the chamber vented. The positions of 105 water vapor and carbon dioxide lines in the ratioed spectrum were compared against the HITRAN data and the following formula was used to calculate a corrected laser wavenumber:

$$LWN_{new}=LWN_{old}*v_{HIT}/v_{obs},$$

where LWN_{new} is the new laser wavenumber, LWN_{old} is the old laser wavenumber, v_{HIT} is the wavenumber of the water vapor line from the HITRAN database, and v_{obs} is the measured position of the line. Even at the highest available spectral resolution of the IFS66V, bands are measured with an unapodized data spacing of 0.1125 cm^{-1}. Zero filling decreased the data spacing only to 0.055 cm^{-1}. As a result, the shapes of very narrow bands are not approximated well, and it is extremely difficult to determine with a high degree of accuracy the point of maximum absorption. This results in the broad scattering of the clusters of rotational bands around a center. Nevertheless, calculating the laser wavenumber 105 times and averaging the result appeared to result in an increasingly more accurate representation of the actual laser wavenumber. The deviation from the expected water vapor lines became smaller each time this process was repeated, starting at close to 0.1 cm^{-1} in the vicinity of 4000 cm^{-1} and reducing it to less than 0.01 cm^{-1}. The graphed response of the instrument toward the end of the iterative process can be seen in Figure 6.

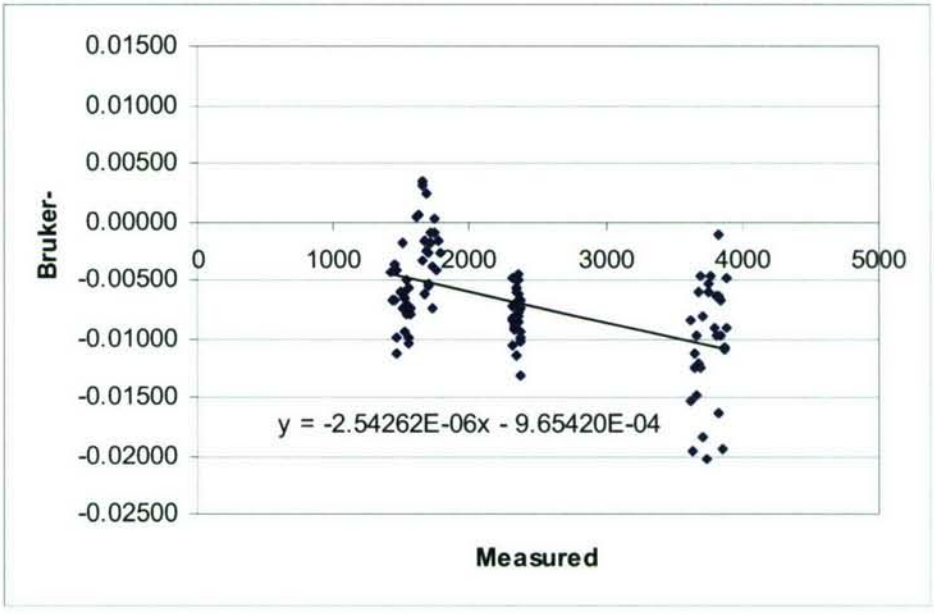

Figure 6. Laser Wavenumber Calibration of Bruker Spectrometer

Final calibration of the wavenumber response of the spectrometer was performed with carbon monoxide (CO) and nitrous oxide (N_2O), two gases for which reference data are available.[7] Compressed gas cylinders of CO at 500 ppm) and nitrous oxide at 200 ppm) in nitrogen were purchased from Matheson Tri-Gas, Montgomeryville, PA. Clean, dry nitrogen was flowed through the gas cell and single beam reference spectra were obtained. The calibration gas was then flowed through the cell until the concentration stabilized, flow rate was reduced to minimize differential pressure in the cell, a single beam spectrum was collected, and the absorbance spectrum of the calibration gas was obtained by ratioing against the pure nitrogen. The differences between the observed and expected positions of 194 lines were then calculated and plotted. At two levels of

zero-filling, with resultant data spacing of 0.055 cm^{-1}, the clustering of the data points was similar to that observed for the water vapor bands. An effort was made to attempt to better approximate the "true" shapes of the bands by increasing the level of zero-fill prior to performing the FT to 16, with a resulting data spacing of 0.007 cm^{-1}. As can be observed in Figure 7, the additional zero-filling resulted not only in the expected "tightening" of the data clusters from the rotational bands around the spectral features, reducing the spread along the y-axis, but also had the effect of moving along the y-axis the center of mass of the bands centered around 600 cm^{-1} (N_2O bend[8]).

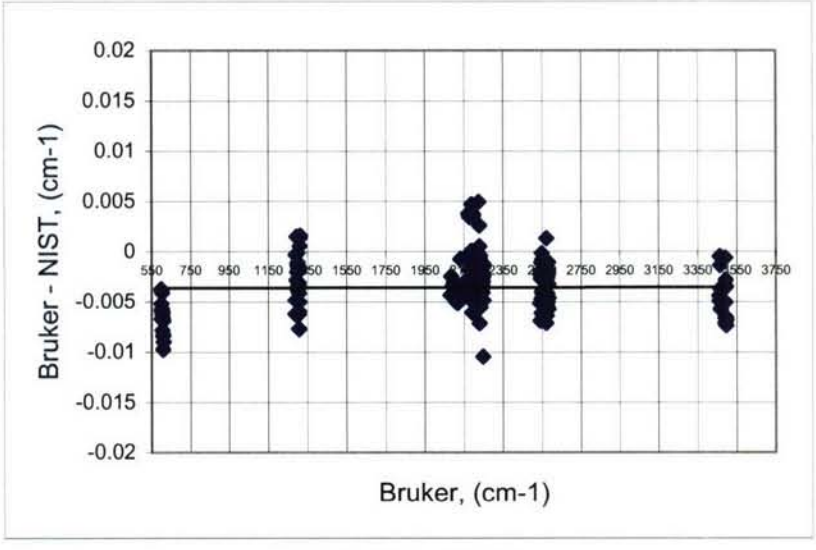

Y = 2E-08x - 0.0036
2 levels of zero fill

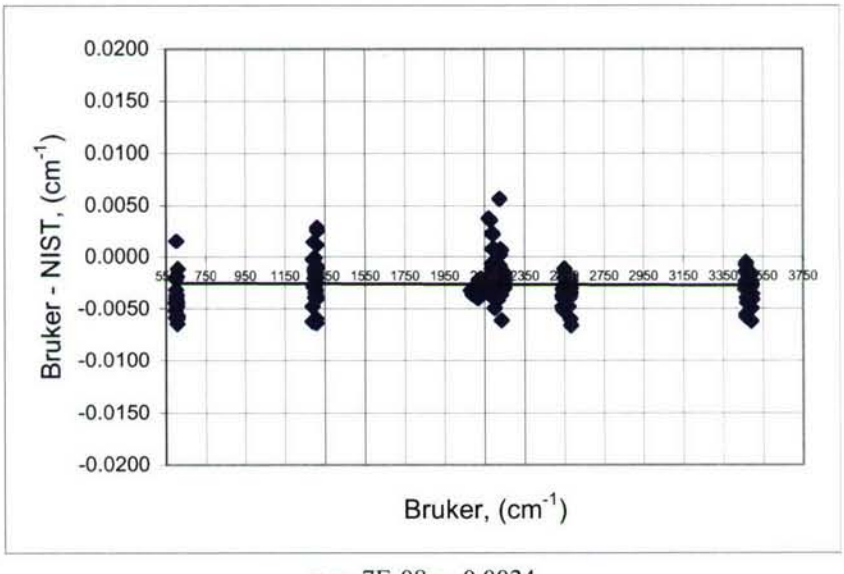

y = -7E-08x - 0.0024
16 levels of zero fill

Figure 7. Wavelength Calibration of IFS66V with Nitrous Oxide and Carbon Monoxide

The equations immediately below the charts in figure 7 represent the "best fit" of the data points, as represented by the lines through the data. It may be observed that the line in the lower chart appears to better fit the centers of masses of the data clusters and gives a y intercept that is closer to zero. When the equations are used to correct the instrument response at each of the lines, both result in average deviations from the reference wavelengths of $<10^{-5}$ cm^{-1}. The standard deviation of the corrected instrument response for the 194 lines is reduced from 0.006 cm^{-1} to 0.002cm^{-1}. The latter represents 1 part in 1,000,000 at 2000 cm^{-1}. The change in the appearance of the spectra associated with the change in zero filling is illustrated in figure 8, which depicts an absorbance peak in a spectrum processed from the same interferogram.

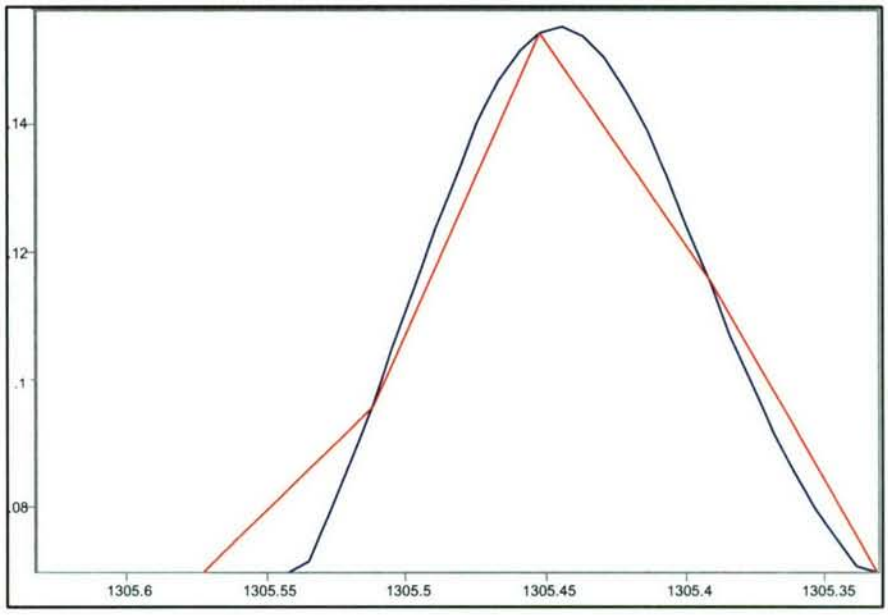

Figure 8. Peak from Spectrum Process with 2 Levels of Zero Fill (Blue) and 16 Levels of Zero Fill (Red)

The calibration procedure, which requires approximately one day to acquire the spectra and one-half day to evaluate the data, should be repeated periodically to verify the instrumental response.

4. PATHLENGTH CALIBRATION OF SCHOTT WHITE CELL

The Schott® cell used in the gas-phase measurements is a multipass variable pathlength White cell with nominal pathlength settings ranging from 1.4 to 20 m. The desired pathlength is set through a micrometer mounted on the top of the cell, which adjusts a movable objective mirror. In order to more accurately establish the true wetted pathlength, we measured the time-of-flight of a laser beam through the cell using the apparatus shown diagrammatically in Figure 9. An Agilent 86100B Infiniium DCA oscilloscope equipped with 86112A dual 20 GHz electrical plug-in modules and an 86103B 10 GHz optical module was used to measure the cell pathlength by recording the time base of a fast rise time laser pulse both with and without the cell in the laser

path. (Figure 8 depicts the White cell inserted in the laser path.) The laser source is a pulsed 1310 nm Mitsubishi ML720J8S laser diode coupled to an optical fiber collimator. Beam divergence is approximately 0.82 milliradians. The use of an optical fiber collimator allows exchanging the infrared diode with a visible diode to aid in system alignment without affecting the optical path. A 10 ns pulse driven by an Avtech model AVO-9B-N-P2-APG pulse generator is used to drive the infrared diode for pathlength measurements with a pulse repetition rate of 100 KHz and a rise time less than 200 ps. Oscilloscope trigger is provided by a beam splitter, which directs 5% of the laser beam to a PIN diode amplifier trigger driver. The 86100B exhibits an internal trigger delay of 24 ns. This delay is compensated by the addition of a 24 ns fiber optic delay cable at the oscilloscope optical input.

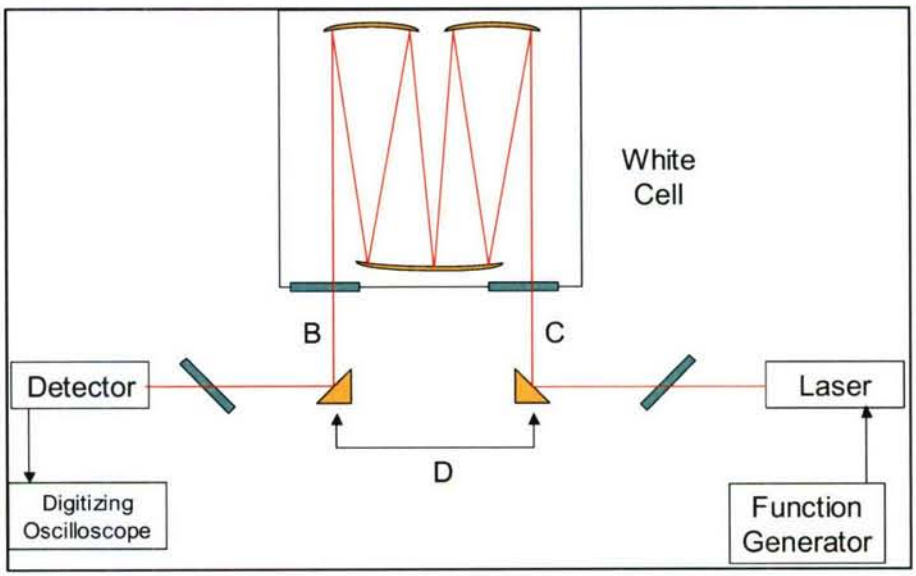

Figure 9. Experimental Setup for White Cell Pathlength Measurements

The first step is to measure the time of the detector output pulse with the gas cell removed. The oscilloscope timebase may be expanded to a resolution as fine as 0.49 ps per division. Time of a convenient waveform feature such as the 50% amplitude point or the peak of observed overshoot is recorded. Data were recorded in computer files for later analysis using an in-house smoothing and peak maximum locating algorithm written under the MatLab® environment. The second step is to repeat the waveform time measurement with the gas cell in place. Cell pathlength (L) is then calculated using the following formula:

$$L-(T1-T2)V-B-C+D,$$

where T1 is the time of flight (TOF) with the cell in place, T2 is the TOF without the cell in place, V-velocity of light (29.979 cm/ns), B = mirror to window distance, C = 2nd mirror to window distance, D = distance between transfer mirrors (see Figure 9).

Table 5. Schott White Cell Pathlengths

Micrometer setting	Manufacturer pathlength	TOF pathlength	Difference (cm)	Relative difference
5.80	1056.00	1066.24	10.24	0.97%
5.99	924.00	934.26	10.26	1.11%
6.20	792.00	802.37	10.37	1.31%
6.99	528.00	537.69	9.69	1.84%
7.76	396.00	405.66	9.66	2.44%
9.36	264.00	272.66	8.66	3.28%
14.33	132.00	140.45	8.45	6.40%

The cell pathlengths determined through the TOF measurements are compared with the manufacturer specified pathlengths in Table 5. It may be noted that the TOF pathlengths are consistently 8-10 cm longer than the manufacturer specifications. The pathlengths provided by the manufacturer are integer multiples of the shortest (1.32 m). This implies that the formula used to calculate the pathlength of the cell was:

$$L = n*l,$$

where n = the number of passes and l = the length of a single pass. Although such a formula apparently simplifies the complex geometry involved, given that the incident traverses the cell at nonperpendicular angles, such a formula also appears to ignore the distances between the lower objective mirror and the two KBr windows at the bottom of the cell, which total 7.5 cm. This implies that a better estimate of the cell pathlengths would be obtained by adding an intercept to the formula:

$$L = n*l + 7.5 \text{ cm},$$

and we have suggested that this may, at least in part, account for the difference between the manufacturer's specifications and the TOF data.

We are attempting to verify the TOF measurements of the pathlengths with two independent methods. The first procedure used standards of benzene in nitrogen provided by NIST, and the results of this effort are described in section 5. The second method will use 555 μmol/mol of butane in nitrogen to be analyzed in the Schott cell at the shortest pathlength setting and an additional gas cell with a fixed length of 20 cm. This will ensure that spectra obtained in both cells have bands in the 3000 cm^{-1} region (C-H stretch) with absorbances that remain within the detector linear range. Influencing the choice of this spectral region has been a desire to minimize the previously cited aperture induced effects. Because integrated band intensities at a fixed concentration are proportional to the pathlength, it should be possible to use the ratios of the response in the two cells to calculate the pathlength of the Schott White cell.

5. ANALYSIS OF NIST-PREPARED BENZENE STANDARDS

5.1 Introduction

Six compressed gas cylinders containing benzene in nitrogen were obtained from NIST. These had been prepared according to the procedures described in reference 3. Because the concentrations were not provided to ECBC personnel prior to analysis, running the samples in the laboratory would provide an independent method of verifying the instrumental setup and data analysis procedures at ECBC. Additionally, the standards provided a way to cross check the TOF measurements of the Schott gas cell.

5.2 Materials and Procedures

Prior to analysis, the standards were equilibrated to ambient room temperature for several hours. Thereafter, the cylinders were placed horizontally on a flat surface and rolled to ensure mixing. A standard high purity regulator was then connected to the cylinders. The regulator was plumbed with ¼" PTFE to the line that would normally be connected to the output from the saturator cells, with a mass flow controller to regulate the flow from the cylinders. Because the flow rate from the benzene cylinders could be expected to have only the small influence upon the concentration-pathlength, arising from dynamic differential pressure effects, it was not necessary to recalibrate the mass flow controller to account for the effect of the low concentrations of benzene upon its response. The secondary stage was set to 20 PSI.

Instrumental parameters were the same as those used in the saturator cell experiments, with the exception that the upper limit for the final spectra was reduced to 4000 cm^{-1}. The desired pathlength was set in the White cell with the micrometer. Dry nitrogen from the boiloff of the liquid nitrogen from the bulk tank (also used in the saturator cell experiments) was then used to collect reference (background) spectra. Finally, the gas flow from the benzene cylinder was set to 5000 sccm, the concentration of benzene in the gas cell was equilibrated, the flow rate was reduced to approximately 400 sccm, and a spectrum of the benzene was acquired. As desired (and as the volume of gas in the cylinder permitted), the pathlength of the gas cell was reset, and additional background and sample spectra were taken. Temperatures and ambient pressure were recorded continuously during the experiments using the Instrunet system and were incorporated into the subsequent calculations of the cylinder concentrations.

Data was acquired using the Opus® software supplied by Bruker Optics. Opus provides a wider variety of baseline handling options in its integration parameters than are available in Grams®, including baseline noise averaging. Opus may, however, have only one integration formula, which is not documented. On the other hand, the Grams software has integration algorithms incorporating several different mathematical formulas, which are readily available to the user. For the most part, therefore, the data processing was undertaken in Grams®/32, version 6.00, after first converting the absorbance spectra to the Grams format.

Grams offers the usual manual and automatic baseline correction methods, with a wide variety of linear and nonlinear fits to the resulting lines. To satisfy the requirement of generating reference quality data, it was desired to remove the subjective judgment involved in the manual baseline correction. Unfortunately, the automatic baseline correction function is not sufficiently robust either. NIST provided an algorithm, abase.ab, written in Grams Array Basic, that averages the y values of the left and right baseline points within a range on either side of the two points and then creates a new baseline by stretching a straight line between these two points.[9] Although improved in its performance versus the automatic baseline correction already available in Grams, it was still insufficiently robust in the case of spectra with significant baseline noise. An additional caveat is that the algorithm selects points in the direction of the peak to be integrated for baseline averaging. The user must be cautious, therefore, not to encompass points within the peak. Abase.ab was then modified to increase the number of data points to be averaged around the selected left and right baseline points and averaging points above and below the baseline points, thereby excluding the possibility of including y-values within the region of the peak. The result of the modification can be seen in Figure 10. The modified algorithm was tested with six spectra with varying concentrations of benzene, in both the 3000 and 674 cm^{-1} regions, with improved results in 5 out of the 6 cases when compared to the algorithm as originally received. Both algorithms produced poor results in one spectrum having a negative peak within the region used for the baseline correction. The anomalous result was duplicated within MatLab.

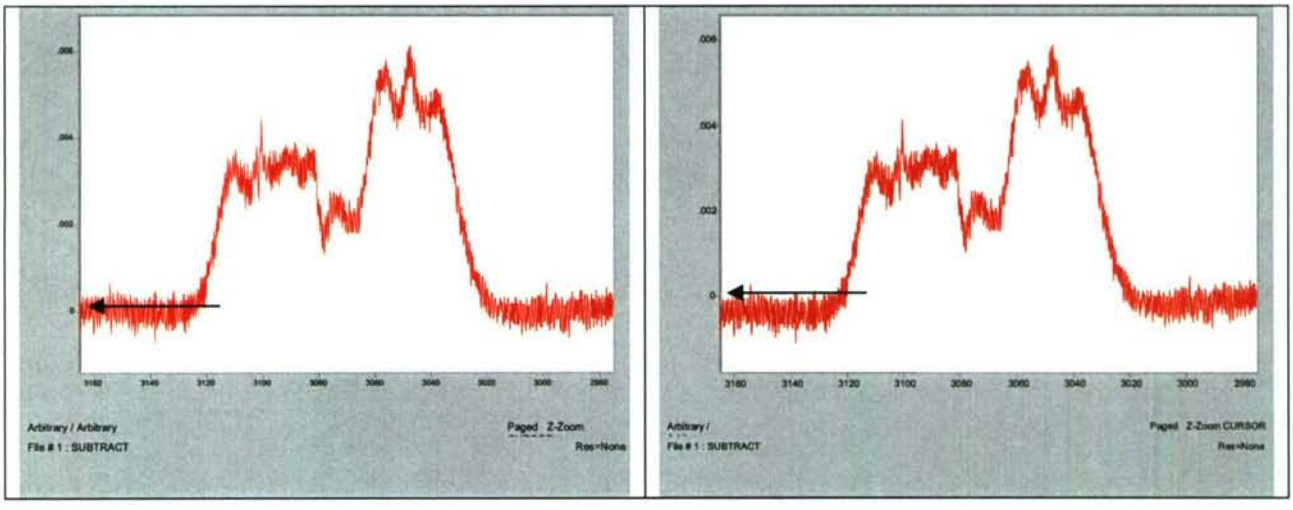

Figure 10. Baseline Corrected Spectra Resulting from Using Modified abase.ab (left) and Original Algorithm (right). Arrows indicate the position of the zero absorbance line.

Although improved in its performance, both the unmodified and the modified code permanently truncate the spectrum to the selected left and right limits, adding a file slot for the baseline corrected spectrum, and replace the original spectrum in the file slot with a spectrum reflecting an intermediate step generated when the algorithm runs.

Furthermore, as currently written, this routine does not provide a means to select specific left and right points for the baseline correction without manually editing and resaving it (presumably to a new file name to preserve the original). The present abase.ab is, therefore, best suited for correcting relatively limited spectral regions to integrate the area within regions of the spectrum. By selecting multiple points across the entire range of the spectrum, it would be possible to perform a baseline correction of the spectrum as a whole. Because neither the logic nor mathematics to perform the required manipulations is inherently complex, it should be relatively straightforward to improve upon the algorithm by adding the desired functionalities. As observed in the case of the manipulation of the spectrum that resulted in a degradation of the baseline, it is always difficult to design an automated function that will completely replace the judgment of an experienced operator.

The mathematical integration method is specified in the Grams software by selecting "type." The "mathematical" method uses the following standard trapezoidal

$$Area = \left[\sum_{n=0}^{i} y_n - \frac{1}{2}\left(y_0 + y_i\right)\right]|\Delta x|$$

formula to calculate the area within the specified range, which may be entered manually or interactively selected:
The operation of the software algorithm was easily confirmed within MatLab by duplicating integration results for a spectral file that had been obtained using Grams. The transparency and simplicity of the operation should enable the procedure to be readily automated through an m-file within MatLab as desired.

Baseline options available during integration are none, custom, both ends, left end, right end, or minimum. Because the baseline is subtracted during integration, this is a critical parameter. Both ends, left end, and right end assign the baseline point to the value of y at the specified x. Baseline noise can place the point randomly within the limits of the noise as shown in Figure 11 and can thus skew the integration. "Minimum" places the left and right baseline points at the minimum y value found across the integrated range, which produces identical results with either the mathematical or absolute integration method. "Custom" permits the user to input the y value to be used at each of the x limits as long as "force to data" is checked "no." If the spectrum has

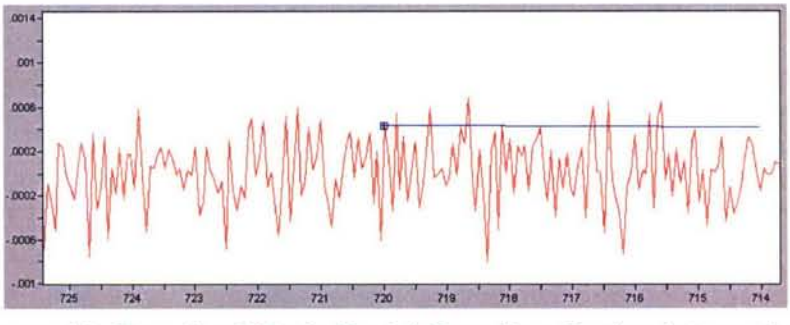

Figure 11. Result of "Both Ends" Baseline Option Integration in Grams Software

been subjected to a baseline correction prior to performing the integration, the user can manually input a numerical zero into the left and right y values on the assumption that the center of mass of the baseline noise is at zero absorbance. The "custom" setting may offer the best option for comparing data recorded with different signal to noise ratios. A comparison of results obtained with a combination of the above parameters is shown in Table 6.

Table 6. Comparison of Grams Integration Parameters

Integration method	Baseline method	Integration results
Mathematical	Both ends	0.2589
	Minimum	0.3828
	Custom (y set to 0)	0.2738
Absolute	Both ends	0.2737
	Minimum	0.3828
	Custom (y set to 0)	0.2821

After integration, the concentrations of benzene in the cylinders were calculated using the following formula:

$$C=A_{\int}/aL,$$

Where $A_{\int}$ = integrated absorbance, a = integrated absorptivity (from NIST absorptivity coefficient data), and L = pathlength. The NIST data is referenced to 296.15K and 760 Torr (101.32 KPa); measured concentrations were adjusted using the ideal gas law as necessary. The spectral region used for calculating the benzene concentrations was either 3160-2980 cm^{-1} or 720-630 cm^{-1}. The selection of the wavenumber region used to calculate the concentration was governed by the need to ensure that only spectra with absorbances within the linearity range of the detector were used ($A \leq 1.2$).

5.3 Results and Discussion

A summary of data from analysis of the benzene cylinders is presented in Table 7. The concentrations of benzene in cylinders CAL015001 and CAL014983 were calculated using the spectral region centered around 674 cm^{-1}; the remaining cylinders were computed using the integrated areas in the 3000 cm^{-1} region. The temperature of the White cell had been fixed to an average of 299.16K using the Omega control system and is not shown in the Table. The respective integrated areas of x001a72.spc, the NIST absorptivity coefficients, were 0.01330 $(\mu mol/mol)^{-1}m^{-1}$ (3160-2980 cm^{-1} region) and 0.01880 $(\mu mol/mol)^{-1}m^{-1}$ (720-630 cm^{-1}). Raw integrated areas were computed from baseline-corrected spectra. Adjusted integrated areas were obtained from the ideal gas law. Table 8 compares the concentrations in the cylinders obtained from measurements at ECBC to the concentrations as certified by NIST, with separate columns for TOF and Bruker-specified pathlengths of the White cell. Figure 12 is a plot of integrated areas (from Table 7) versus TOF and Bruker-specified pathlengths, i.e., a Beer's Law plot.

Table 7. Summary of Data from Analysis of NIST Benzene Cylinders

Cylinder number	Data file name	Integrated area (raw)*	Pressure (Torr)	Integrated area (adjusted)**	TOF data		Bruker data	
					Pathlength (m)	Conc (μmol/mol)	Pathlength (m)	Conc (μmol/mol)
CAL015001	04080901.0	0.2746	765.7	0.2755	1.4045	10.43	1.32	11.10
	04080902.0	0.5222	765.7	0.5238	2.7266	10.22	2.64	10.56
	04080903.0	0.7834	765.7	0.7859	4.0566	10.31	3.96	10.56
	04081001.2	1.017	762.7	1.024	5.377	10.13	5.28	10.31
					Mean	10.27	Mean	10.63
					d (2 σ)	0.26	*d* (2 σ)	0.67
					Rel *d* (2 σ)	0.025	Rel *d* (2 σ)	0.063
CAL014983	04081002.0	0.2770	761.6	0.2783	1.4045	10.58	1.32	11.26
	04081003.0	0.5354	761.6	0.5400	2.7266	10.54	2.64	10.88
	04081004.0	0.7879	760.6	0.7957	4.0566	10.43	3.96	10.69
	04081101.1	1.019	758.6	1.0315	5.377	10.20	5.28	10.39
					Mean	10.44	Mean	10.80
					d (2 σ)	0.15	*d* (2 σ)	0.58
					Rel *d* (2 σ)	0.014	Rel *d* (2 σ)	0.053
CAL015010	04081202.0	4.114	759.8	4.159	1.4045	222.6	1.32	236.9
	04081202.1	4.130	759.5	4.176	1.4045	223.5	1.32	237.8
	04081202.2	8.055	759.2	8.149	2.7266	224.7	2.64	232.0
	04081301.1	11.90	759.8	12.03	4.0566	223.0	3.96	228.4
					Mean	223.4	Mean	233.8
					d (2 σ)	1.8	*d* (2 σ)	8.8
					Rel *d* (2 σ)	0.008	Rel *d* (2 σ)	0.037
CAL014998	04081601.0	4.138	766.0	4.149	1.4045	222.1	1.32	236.3
	04081601.1	8.153	766.0	8.175	2.7266	225.4	2.64	232.8
	04081702.0	15.60	765.5	16.05	5.377	224.4	5.28	228.5
	04081702.1	20.09	765.4	20.16	6.70	226.2	6.60	229.6
					Mean	224.5	Mean	231.8
					d (2 σ)	3.6	*d* (2 σ)	7.0
					Rel *d* (2 σ)	0.016	Rel *d* (2 σ)	0.030

Table 7 (Continued)

Cylinder number	Data file name	Integrated area (raw)*	Pressure (Torr)	Integrated area (adjusted)**	TOF data		Bruker data	
					Pathlength (m)	Conc (μmol/mol)	Pathlength (m)	Conc (μmol/mol)
CAL014985	04082701.0	8.644	766.5	8.662	1.4045	463.5	1.32	493.3
	04082702.0	17.02	766.4	17.06	2.7266	470.3	2.64	485.7
	04083101.0	24.95	762.0	25.15	4.0566	466.1	3.96	477.5
	04083102.0	33.45	762.4	33.70	5.377	471.1	5.28	479.7
					Mean	467.8	Mean	484.1
					d (2 σ)	3.5	*d* (2 σ)	7.1
					Rel *d* (2 σ)	0.008	Rel *d* (2 σ)	0.015
CAL014988	04083103.0	8.719	762.9	8.779	1.4045	469.9	1.32	499.9
	04083104.0	17.09	762.9	17.20	2.7266	474.3	2.64	489.8
	04090101.0	25.42	766.6	25.48	4.0566	472.1	3.96	483.6
	04090101.1	33.82	766.4	33.90	5.377	473.9	5.28	482.6
					Mean	472.5	Mean	489.0
					d (2 σ)	2.0	*d* (2 σ)	8.0
					Rel *d* (2 σ)	0.004	Rel *d* (2 σ)	0.016

*Obtained from baseline-corrected spectra.

**Obtained from raw areas by applying the ideal gas law.

Table 8. NIST Gravimetrically-Prepared Cylinders: Comparison between Gravimetric Concentrations and Concentrations Obtained from TOF and Bruker Specified Pathlengths

Serial Number	NIST Grav	ECBC (TOF)	ECBC-NIST/ NIST	ECBC (Brucker)	ECBC-NIST/ NIST
Cal-15001	9.9	10.3	4.6%	10.6	7.9%
Cal-014983	10.0	10.4	4.0%	10.8	8.0%
Cal-015010	225.8	223.4	-1.1%	233.8	3.5%
Cal-014998	226.0	224.5	-0.7%	231.8	2.6%
Cal-014985	470.3	467.8	-0.5%	484.1	2.9%
Cal-014988	475.4	472.5	-0.6%	489.0	2.9%

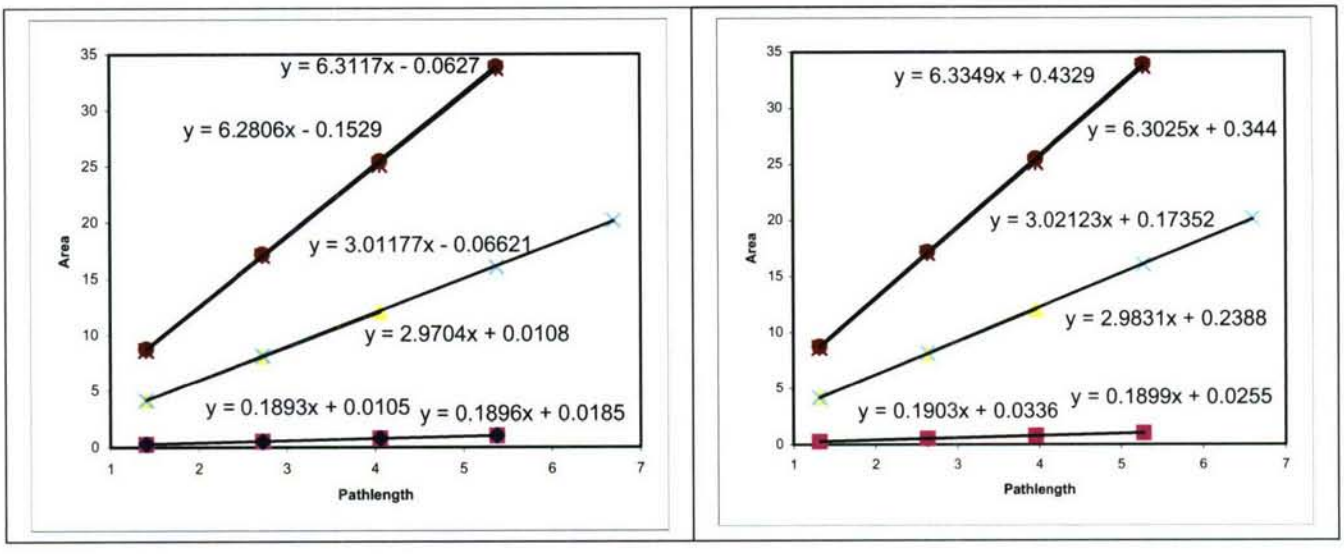

Figure 12. Integrated Areas in Spectra of Benzene Cylinders versus TOF (left) and Bruker Pathlengths (right)

A number of observations can be made about Tables 7 and 8 and Figure 12. Used to verify the pathlengths of the White cell, several aspects of the data appear to provide evidence that the TOF data are significantly more accurate than the Bruker-provided pathlengths. First, the standard deviations of the means of the calculated benzene concentrations in Table 7 are two to four times higher for the Bruker pathlengths versus the TOF data. Column 8 (Bruker) also shows, *for each cylinder tested*, a distinct trend resulting in calculated concentrations that decrease from longer to shorter paths, an indication of poor adherence to Beer's Law. Such a trend is much less evident in the TOF calculations, which show more of a scattering aspect to the data. This is further illustrated in Figure 12. The lines are derived from least squares fits of the integrated peak areas and pathlengths from Table 7. All of the plots in the graph on the right (Bruker data) have positive y-intercepts. The lines derived from TOF paths again show no particular trend, with three of the six having slightly positive y-intercepts and three having slightly negative y-intercepts.

Referring back to Figure 9, the accuracy of the TOF data depends in part upon the accuracy of D (distance between the transfer mirrors) as well as B and C (distance between the transfer mirrors and the "wetted" side of the KBr windows), which were measured by a direct method. Because these distances were a constant in the calculations of all of the pathlengths, any errors would propagate, producing a false intercept in the plotted pathlength calculations (similar to that caused by the distance between the KBr windows and the field mirror, inherent in the design of a White cell and discussed in section 4). Besides depending upon the limitations of the method used to measure them, the accuracy of these distances are dependent upon knowing as well as possible the incident point of the incoming light and the corresponding point of the exiting light on the transfer mirrors. It may be noted from the diagram that moving either the incident or exit point changes both B and D or C and D simultaneously and in the same direction, with both distances decreasing as the beam moves toward the windows and increasing as the beam moves away from windows. Furthermore, the assumption must be made that no changes in beam alignment between the bench test and the cell as installed in the spectrometer have occurred if the data are to be related to the cell as used in the spectrometer. The data in Table 9 include the y-intercepts from Figure 12, along with their respective averages. Although it is apparent from the average intercepts that the TOF pathlengths provide a better fit than the Bruker, the sensitivity that can be caused by small changes in B, C, and D is illustrated by the last column, generated by subtracting 0.01 m (1 cm) from each of the TOF pathlengths. Although this represents a change of only 3.3 mm each in B, C, and D, the average y-intercept is reduced by 70%. Given that a change of ±1 cm in the length of the shortest possible path of 1.40 m is well within the 1% estimated uncertainty for the TOF method, the data appear to provide good evidence of the usefulness of the method.

Table 9. Y-Intercepts from Equations of Least Squares Fits of Area vs. Pathlength

	TOF	Bruker	Artificial
	-0.0627	0.4329	-0.0047
	-0.1529	0.344	-0.0913
	-0.06621	0.2388	-0.0456
	0.0108	0.17352	0.0367
	0.0105	0.0336	0.0204
	0.0185	0.0255	0.0124
average	-0.040	0.208	-0.012

On the assumption that the above evidence points strongly to the validity of the TOF pathlengths, the results in Table 8 appear to support the measurement and data analysis process in the laboratory. Average deviation of the measured from the prepared concentrations, excluding the two standards with the lowest concentrations, which rely upon the difficult 674 cm^{-1} band, is 0.7%, within the estimated uncertainties of the pathlengths, even if other possible sources of error are excluded. Average deviation in the determinations of the two lowest concentration cylinders is 4.3%.

6. QUANTITATIVE CONDENSED-PHASE MEASUREMENTS OF DIMETHYL METHYLPHOSPHONATE

6.1 Introduction

The currently used condensed-phase absorptivity coefficients of the chemical agents were measured in the 1960's on grating instruments.[10] Instruments and apparatus have evolved significantly since these tests were done. The experiments were intended to develop and test proposed procedures to be used to repeat this earlier work.

Dimethyl methylphosphonate (DMMP, CAS RN 756-79-6) has the structure shown in Figure 13. Having several functional groups and, therefore, infrared spectral features common to the organophosponofluoridate nerve agents and a similar volatility, but with a much lower toxicity, DMMP was chosen as a simulant for these tests.

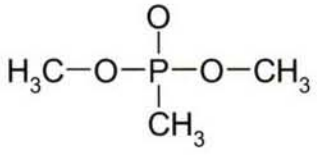

Figure 13. Dimethyl Methylphosphonate

The experimental approach was similar to that in the earlier cited work by Barrett, *et al.* A series of standards of dimethyl methylphosphonate were diluted quantitatively in carbon disulfide and carbon tetrachloride. Short path liquid cells were filled with the solutions and analyzed with an FTIR spectrometer. The resulting spectra were then processed mathematically to determine their adherence to Beer's Law.

6.2 Methods and Materials

In order to ensure that the resulting spectra of the DMMP adhered to Beer's Law, it was desirable to obtain spectra in which the absorbances did not exceed 1.0. The most intense band in DMMP, at 1037 cm^{-1}, arises from P-O-C stretching modes, common to all of the organophosphonate nerve agents. The concentration-pathlengths (CL) of DMMP necessary to obtain usable data could thus be estimated using the earlier data. The data indicated that concentration-pathlengths of $\leq$40 mg/cm^2 would meet the requirement. This CL is significant, because, at a pathlength of 0.05 cm, the concentration of analyte is 2 mg/mL, the maximum concentration of RDTE dilute VX.

Stock dilutions of the dimethyl methylphosphonate at approximately 10 mg/mL were prepared by weighing the neat material in 10-mL class A volumetric flasks and diluting with the appropriate solvents. Further dilutions were prepared from the stock solutions at concentrations of approximately 0.25, 0.5, 1.0, 1.5 and 2.0 mg/mL by transferring known volumes of the stock solution into 7-mL screw cap vials and diluting to 5-mL using Finnpipette digital pipettors. Actual concentrations of the solutions obtained are shown in Table 10.

Table 10. Concentrations of DMMP Solutions

CS_2	CCl_4
Concentration (mg/mL)	Concentration (mg/mL)
10.45	10.38
2.089	2.077
1.567	1.558
0.9497	1.038
0.5224	0.5192
0.2625	0.2609

Initial data from the carbon disulfide solutions showed significant nonlinearities. Investigation eventually indicated that the problem was most likely attributable to the 5 mL digital pipettor. Disassembly showed that the o-ring in the pipettor was causing the plunger to stick. Because the problem did not occur when pipetting the carbon tetrachloride, it appears that the carbon disulfide vapor in the headspace above the pipette tip may have been swelling the o-ring of the plunger and causing it to stick. A call was placed to the manufacturer to determine the material in the o-ring and its compatibility with the solvent. To date a response has not been obtained. The symptoms that can be observed to indicate that the problem is occurring are: solvent that moves up into the tip in a jerking manner rather than smoothly or that the manual button on the plunger does not return to its original setpoint without pulling up on it. As long as repeated attempts are not made over a short period of time to pipette the solvent, the pipettor appears to be suitable. Furthermore, the swelling of the o-ring appears to be reversible. Several of the carbon disulfide solutions were reprepared and reanalyzed.

In the course of the investigation of the problem with the CS_2 data, the calibrations of the 200, 1000 and 5000 μL pipettors were verified. Although manufacturer instructions, which specify a series of 10 checks each at multiple volumes, were not followed exactly and no calculation of precision could be obtained, the data appeared to indicate that the accuracies of the devices exceed the specifications (generally better than 1%).

There is a wide variety of liquid cells that are compatible with the instrument. Of these, two types were purchased for the initial investigations. Thermo-Spectra-Tech sealed precision pathlength (series 0003-5XX) cells are sealed with an epoxy-mercury amalgam and can be supplied with either KBr or NaCl windows. Pathlengths from 0.015-0.5 mm are available and must be specified when ordering. Two of these cells are available for use in the laboratory. One of the two cells was used for tests with DMMP in carbon tetrachloride.

Two additional demountable cells of the 0003-000 series with KBr windows are available. The pathlength is set by the operator during assembly using Teflon spacers with widths of 0.015, 0.025, 0.05, 0.1, 0.2, and 0.5 mm. The tests described in this report were conducted using the 0.5 mm (0.05 cm) spacer. A completed cell includes

bottom and top stainless steel rectangular mounting plates with threaded holes in each corner. The top mounting plate also has Luer compatible ports for filling and flushing the cell. Two rubber gaskets provide a seal between the stainless steel plates and the KBr windows. The rectangular Teflon spacer is positioned between the KBr windows. Assembling the cells requires aligning the Teflon spacer with the fill holes in the upper KBr window, followed by the rubber gasket, and then the upper stainless steel mounting plate. Because the holes on the lower (window) side of the mounting plate have a diameter of only about 1-mm, this operation requires significant manual dexterity. It was necessary to insert a thin fiber, paperclip, or other object through the fill ports and the hole in the upper KBr window to maintain alignment between these parts of the cell during assembly.

The assembled cells have internal volumes of less than 1-mL and require a filling device with a small volume to avoid having liquid spurting out of the upper fill port, which could contaminate the cell and operator. The cells were filled for this series of tests using 1-mL disposable polyethylene syringes with Luer slip tips. These were selected primarily because of their low cost and because a few of them were available for immediate use. Other similar polyethylene syringes with a rubber o-ring at the distal end of the plunger were also tested and found to be incompatible with the carbon disulfide, which appeared to cause the o-ring to swell and stick.

The cells were filled by positioning the cell vertically, and then (1) inserting an empty syringe into the upper fill port, (2) drawing up 0.5-1.0 mL of the appropriate solvent or standard solution into a second syringe and wiping the tip of the syringe with a laboratory tissue wiper, (3) inserting the syringe into the lower fill port of the cell (4) withdrawing the plunger on the empty syringe about one-half, (5) observing the level of liquid in the cell through the KBr windows while carefully depressing the plunger of the liquid filled syringe. When the liquid first appeared in the upper syringe, it was withdrawn, a Teflon stopper was inserted, the cell was placed horizontally, the lower syringe was withdrawn from the lower fill port, and the second Teflon stopper was inserted.

In order to empty and clean the cell, the above fill procedure was more or less reversed: (1) place the cell horizontal and remove the Teflon plugs (2) insert a syringe with the plunger fully retracted into the lower fill port and a second syringe into the upper port (3) invert the cell (4) withdraw the barrel of the second plunger gradually while depressing the plunger of the first syringe. The cell was flushed several times with solvent, and then the fill port was connected to dry nitrogen at approximately 500 mL/min for several minutes. Repeated analysis of blank solvent between spectra of DMMP standards showed that this cleaning step was sufficient to reduce the concentration of the material in the cell sufficiently such that spectral features of the compound were not observed.

Repeated measurements were made of the empty cell, the cell filled with blank solvent, and the DMMP standards in carbon disulfide and carbon tetrachloride. The

instrument used was a Thermo-Nicolet Model 670 FTIR spectrometer with the following parameters:

Detector: Mercury-Cadmium-Telluride (MCT)
Number of scans: 128
Mirror velocity: 1.8988 cm/sec
Apodization: Happ-Genzel
Phase correction: Mertz
Resolution: 0.5 cm^{-1}
Spectral range: 4000-650 cm^{-1}

Absorbance spectra of blank solvent were ratioed against the single beam spectra of the empty cell. Spectra of the DMMP in the solvents were ratioed against single beam spectra of the solvents. All interferograms were saved, enabling additional post-processing of data.

6.3 Results and Discussion

The pathlength of the demountable cell, nominally 0.05 cm, was determined using the interference fringes observed in the single beam spectra of the empty cell (Figure 14) on the basis of the following equation[11]:

$$L = n/(\nu_1-\nu_0)*2,$$

Where L = pathlength in centimeters, n = number of fringes, and ν = wavenumber (cm^{-1}) position of the left and right fringes used for the calculation. Repeated measurements of the pathlength showed no significant change during the course of the experiments. A summary of the data collected is presented in Table 11.

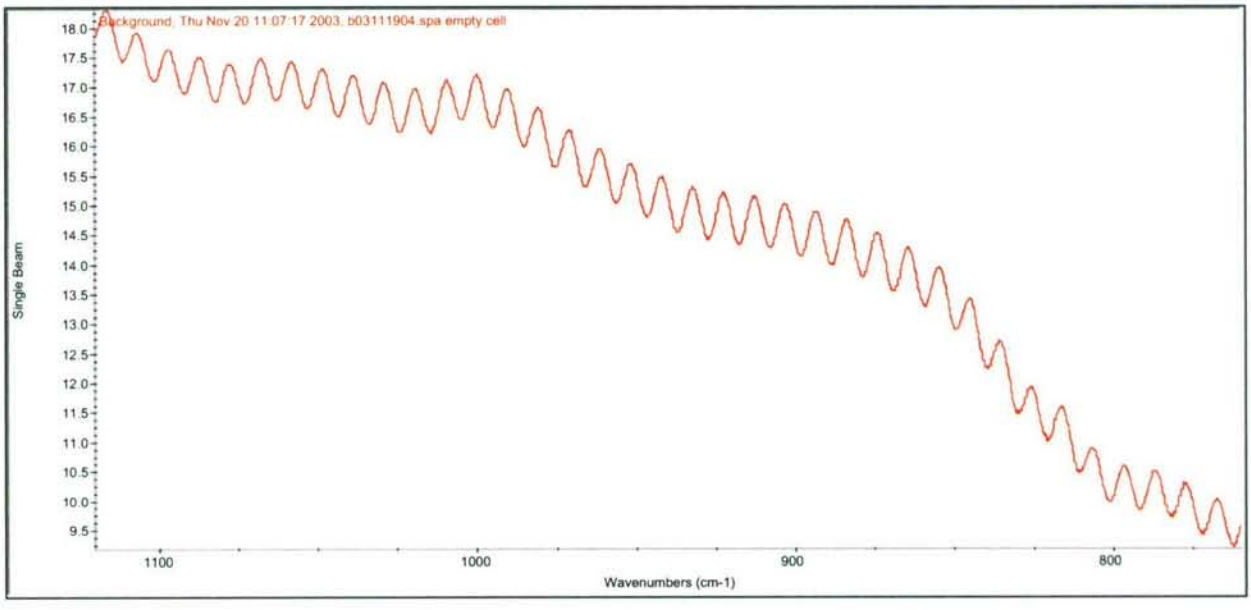

Figure 14. Interference Fringes in Empty Demountable Transmission Cell

Table 11. Pathlength Measurements of Demountable Cell

n	$\Delta\nu$	L in cm (mm)
35	341.9	0.0513 (0.513)
24	235.4	0.0510 (0.510)
34	331.1	0.0513 (0.513)
35	341.5	0.0512 (0.512)
35	331.9	0.0512 (0.512)
35	341.6	0.0512 (0.512)
35	340.0	0.0515 (0.515)
35	339.1	0.0516 (0.516)
	Mean	0.0513 (0.513)

The data from Barrett and Dismukes were recorded using a pathlength of 0.1 mm and with maximum concentrations of agents in the range of 40-60 mg/mL. To avoid using spectral data in the regions in which the solvents were apparently presumed to have significant absorption bands, the absorption coefficients were calculated using data in the range of 3998-1299 cm^{-1} (solutions in CCl_4) and 1399-400 cm^{-1} (solutions in CS_2). The report states that, "The spectrum of the solvent was scanned likewise each time the spectrum of a solution was recorded." It is not clear from this statement whether the spectra of the solvent and solvent/analyte solution were recorded simultaneously (double beam mode) or separately. In either case, the maximum concentrations of solute to solvent analyzed were well into the percent range. There is no indication in the report that any attempt was made to characterize the solvents beyond the statement that, "Spectral-grade solvents were used."

By taking advantage of the increased sensitivity and signal to noise potential of a modern FT instrument and detector, it was hoped that it would be possible to decrease the maximum concentration of analytes. This carries two potential benefits. First, the handling and storage requirements for RDTE dilute solutions are significantly reduced versus those at higher concentrations. Additionally, the safety concerns associated with agents in the percent range are not insignificant. In particular, filling and rinsing the liquid transmission cells without contaminating the exterior of the cell, the fume hood, or the operator requires a slow, careful technique.

Figure 15 includes spectra of carbon tetrachloride acquired in room 18, (ratioed against the empty cell) and from the NIST Webbook in the range 4000-870 cm^{-1}. The spectra are qualitatively similar. The most intense band in the range of 4000-1300 cm^{-1} is found at 1550 cm^{-1}. The band is broad and has an absorbance of 1.45 at the 0.05 cm pathlength. If the pathlength were to be reduced from 0.05 to 0.01 cm to correspond to the historic data, this would still imply an absorbance for this band of nearly 0.3. It will most likely be difficult to subtract this band with a high degree of accuracy and may result in distortion of any spectral features of the analytes in this region of the spectrum. If higher concentrations of analytes (relative to the solvent) are analyzed, it will most

likely be necessary to ratio using a spectrum of the solvent generated with a mathematical algorithm.

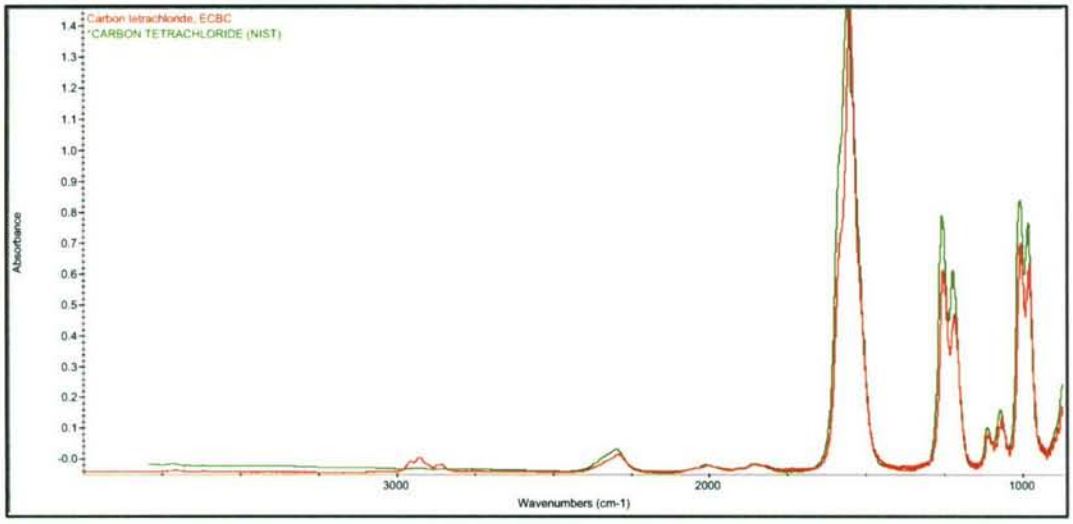

Figure 15. Spectra of Carbon Tetrachloride from ECBC (red) and NIST (green)

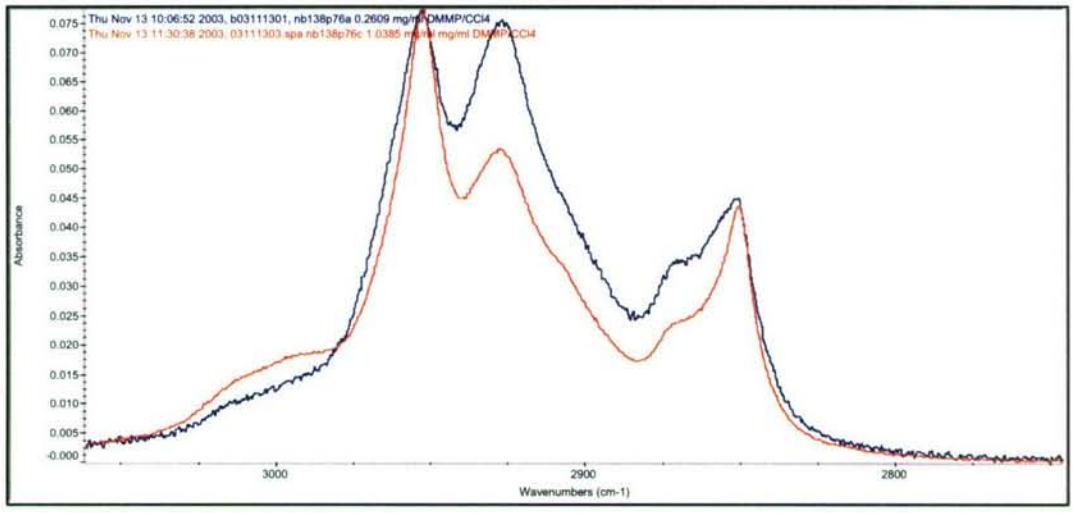

Figure 16. C-H Stretch Region of Ratioed DMMP Spectra

More troublesome in the spectra of the carbon tetrachloride were persistent features appearing in the C-H stretching region in the vicinity of 3000 cm^{-1}. These varied in shape and intensity, and subtracting these features from those attributable to the DMMP proved problematic. As a result, the relative shapes and intensities of those stretching bands in the DMMP were not consistent in all of the spectra (Figure 16). The source of these anomalous features was not determined. They could have arisen from impurities in the solvent. The purity of the CCl_4 is indicated at 99.5%, i.e., potentially as much 0.5% impurities, contrasted to a ratio of solute to solvent in the DMMP solutions of 0.025-0.2%. Arguing against this hypothesis is the fact that the features showed no observable trend as the concentration of DMMP changed. Nevertheless, if the bands stem from solvent impurities, reducing the pathlength of the cell could improve the

resulting spectra. Another possibility could have been organic compounds leaching from the syringes. Testing with glass, as opposed to disposable plastic syringes, could assist in confirming or eliminating this hypothesis. The conclusion for now must be that the phenomenon requires further investigation.

Carbon disulfide is used in parallel with carbon tetrachloride for obtaining absorptivity coefficients of organic compounds because their bands of maximum intensity do not overlap. The most intense absorptions in the infrared spectrum of carbon disulfide occur between 1600 and 1400 cm^{-1}, the upper end of which, however, does include one of the absorptions of carbon tetrachloride. The accuracy of the absorptivity coefficients in this region may be limited.

The method used for acquiring spectra of the DMMP in carbon disulfide was similar to the carbon tetrachloride. Single beam spectra of the empty cell were taken, then the blank CS_2, then the DMMP in solution. The spectra of the DMMP were then obtained by ratioing the solution spectra with the blank solvent. In general this method obtained reasonably consistent spectra in the fingerprint region. Figure 17, showing spectra of DMMP at 1.567 and 2.089 mg/mL (to the same scale), illustrates that proportionalities of the bands were maintained.

As can be noted in Figure 17, the most intense bands in the infrared spectra of the organophosphonates are typically observed in the vicinity of 1000 cm^{-1}.[12] Although this spans some weaker bands of carbon tetrachloride, it was useful to compare data obtained with the two solvents. Figure 18 is a plot showing that the 1037 cm^{-1} band in the DMMP spectrum does appear to follow Beer's Law in both the CS_2 and the CCl_4.

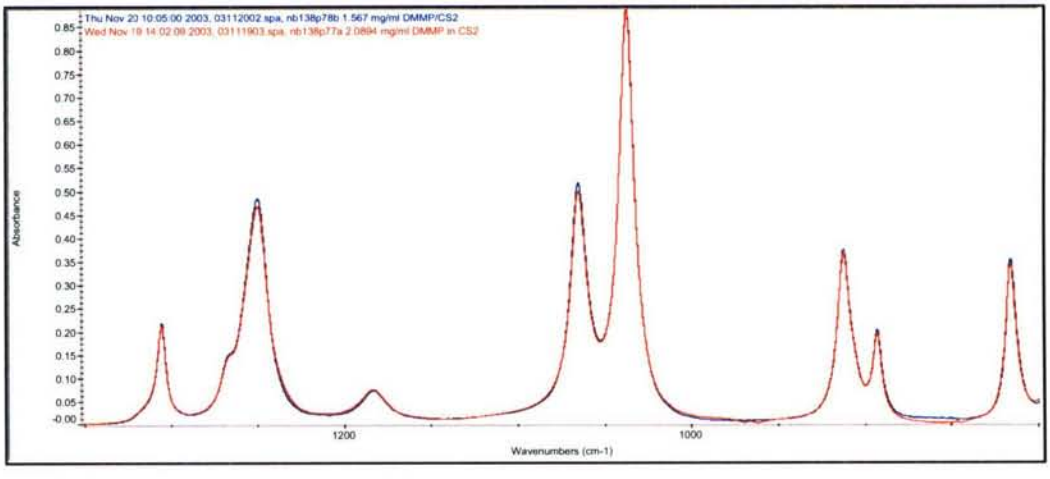

Figure 17. Spectra of DMMP in CS_2 at 1.567 and 2.089 mg/mL (common scale)

As noted earlier, tests of the two sealed precision pathlength cells were conducted in the laboratory. According to the manufacturer, these cells have pathlengths with accuracies of ±2%, a desirable feature for precise quantitative work. Because the pathlengths of the cells were not noted on either the polymer shipping bags or the stainless steel mounting plates, these were unknown at the time of the experiments.

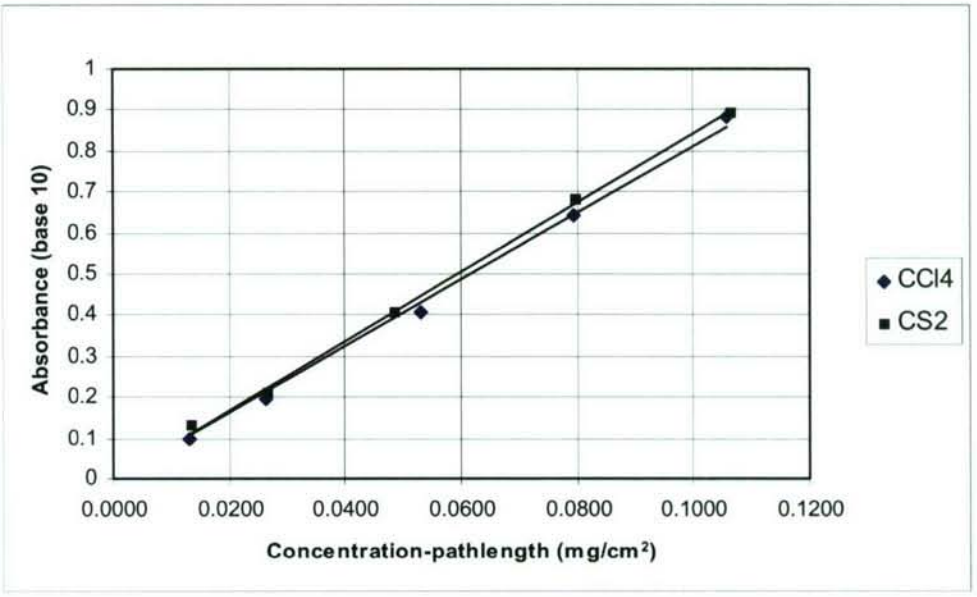

Figure 18. Beer's Law Plots of Dimethyl Methylphosphonate in CS_2 and CCl_4

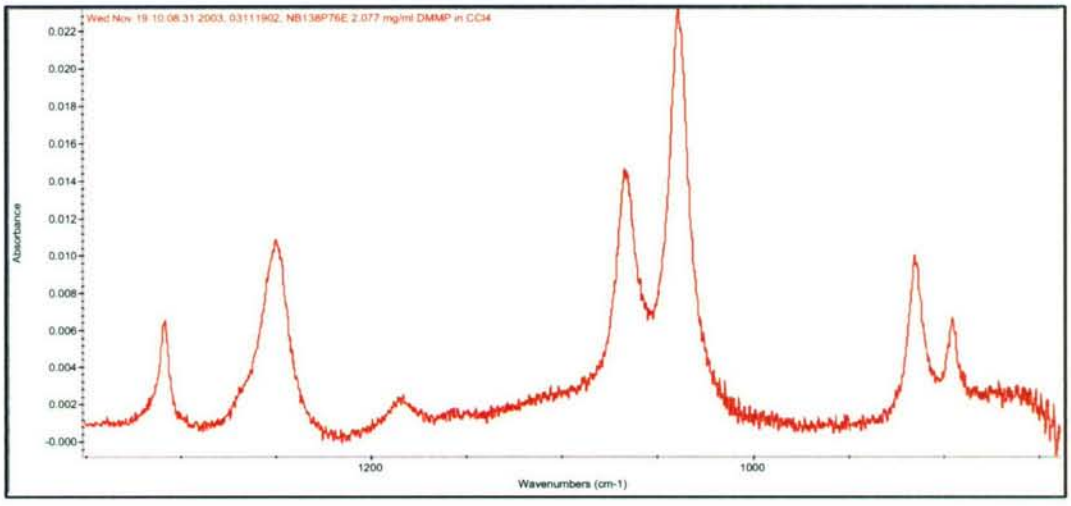

Figure 19. Spectrum of DMMP in Sealed Fixed Pathlength Cell

One of the two cells was selected for the tests. The single beam spectrum of the empty cell was obtained, then of the cell filled with carbon tetrachloride, then of the cell containing the DMMP at a concentration of 2.077 mg/mL. The single beam spectrum of the empty cell did not show the pronounced interference fringes noted earlier; therefore, the 1037 cm^{-1} peak of the spectrum of DMMP taken in the sealed cell (Figure 19) was used to determine the pathlength based upon the absorptivity of this band obtained previously in the demountable cell (Figure 18). This resulted in a calculated distance of 0.014 mm (14 μm). Because this is close to one of the standard spacings of 0.015 mm available from the manufacturer, it is probable that the actual spacing is 0.015 mm±2%.

In principle, the above ratio method that was used does differs little from that proposed for use in verifying the pathlength of the Schott gas cell, as described in section 5.3.

When the sealed cell was being flushed after acquiring the spectra of the DMMP, it was noted that solvent appeared to be leaking between the KBr plates. After several calls to the manufacturer, it was ascertained that the amalgam used to the seal the cells is not generally compatible with organic solvents except for alcohols. This would obviously severely limit their effectiveness for future work. It should be noted that Thermo-SpectraTech no longer supplies the demountable cells. We were referred to Wilmad Labglass as the current manufacturer of equivalent cells. A phone call to Wilmad indicated that they might be a custom manufacture, although this has not been confirmed.

Infrared band positions and intensities are subject to intermolecular effects, either between adjacent molecules of the same type or different molecular species (solute-solvent effects). Perhaps the most easily recognizable, and one of the most dramatic, among these is hydrogen bonding. Within species containing an –OH functional group (alcohols, acids, etc.), the O-H stretching frequency will shift by 300-400 cm^{-1}, and intensities can vary greatly between neat liquid, dilute solution, and vapor-phase. Among the organophosphorous esters, for example, the phosphoryl stretching band arising from P=O increases by up to 65 cm^{-1} in the vapor-phase.[13] In some cases, band intensities have also been observed to change.

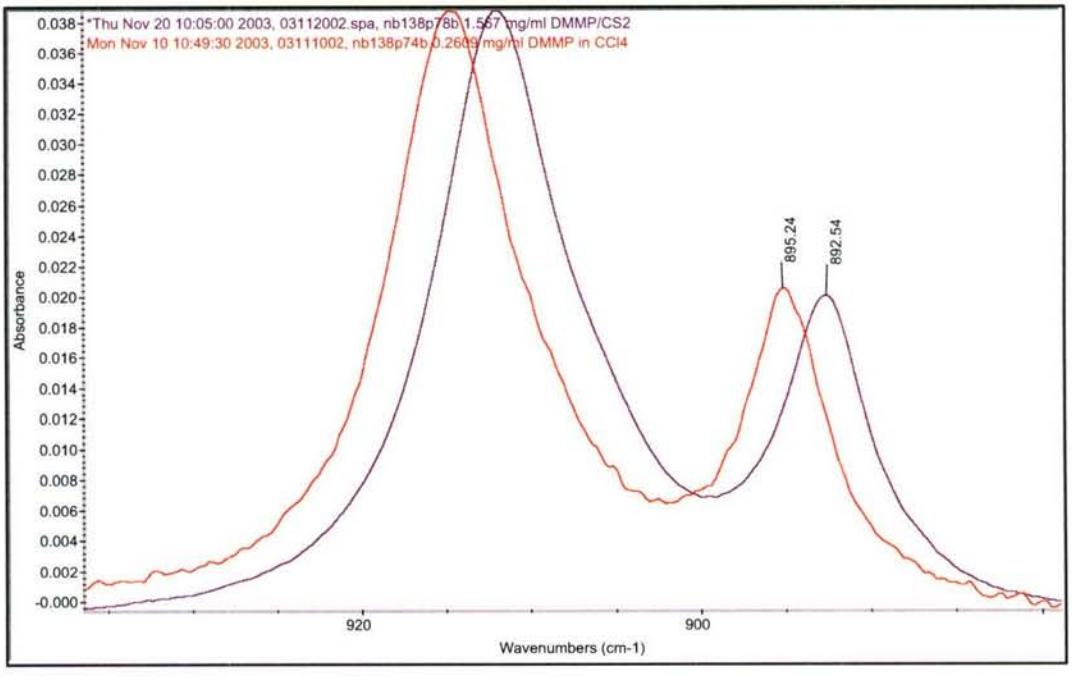

Figure 20. Spectra of DMMP in Carbon Tetrachloride (red) and CS_2 (violet)

Carbon disulfide is a more polar solvent that carbon tetrachloride. It is not surprising, therefore, that solvent/solute effects resulted in differences in the observed frequencies of some of the infrared bands of the DMMP, although in general the shifts were ≤2-3 cm^{-1} (Figure 20). It was noted that effects on relative band intensities were very small. Nevertheless, the spectral data reminded us that a caveat should be applied to all quantitative infrared measurements: Positions, widths, and intensities of bands are dependent upon temperature, pressure, and matrix. While it is not impossible to apply such data outside of the specific conditions of the experiment in which the spectra were obtained, the resulting data represents, to a greater or lesser extent, only an approximation. Given that spectra can differ significantly by technique and matrix, the question is sometimes asked, "How does one obtain the *true* spectrum of a material?" The answer may be that merely because a spectrum alters in going from thin film, to solvent, and then to vapor-phase, it has not become more or less *true* in the absolute sense, but merely different. For this reason, spectra acquired for reference databases should always be supplied with as much detail as possible concerning the experimental conditions, and a comprehensive database should maximize not only the number of compounds but also the spectral technique and matrix types.

No attempt was made to calculate the absorptivity coefficients of the DMMP, other than the simple plot in Figure 18. The algorithm assumes that positions of bands remain constant. It is possible that an attempt could be made to do an averaging of the frequencies of the bands between the two sets of spectra, although this is currently beyond the scope of the MatLab script as written.

Transitioning between analyzing relatively nontoxic solutions of DMMP and toxic chemical agents will require some care to ensure that the materials are handled safely. The single demountable cell used in the tests proved to be relatively robust and appeared to be well sealed against at least visible leaks. The additional considerations come at least in part, and unexpectedly, from the fact that the internal volumes of the cells are very small, ranging from 6 μL for the 0.015 mm pathlength to 200 μL for the 0.5 mm. When filling the sealed cell (0.015 mm), it was very nearly impossible to ascertain by sight the level of liquid in the cell, making it easy to overfill the cell. With a 1 mL syringe this proved to be challenging. The demountable cell, assembled with 0.5 mm spacer, was somewhat easier to fill. By partially withdrawing the plunger on the second syringe and using care not to depress the liquid filled syringe beyond the retracted volume of the second syringe, the risk of causing liquid to leak from the cell was minimized.

7. QUANTITATIVE MEASUREMENTS OF BACILLUS ATROPHAEUS IN KBr PELLETS

7.1 Introduction

Bacillus atrophaeus (often called by its former name, *bacillus globigii* or BG) is routinely used in military field trials to emulate the properties of a threat *bacillus anthracis* aerosol. To date, no rigorously quantitative (Beer's Law) mid and long wavelength infrared cross-section data of these materials have been reported (to our knowledge). The KBr pellet methodology reported here has been developed to obtain the Beer's Law plots and absorptivity (extinction) coefficients of the variants historically and currently in use.

The series of experiments have been initiated to compare the quality of the KBr pellet data with those of thin films of the microbes (measured in the biosafety level 3 laboratory). We anticipate that we can then use the qualitative thin film data of select pathogens in conjunction with quantitative pellet data of analogous microbes to infer the cross-sections of the live biological agents.

BG is a non-etiologic organism, presenting little health threat to non-immunocompromised individuals. This, and other similar non-etiologic organisms, can be handled in a BSL-1 environment.

7.2 Materials and Methods

The experiments described in this section were performed in accordance with the procedures in SOP CR8-OSP-142 (currently numbered RNB-093). This SOP, originally developed for the purpose of acquiring condensed-phase quantitative infrared spectra of chemical agents in a solid matrix, was amended to include additional requirements for handling and disposal of BSL-1 microbes.

In addition to the Thermo-Nicolet 670 spectrometer, other equipment and apparatus used in the procedure included:

- Gloveboxes purged with dry nitrogen
- Carver 10-ton hydraulic press
- 13-mm press die with vacuum port
- Mortar and pestle
- Sartorious model BP211B analytical balance-
- Mitutoyo model C112EB digital comparator

Potassium bromide (CAS RN 7758-02-3, Thermo-SpectraTech part number B927232) was used as diluent for the pellets. In order to obtain consistent spectra free from scattering, materials used in making the pellets should have maximum diameters of a few micrometers. The material as received from the manufacturer was further ground with an agate mortar and pestle until a smooth, even texture was achieved, with

little visible speckle from larger grains of the salt when an aliquot of the material was viewed at an oblique angle. KBr is an extremely hygroscopic material, and after grinding it was dried for several hours at 105° C. Even with drying, during conditions of high humidity, it was difficult to obtain a clear pellet free of bands from adsorbed water. For this reason, we emplaced a glovebox for sample preparation (additional to the larger glovebox in which the spectrometer is installed) behind the 20-cm line in a fume hood. Although not necessary for BSL-1 work, the configuration permits dual use of the glovebox for both chemical and biological materials. When mixing samples for weighing, a port on the side of the glovebox was connected to dry nitrogen flowing at 1-2 liters per minute.

The biosamples were from a selection of BG spores in varieties that either have been or are currently being used in military field trials. The historical sample selected was a "Bioferm," designated BG-BF-01, and the current sample was from Danish milled spores numbered BG-DAN-01. BG-DAN-04 was selected on the basis of its having been used in a chamber experiment in 2003. All variants were fluidized with silica. No additional preparation or grinding of the spores was done.

Dilutions of the biosamples in the powdered potassium bromide were prepared gravimetrically and hand mixed in 7-mL Teflon lined screw cap glass vials. BG-DAN-04, the last sample set addressed in this report, was mixed with a Retsch® grinder/mixer after this apparatus became available in the laboratory. In order to ensure data within the linear range of the detector, pellets were prepared in concentrations ensuring that absorbance in the strongest spectral band (1655 cm^{-1}) did not exceed 1.2, although subsequent experiments with BG-DAN-04 indicated that this limitation may have been somewhat pessimistic, and data from the latter set were calculated after preparing an additional eight pellets and using a maximum absorbance of 1.3. To ensure an adequate signal to noise ratio, pellets were prepared having a minimum absorbance in the most intense band of 0.05. This was achieved by preparing an initial single pellet to estimate the absorptivity coefficient of the band. Thereafter, serial dilutions were prepared from the initial sample to obtain five 1-gram aliquots expected to produce pellets with spectra with the range of 0.05 to 1.2 absorbance. Three replicates were prepared from each of the five final dilutions, resulting in a total of a total of fifteen pellets.

A nominal 0.22 g amount of each powdered sample was added to a ten-ton pellet die, and then pressed at 18,000 pounds (8,000 Kg) under vacuum for five minutes. All pellets were then weighed three times on the analytical balance, with weights recorded to the nearest 0.01 mg. Thereafter, the pellets were transferred to the glovebox containing the FTIR instrument.

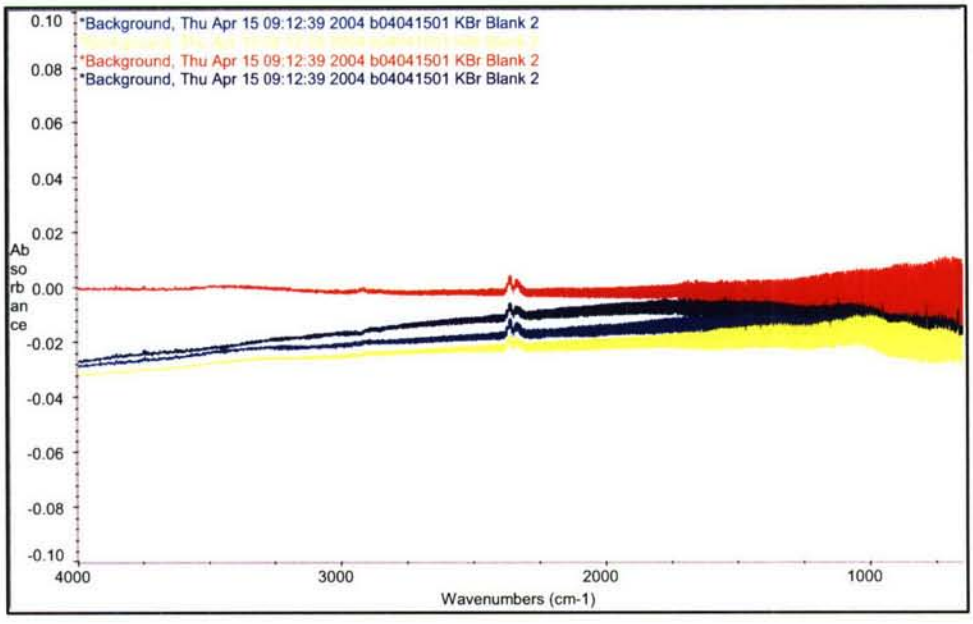

Figure 21. Spectra of Blank KBr Pellets

Spectra were acquired with a Thermo-Nicolet Model 670 FTIR spectrometer using the following instrumental parameters:

Detector: Mercury-Cadmium-Telluride (MCT)
Number of scans: 64
Mirror velocity: 1.8988 cm/sec
Apodization: Happ-Genzel
Phase correction: Mertz
Resolution: 2 cm^{-1}
Spectral range: 4000-650 cm^{-1}

All background and sample interferograms were archived, enabling future processing of interferograms as desired. Absorbance spectra were saved in Grams format (.spc) for additional processing in Grams and MatLab.

It is not possible in a consistent way to prepare multiple blank or analyte containing KBr pellets in which the transmission properties (i.e., scattering, thickness) are exactly reproduced. Despite our best efforts, small differences in pellet densities, masses, and thicknesses, as well as differences in scattering properties, resulted in baseline shifts among pellets. Indeed, because of this lack of reproducibility, some references suggest that pellets should be ratioed against the blank pellet holder rather a KBr blank.[14] Other authors specify the use of a blank KBr pellet for the background sample.[15] During the work by Barrett and Dismukes, the spectra of the agent-containing pellets were compared with a blank KBr pellet, and such a procedure does have advantages. Any absorbance features present in the salt (i.e., impurities and water) are subtracted from the final absorbance spectrum, and the resulting baseline, in which the attenuating properties are more closely matched using the blank salt as opposed to the

empty holder, is closer to zero. By matching the mass of KBr as closely as practicable to that of the sample pellets, evacuating the die while pressing, and using the same pressure and pressing time in each case, it was possible to produce pellets with a reasonable degree of reproducibility, as seen in Figure 21.

What appears to be noise in the region of the spectra below 1000 cm^{-1} are interference fringes resulting from the high specularity of the pellets. An ideal pellet should also be nearly transparent. The latter factor may, however, in some cases become a disadvantage. Because a very smooth, transparent pellet may also have highly specular properties, this may result in interference fringes when the spectrum of the pellet is taken. To minimize such effects, we have rotated the solid sample accessory, normally with the sample plane at 90° with respect to the infrared beam, to an angle of approximately 88.5°. Nevertheless, interference fringes are still sometimes observed, as can be seen in Figure 22. Indeed, because of the large number of factors that can affect the properties of a KBr pellet, it is extremely difficult to isolate and investigate them individually, and we have provided additional discussion of the effects of pellet variability, some possible sources of errors, and baseline correction in Appendix B.

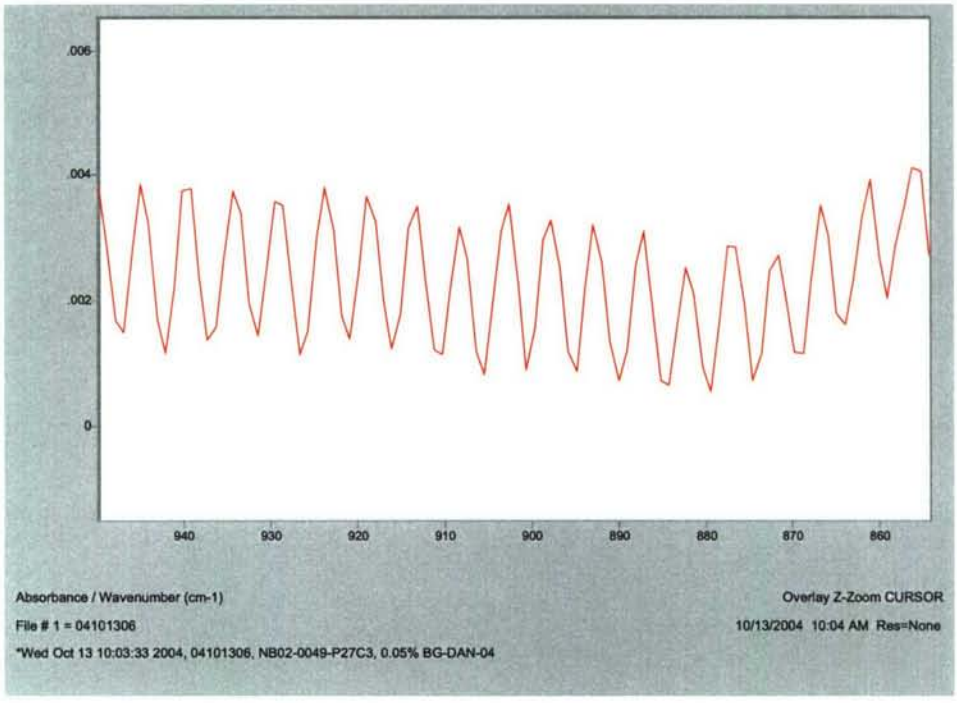

Figure 22. KBr Pellet of BG Showing Interference Fringes

Five blank KBr pellets were made with each sample set (variant) to ratio against the BG-containing pellets. During data analysis, the single beam spectrum of each blank pellet was ratioed against the single beam spectra of each of the BG pellets to obtain five absorbance spectra for each of the 15 pellets. To obtain the final absorbance spectrum from each pellet, the blank KBr pellet that gave an absorbance

spectrum with the least slope in the baseline and with the baseline closest to the zero absorbance line was used. Typical sample-to-sample baseline variation in a set of pellets at approximately the same concentration-pathlength may be observed in Figure 23. Remaining deviations in the baselines of the absorbance spectra were corrected using Grams software by selecting two points in non-absorbing regions of the spectra (3990 and 2260 cm^{-1}) and using a straight-line function. Because the correction required each time manually inputting the wavenumber points within the baseline to be used for zeroing, it may be worthwhile considering the development of an algorithm to automate this process (see section 5.2 for an example).

After the spectra were acquired, the physical cross sections (thickness) of the pellets were measured with the Mitutoyo comparator. Each sample and blank pellet was marked with an arbitrary orientation mark on the outer perimeter. With the orientation mark denoted as 12 o'clock, five measurements were conducted at the 12, 3, 6 and 9 o'clock and center positions, with readings recorded to the nearest 0.001 mm (1 μm).

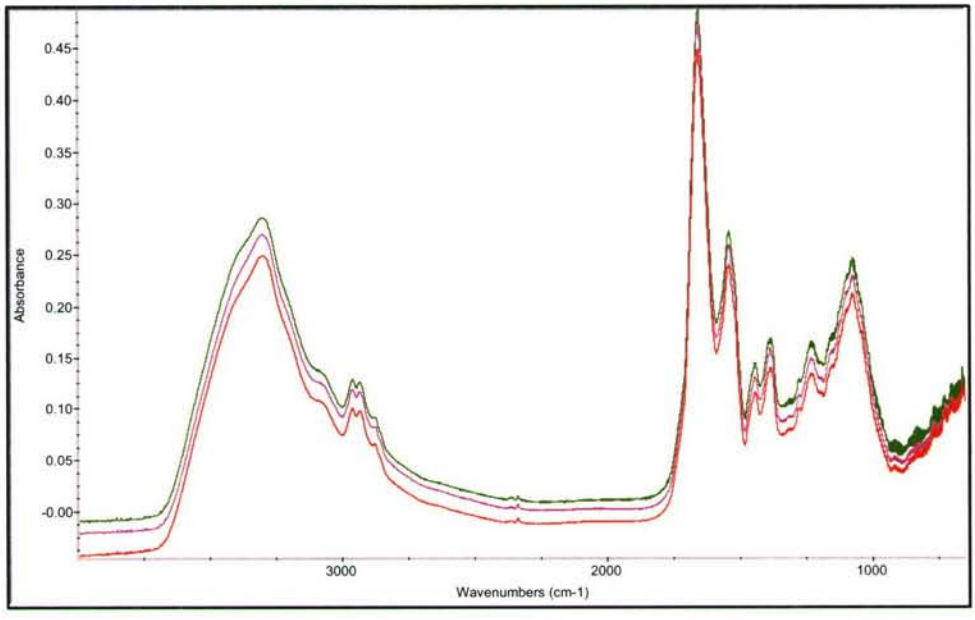

Figure 23. Spectra of BG Pellets at Approximately the Same Concentration-Pathlength

In addition to the concentration-pathlengths of the pellets in mg/m^2, an additional calculation was performed to obtain the density of the pellets in g/cm^3. Although not necessary for the computation of the concentration-pathlength, because the bulk material in the pellets was comprised of potassium bromide, the degree to which the density of the pellets approached that of crystalline KBr (2.75 g/cm^3) was considered a potential indication of the relative consistency of the pellets.

7.3 Results and Discussion

Data from the dimensional analysis and calculation of the concentration-pathlength products of the pellets is presented in Appendix C.

The absorptivity coefficients were obtained from the spectral data using the MatLab algorithm that had been originally developed for use with the vapor-phase spectra. Because baseline control is more difficult in the case of the pellets due to scattering and pathlength differences between the background and sample pellets, the algorithm was ultimately modified to include the calculation of the y-intercepts of the coefficient.

Initial analysis of spectra from BG-DAN-01 resulted in what appeared to be a discontinuity in the standard deviation of the absorptivity coefficient, with a large relative error in the vicinity of 1655 cm^{-1}. This can be seen in Figure 24. After several days of investigation, including crosschecks of the output of the MatLab code through use of a simplified algorithm that had been developed prior to the implementation of the more sophisticated software, the source of the discontinuity was traced back to an apparent bug in the Omnic software used with the FTIR spectrometer. Apparently when Omnic writes to the Grams format, the exponent for scaling the Y data that is exported to the binary file does not get converted correctly if the spectra contain points with absorbances ≥1. Curiously, although the resulting spectra scale correctly when opened in Grams, when read subsequently by *readspc*, a subroutine in the MatLab algorithm developed at ECBC, the exponent is interpreted incorrectly. Fortunately a simple fix to the problem was intuited: As long as the spectra are resaved within Grams after they have been written from the Omnic, the exponent is then reinterpreted correctly.

Absorptivity coefficients of the three most intense bands in the spectra of the materials are listed in Table 12. It may be noted that the apex of the band in the 1100 cm^{-1} region of BG-BF-01 is approximately 25 cm^{-1} lower than in the other two variants. The materials studied are a complex mixture of spores, growth media, metabolic byproducts, and fluidizer. It is likely that the shift in the position of the peak arises from differences in the concentrations of fluidizer to biological materials in the variant. Evidence for this hypothesis may be indicated by the fact that the variant showing with the greatest shift in the band position also has the largest ratios of band intensities. A future planned study of "cleaned" BG spores may elucidate the problem.

Plots of absorptivity coefficients and statistical uncertainties (2σ) for the three sets of spores are available in Figures 25, 26, and 27. In general, the relative expanded uncertainties are 2-10% of the absorptivity coefficient for α greater than approximately 15% of the maximum coefficient. Additional discussion of uncertainties may be found in Appendix B. In order to illustrate the similarities and differences among the three different spore types, the y-intercepts obtained from the least squares fits of the data have been combined in one plot (Figure 28). There is a noticeable trend for y-intercepts to be greater in regions where absorption bands are present. We discuss a possible cause of this effect in Appendix B.

Table 12. Absorptivity Coefficients [$(mg/m^2)^{-1}$ X 10^{-4}] of BG Variants in Regions with the Most Intense Absorption Features

Variant	Band position cm^{-1}		
	1100 region	1655	3296
BG-DAN-01	0.607 (1110 cm^{-1})	0.682	0.479
BG-BF-01	0.635 (1076 cm^{-1}) 0.555 (1110 cm^{-1})	1.33	0.714
BG-DAN-04	0.582 (1108 cm^{-1})	0.707	0.378

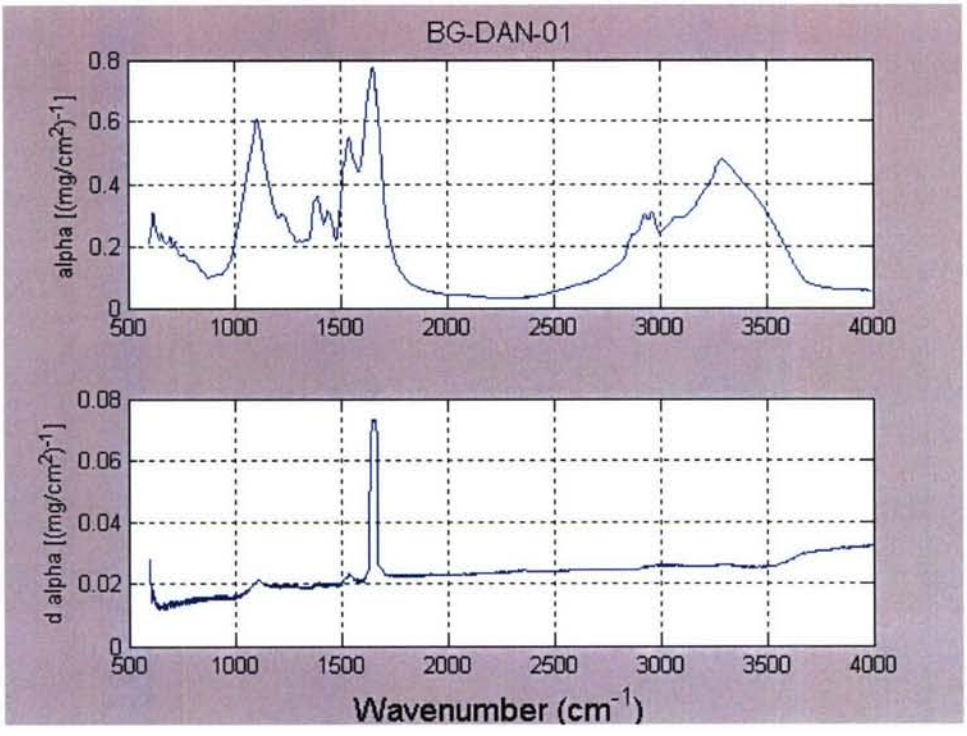

Figure 24. Absorptivity Coefficient Data of BG-DAN-01 Showing Apparent Discontinuity in Standard Deviation (lower graph) prior to Recalculation of Data

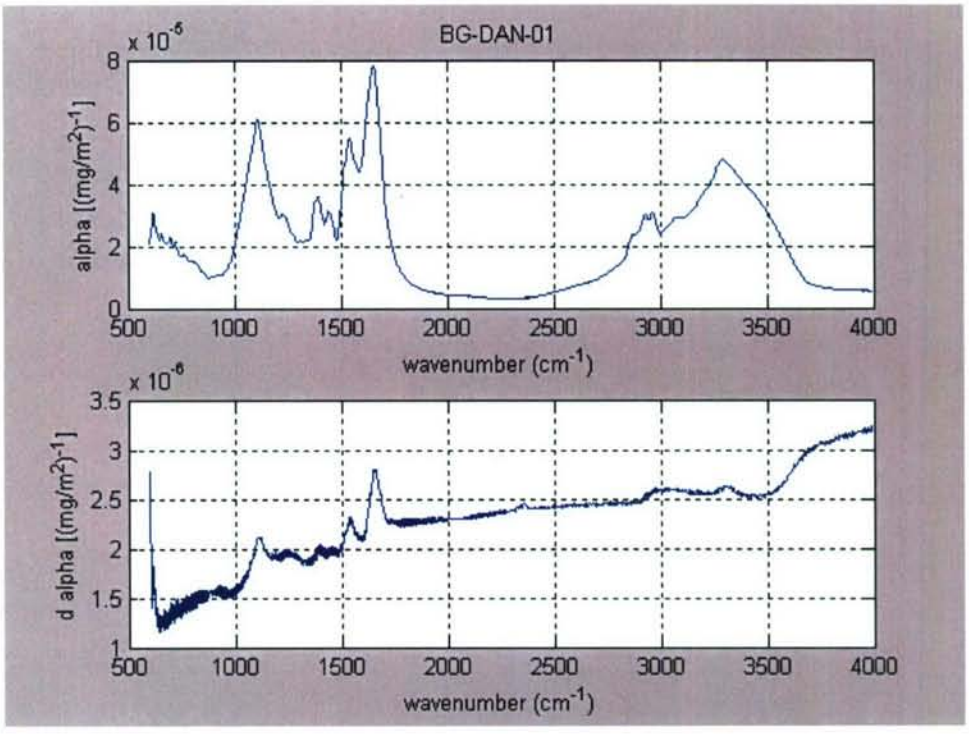

Figure 25. Absorptivity Coefficient (upper) and Statistical Uncertainty (2σ) (lower) for BG-DAN-01

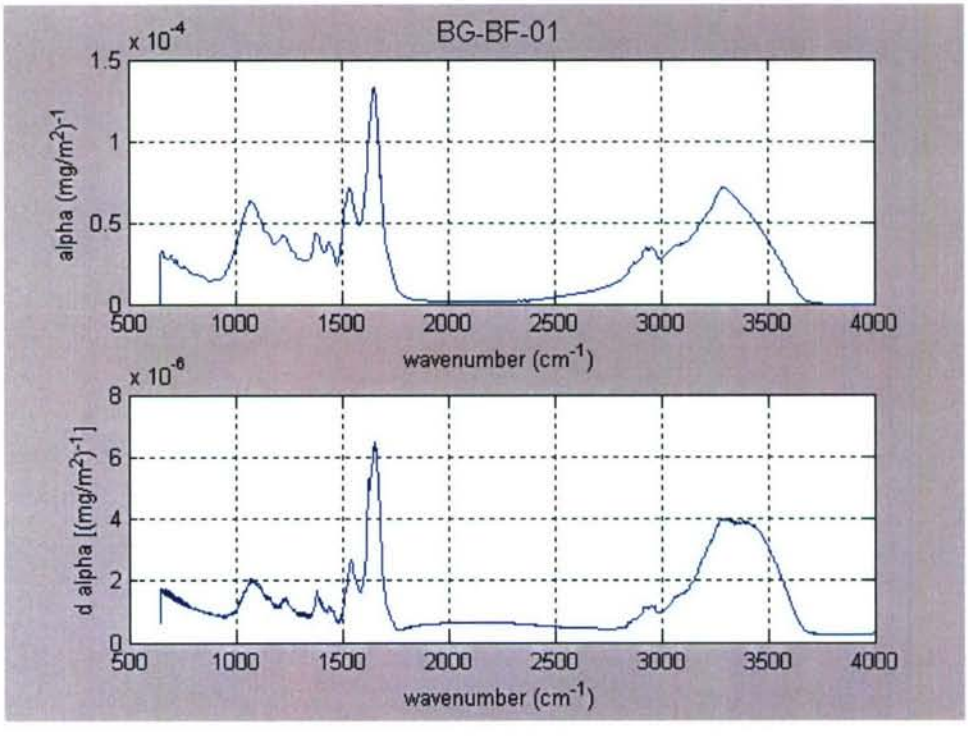

Figure 26. Absorptivity Coefficient (upper) and Statistical Uncertainty (2σ) (lower) for BG-BF-01

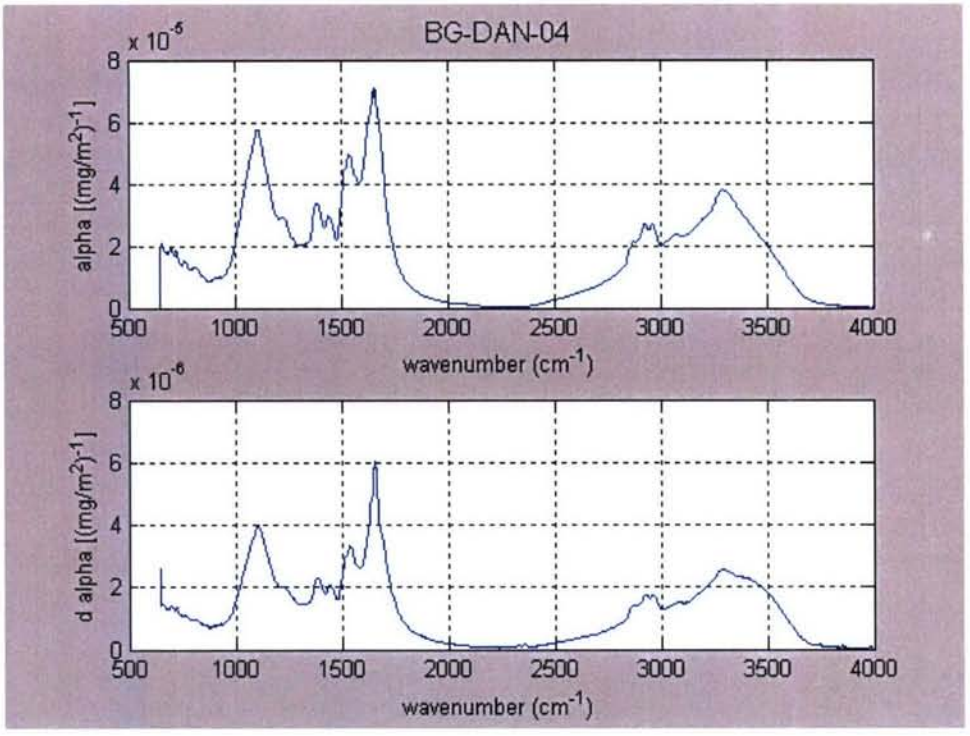

Figure 27. Absorptivity Coefficient (upper) and Statistical Uncertainty (2σ) (lower) for BG-DAN-04

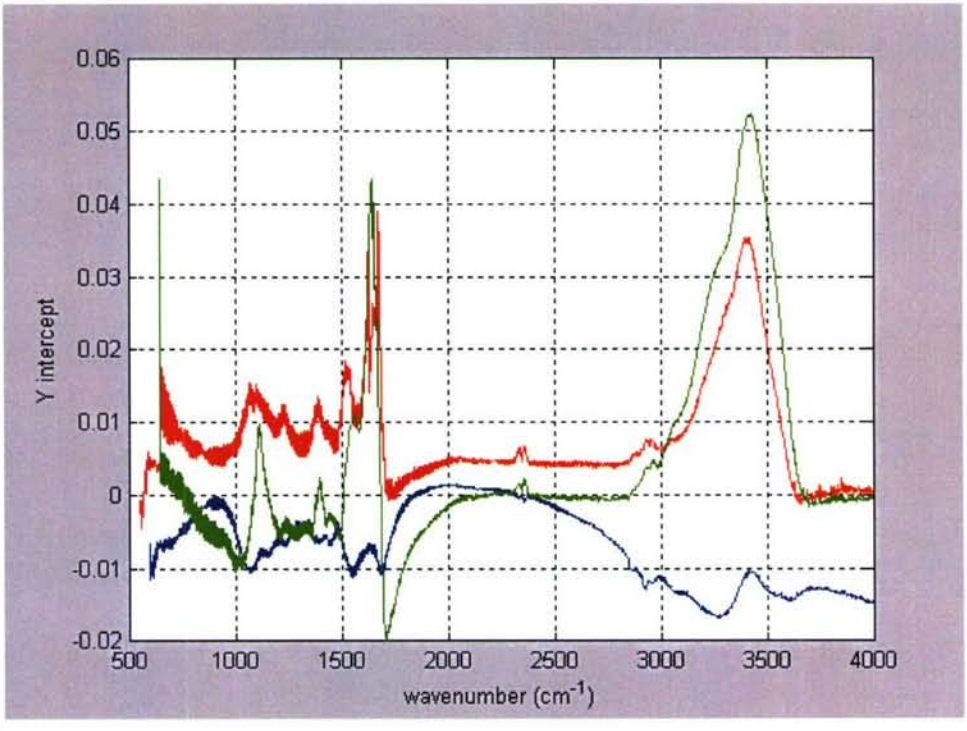

Figure 28. Y-intercepts of the Absorptivity Coefficients (BG-DAN-01, blue; BG-BF-01, red; BG-DAN-04, green)

Biological materials have been studied with a variety of reflectance techniques, and a study is currently ongoing within the Passive Standoff Team to obtain the infrared reflectance spectra of a variety of biosimulants deposited on a reflective substrate, Transflex®, using a Digilab FTIR spectrometer. Because of the very preliminary state of this work, a complete report of the data is not possible at the time of this report.

It is useful, however, to present a spectrum from one of the BG variants covered in this report (BG-DAN-04, seen in Figure 29) that was obtained using this technique. The similarities in positions of the bands in the spectrum below to those in Figure 27 may provide evidence that the high pressure applied in the pellet press does not adversely affect the gross morphology and chemistry of the spores. Although variations in relative band intensities may be noted, these may arise from differences inherent in transmission versus reflectance infrared spectroscopy or may indicate saturation in the more intense bands.[13]

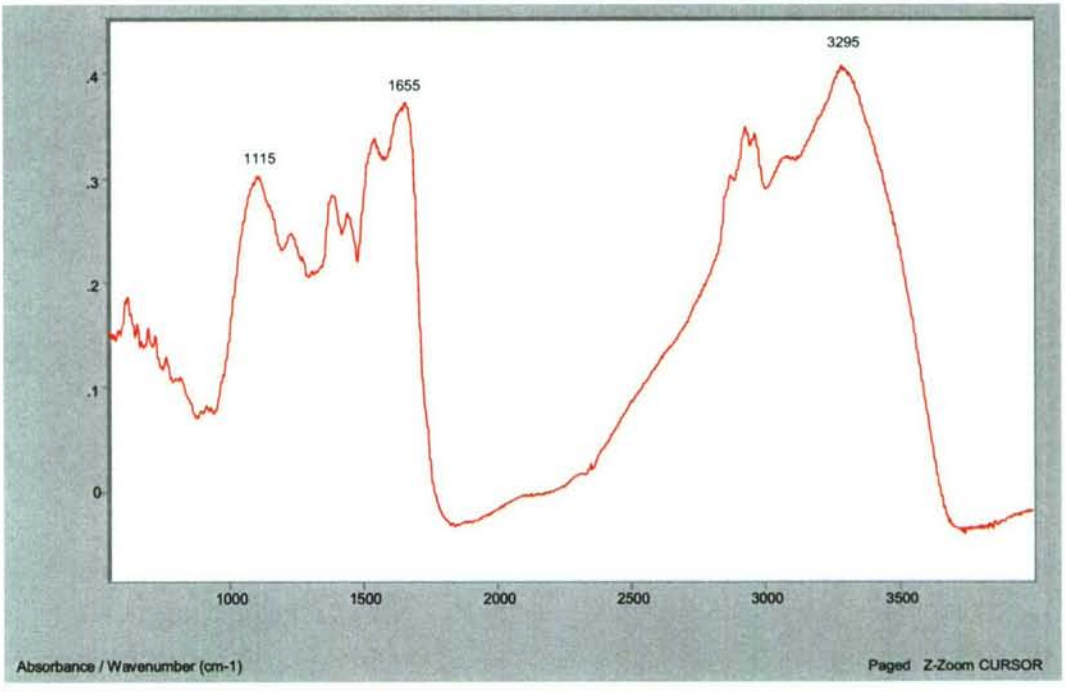

Figure 29. Reflectance Spectrum of BG-DAN-04 Deposited on Transflex Substrate

7.4 Conclusions

We believe that these experiments have provided the first quantitative infrared spectral data of these variants of fluidized spores of BG. The data indicate the usefulness of the technique for future use in obtaining the absorptivity coefficients of additional biological materials.

8. SUMMARY AND FUTURE WORK

Work addressed in detail in this report included the following laboratory experiments:

- Absorptivity coefficients of benzene in the vapor phase.
- Analysis of NIST prepared benzene standards to validate the vapor-phase laboratory capability.
- Wavelength calibration of the Bruker IFS66V FTIR spectrometer.
- Experiments to verify the pathlength settings of the Schott variable-pathlength gas cell.
- Development and testing of algorithms to calculate absorptivity coefficients and statistical errors from quantitative spectra of materials measured in condensed and vapor-phase.
- Quantitative measurements of dimethyl methylphosphonate in liquid-phase.
- Quantitative measurements of bacillus atrophaeus (bacillus globigii, BG) in KBr pellets.

Additional work conducted included the successful publication of three new SOP's, theoretical studies of baseline effects in diffuse reflectance, as well as additional laboratory work to be published separately, and presentation of papers at scientific conferences.

We believe that the experiments conducted in the laboratory have validated the equipment and procedures to be used in the future to obtain quantitative infrared spectral data of the required chemical and biological materials in a variety of matrices. Future work will encompass additional biological materials, including other microbial species, and the chemical agents.

REFERENCES

1. B. R. Williams, M. Hulet, A. Ben-David, R. Miles, G. Roelant, A. Samuels, C. Zhu. *Validation and Support of a Quantitative Vapor-Phase Infrared Instrument Facility and Generation of a Library of Chemical Warfare Agents and Related Materials by Fourier Transform Infrared Spectroscopy,* EAI Report No. 4000040/03/001F, September 2003.

2. A. C. Samuels, B. R. Williams, A. Ben-David, M. Hulet, G. J. Roelant, R. W. Miles, C. Zhu. "A Traceable Quantitative Infrared Spectral Database of Chemical Agents," in *Optically Based Biological and Chemical Sensing for Defence*, edited by John Carrano and Arturas Zukauskas, Proceedings of SPIE Vol. 5617 (SPIE, Bellingham, WA, 2004) 166-178.

3. A. C. Samuels, B. R. Williams, A. Ben-David, M. Hulet, G. J. Roelant, R. W. Miles, N. Green, C. Zhu. "A Traceable Quantitative Infrared Spectral Database of Chemical Agents." 6th Conference on Standoff Detection for Chemical and Biological Defense, 25-28. October 2004.

4. T. J. Johnson, R. L. Sams, T. A. Blake, S. W. Sharpe, P. M. Chu. *Applied Optics,* 41(15), 2831-2839.

5. P. M. Chu, F. R. Guenther, G. C. Rhoderick, W. J. Lafferty. *J. Res. Natl. Inst. Stand. Technol.,* 104, 59 (1999).

6. S. Sharpe. Pacific Northwest National Laboratory, personal communication.

7. A. G. Maki, J. S. Wells. *Wavenumber Calibration Tables from Heterodyne Frequency Measurements* (version 1.3), [Online] http://physics.nist.gov/wavenum [2004, November 8], National Institute of Standards and Technology, Gaithersburg, MD.

8. E. K. Plyler, E.F. Barker. *Phys. Rev.,* 18, 1551 (1931).

9. P. M. Chu. personal communication.

10. W. J. Barrett, E. B. Dismukes. AD 506023, *Infrared Spectral Studies of Agents and Field Contaminants,* Southern Research Institute, January 1969.

11. N. B. Colthup, L. H. Daly, S. E. Wilberley. *Introduction to Infrared and Raman Spectroscopy,* Academic Press, New York, 1990.

12. L. C. Thomas. *Interpretation of the Infrared Spectra Organophosphorous Compounds,* Heyden & Sons Ltd., London, 1974.

13. R. A. Nyquist. *The Interpretation of Vapor-Phase Infrared Spectra,* Sadtler Research Laboratories, Philadelphia, 1984.

14. B. C. Smith. *Fundamentals of Fourier Transform Infrared Spectroscopy,* CRC Press, Boca Raton, FL, 1996.

15. Patricia B. Coleman, Ed. *Practical Sampling Techniques for Infrared Analysis,* CRC Press, Boca Raton, FL, 1993.

APPENDIX A

MATLAB CODE

Avishai Ben-David
ATTN: AMSRD-ECB-RT-DP
5183 Blackhawk Rd.
Aberdeen Proving Ground, MD 21010-5424
Telephone: 410-436-6631
Email: avishai.bendavid@us.army.mil

run_analyze_vapor_absorption_coeff_offset.m

```
function
[wavel,alfa,d_alfa,R2,offset,d_offset,f_names_used,suspect_fnames,saturated_wavel,w
avel_without_alfa_results]=run_analyze_vapor_absorption_coeff(vapor_name,dir_name
,fnames_to_read,max_error,y_saturation)
% a program to compute vapor absorption coefficients from absorbance measurements
%
%
[wavel,alfa,d_alfa,R2,f_names_used,suspect_fnames,saturated_wavel,wavel_without_a
lfa_results]=run_analyze_vapor_absorption_coeff(vapor_name,dir_name,fnames_to_re
ad,max_error,y_saturation)
%
% INPUT
%
% vapor_name = string  containing vapor name ( e.g., 'dpgme' or 'sf96')
(required)
% dir_name = string containing directory name (e.g., 'D:/All_Avi_part_1/passive_ir')
(required)
%              = []  (default  all files with vapor_name be read from dir_name)
% fnames_to_read = (n,1) cell array with specific n filenames filename.spc to be read
(optional)
%                (default  all files with vapor_name be read from dir_name)
% ********************************************************************************
% the syntax for all *. SPC file_names is :  vapornname_xeyz_i.spc  (e.g.,
dimp_1025em1_5.spc)
%
% i = measurement serial number
% vapornname = ascii characters for the vapornname (e.g., sf6 , dimmp )
%
% The CL value (ppm-m) is coded in the field : xeyz
```

```
% where:  CL = x*10^(z)   for y = p
%        CL = x*10^(-z)  for y = m
% the number of digits of x or z is arbitrary (e.g., can be xxxeyz or xxeyzz or xxxxxxeyz)
% Examples: xxxxeyz=0081em1  CL=0081E-1=8.1  ;  xxxxeyz=0081ep1
CL=0081E+1=810
%         xxxxeyz=8081em3  CL=8081E-3=8.081  ;  xxxxeyz=0781ep2
CL=0781E+2=78100
% ********************************************************************************************
% max_error = (1,1), 0 < max_error < 1 , allowable error between
(optional)
%            the normalized peak value by concentration of all measured absorbance
spectra
%           (i.e., max(absorbance)/CL) spectra. (default: max_error=0.05 i.e., a 3 percent
error)
%            max_error is not used if there is saturation in the absorbance spectra.
% y_saturation = (1,1) saturation value of the absorbance measurements
(optional)
%             (i.e., saturation value for optical depth) default=0.05
%
% OUTPUT
%
% wavel = (L,1) vector wavenumber (1/cm)
% alfa = (L,1), alfa(wavel), absorption coefficient [1/(ppm-m)] as a function of
wavenumber
%             alfa(wavel) can be computed for a minimum of two valid absorbances
(optical depth values).
% d_alfa = (L,1) error in alfa [1/(ppm-m)]
%         Note: d_alfa(wavel) can be computed only if there are at least three valid
absorbances.
%         Thus, if the number of absorbances (optical depth values) is 2 for a specific
wavel
%              then d_alfa(wavel)=nan for that specific wavel
%              whereas alfa(wavlel) and R2(wavel) are computed correctly
% R2 = (L,1) the computed coeficcient of determination R^2 value for each wavel
% offset = (L,1) [absorbance units] the (intercept) offset(wavel) of the least-squares
regression (b(:,1) in linear_regression.m)
%       = we expect it to be zero  (note the units of offset is optical depth (i.e.,
absorbance units)
%         (i.e.,the regression line of absorbance-vs-CL cross the zero for CL=0)
% d_offset = (L,1) [absorbance units] the error in offset as a function of wavel
% f_names_used = (k,1) cell array of file names that were were processed
%              k < n
% suspect_fnames = (j,1) cell array files that were excluded (i.e., were not used).
%                suspected to be incorrect in the recorded CL value in file name
%              = 'none' if all files were processed
```

```
% saturated_wavel = a column vector with the wavel that were saturated (i.e.
absorbance>y_saturation)
%                 = 'none' if no saturation was found
% wavel_without_alfa_results = a column vector with the wavel for which there were no
good
%                         (i.e., at least) two absorbance value (e.g., not saturated)
%                          and thus there  no results for alfa for these wavelengths
%                         The user is encouraged to do more measurements or to
%                         relax the input parameters max_error and/or y_saturation.
%                        = 'none' if all wavel in absorbance (SPC files) werre processed
successfully
%
% DEFAULTS:
%
% fnames_to_read=[] : all fname with vapor_name will be read from dir_name
% dir_name=[] current director (dir_name=pwd)
% max_error=[] : max_error=0.05;
% y_saturation=[] : y_saturation=1 ;
%
% Notes:
%
% The check for max_error is affected by outliers: thus to get 2% error, I suggest to set
max_error=0.05
% You can put [] for any of the optional input values
%
% Examples
%
%
[wavel,alfa,d_alfa,R2,offset,d_offset,f_names_used,suspect_fnames,saturated_wavel,w
avel_without_alfa_results]=run_analyze_vapor_absorption_coeff('dpgme','D:\Barry_data
\vapor');
%
[wavel,alfa,d_alfa,R2,offset,d_offset,f_names_used,suspect_fnames,saturated_wavel,w
avel_without_alfa_results]=run_analyze_vapor_absorption_coeff('benzene','D:\Barry_da
ta\vapor');
%
[wavel,alfa,d_alfa,R2,offset,d_offset]=run_analyze_vapor_absorption_coeff('benzene','D
:\Barry_data\vapor',[],0.03,1.5);
%
[wavel,alfa,d_alfa,R2]=run_analyze_analyze_vapor_absorption_coeff('benzene','D:\Barr
y_data\vapor',[],0.03,1.2);
%
[wavel,alfa,d_alfa,R2,offset,d_offset]=run_analyze_vapor_absorption_coeff('dpgme','D:\
Barry_data\vapor',[],[],0.9);
% [wavel,alfa,d_alfa,R2]=run_analyze_vapor_absorption_coeff('dpgme',[],[],[],0.9); %
current directory
```

```
%
[wavel,alfa,d_alfa,R2,f_names_used,suspect_fnames,saturated_wavel,wavel_without_a
lfa_results]=run_analyze_vapor_absorption_coeff('dpgme');
%
% Avishai Ben-David 7/26/04
%

%  running the p code analyze_vapor_absorption_coeff.p
if ~exist('dir_name'),dir_name=[]; end
if ~exist('y_saturation'),y_saturation=[]; end
if ~exist('max_error'),max_error=[]; end
if ~exist('fnames_to_read'),fnames_to_read=[]; end
[wavel,alfa,d_alfa,R2,offset,d_offset,f_names_used,suspect_fnames,saturated_wavel,w
avel_without_alfa_results]=analyze_vapor_absorption_coeff(vapor_name,dir_name,fna
mes_to_read,max_error,y_saturation);
```

APPENDIX B

DISCUSSION OF SOME UNCERTAINTIES OBSERVED IN FTIR ANALYSIS OF POTASSIUM BROMIDE PELLETS OF MICROBIAL SPORES

1. ABSTRACT

A series of KBr pellets were prepared quantitatively from samples of bacillus atrophaeus (also known as bacillus globigii, BG), subsequently analyzed by FTIR, and the absorptivity coefficients were calculated. Possible causes of spreads in the data from KBr pellets and the baseline correction routine are discussed.

2. INTRODUCTION

As compared with other quantitative FTIR techniques tested in the laboratory, such as variable path liquid cells and gas cell, the data from the KBr pellet experiments with biological materials showed significant scattering. Pellets were prepared from three variants, BG-DAN-01, BG-BF-01, and BG-DAN-04. In the case of the first two variants, data from three pellets of the fifteen total prepared in each case were discarded before computing the final absorptivity coefficients. Thereafter, typical relative uncertainties in the plots were about 2-10% of the coefficient in regions where absorption bands were present.

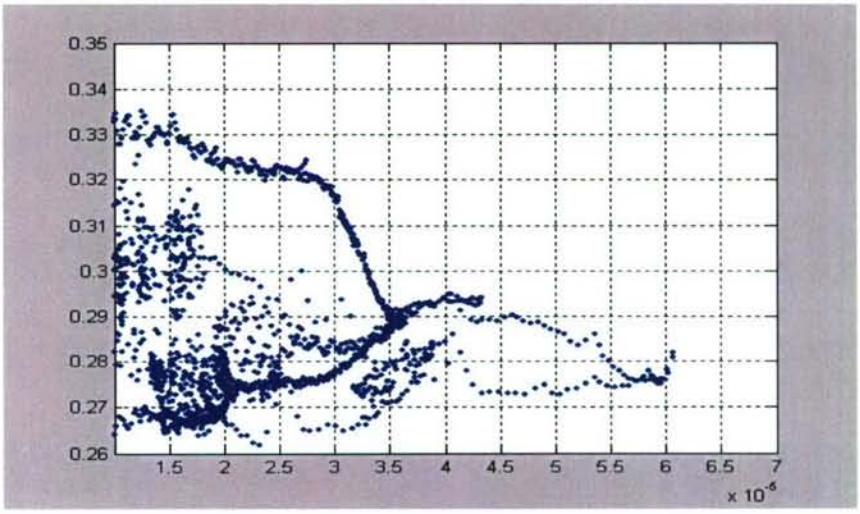

Figure 1. Relative Standard Deviation (2σ) Versus Absorptivity Coefficient of Data Obtained with KBr Pellets Prepared from BG-DAN-04

The analysis of data from the initial series of 15 pellets prepared from BG-DAN-04 demonstrated poor statistical fits even as compared with the prior two sets of spores. In particular, this can be observed in the plot of the relative standard uncertainty (type A, 2σ) of the absorptivity coefficient (Figure 1), which ranged from approximately 26-33% for coefficients >1X10^{-5} m²/mg. Much of the reason for the problems appeared to arise from a spread in the data at the mid and higher concentrations. This can be observed

when the data from the bands at 1655 and 1110 cm^{-1} are plotted manually (Figure 2). By selectively rejecting the data from different combinations of three pellets at approximately 3000 and 7000 mg/m^2, the estimated alpha value (absorptivity coefficient) of the 1655 cm^{-1} line varies between 0.00006 and 0.0001 m^2/mg. The poor statistical fits noted in Figure 1 resulted, by the way, even after removing data from three pellets and calculating the absorptivity coefficients with the remaining twelve.

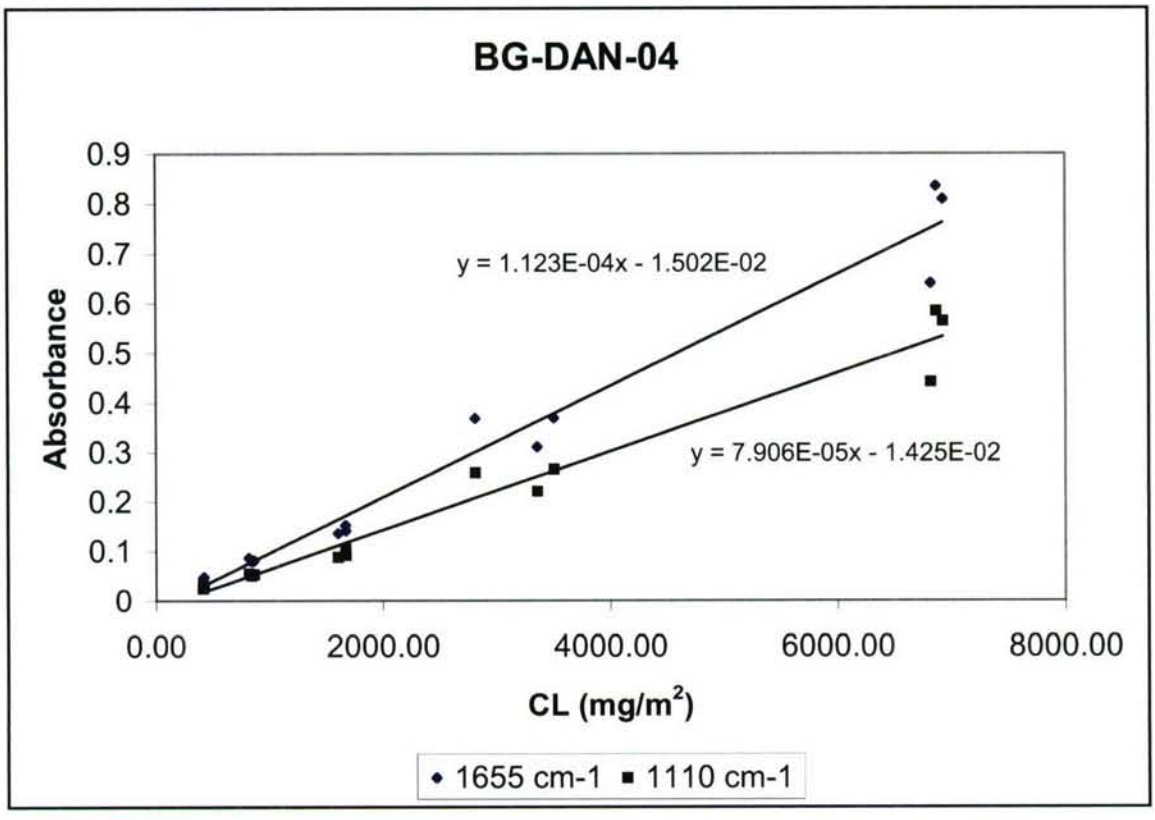

Figure 2. Beer's Law Plot of Initial Data Acquired from KBr Pellets of BG-DAN-04

The decision was made to prepare additional pellets at higher concentrations in an attempt to better estimate the absorptivity coefficients of the material.

3. PREPARATION OF PELLETS AND BASELINE CORRECTIONS

We have steadily added to the equipment available in the laboratory since the preparation of the first pellets. Noteworthy acquisitions are the Carver hydraulic press, purged glovebox, Mitutoyo digital comparator, and Retsch grinder/mixer. This has allowed us to standardize and refine the technique, which is in the process of being published as a standard laboratory protocol.

In general, KBr that has been finely ground and dried for several hours is added to a weighed and tared sample of the material to be investigated in 4-7 mL screw cap vials. From this stock material, serial dilutions are prepared as necessary to obtain the

desired concentrations. Because of their higher relative concentrations, the newer set of eight pellets from BG-DAN-04 were prepared without serial dilution. Approximately 225 mg aliquots of the final dilution are then pressed for several minutes in an evacuated 13-mm die at 9000 PSI. The techniques are addressed in more detail in Section 7.2 of the main report.

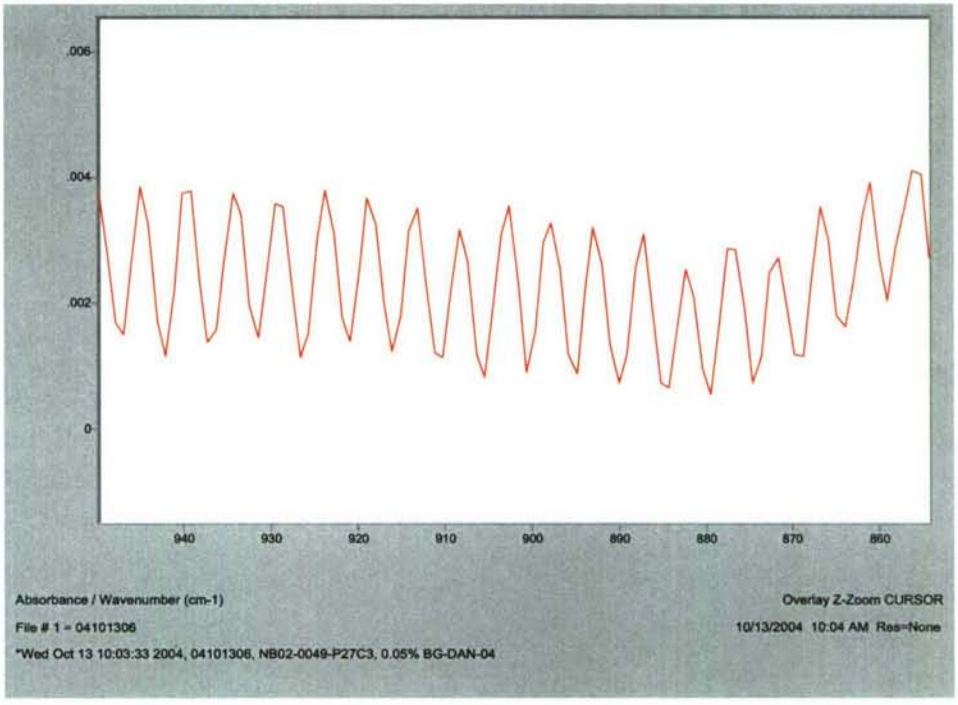

Figure 3. KBr Pellet Prepared From BG Showing Interference Fringes

Making reproducible KBr pellets is not trivial. Among the factors influencing the quality of a pellet are the size of the particles in the sample, sample moisture, environmental humidity and temperature, pellet mass, and force used to press the pellet. For quantitative purposes, pellet masses and thicknesses should be kept as uniform as practicable.

An ideal pellet should also be nearly transparent. The latter factor may, however, in some cases become a disadvantage. Because a very smooth, transparent pellet may also have highly specular properties, this may result in interference fringes when the spectrum of the pellet is taken. To minimize such effects, we have rotated the solid sample accessory, normally with the sample plane at 90° with respect to the infrared beam, to an angle of approximately 88.5°. Nevertheless, interference fringes are still sometimes observed, as can be seen in figure 3. Because of the large number of factors that can affect the properties of a KBr pellet, it is extremely difficult to isolate and investigate them individually.

Despite our best efforts, small differences in pellet densities, masses, and thicknesses, as well as differences in scattering properties, resulted in baseline shifts

among pellets (Figure 4). Before using the spectra in calculations, they are subjected to a baseline correction routine, using a straight line drawn through two nonabsorbing points in the vicinity of 3990 and 2260 cm^{-1}. Such a procedure makes at least three

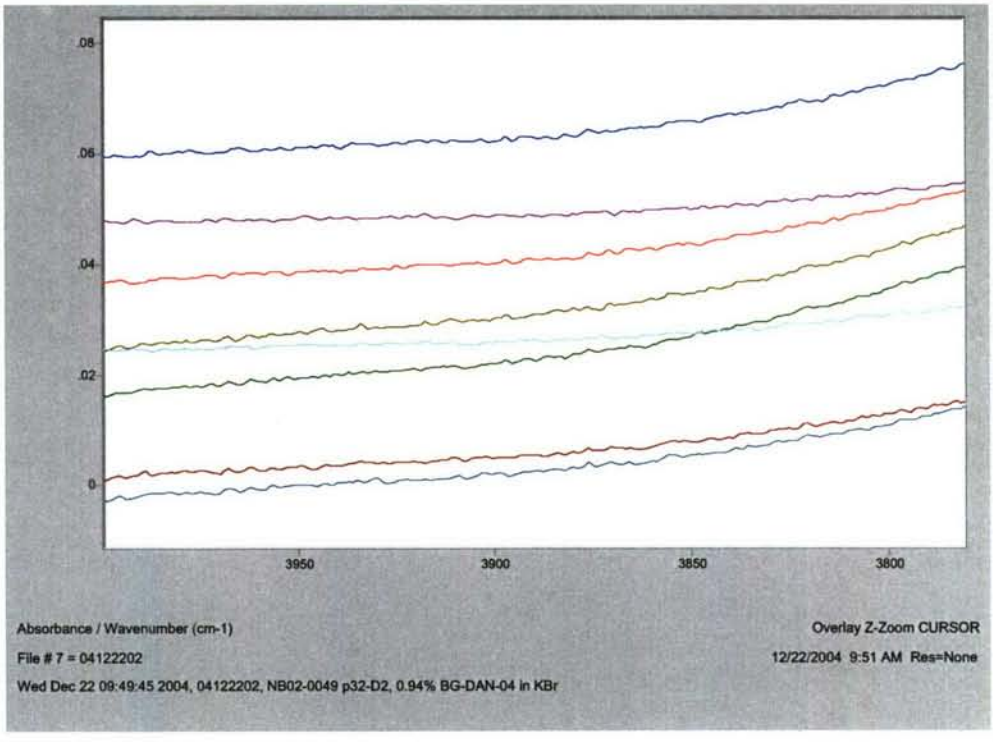

Figure 4. Baseline in Nonabsorbing Region of Spectra Obtained from Eight Blank KBr Pellets

assumptions that can be seen by examining the process in more detail. The baseline correction that was used is a simple mathematical subtraction. Although performed in a semi-automated manner through the instrument software, in principle the deviation of each point in the uncorrected spectrum from the true can be described by the equation: $y=mx+b$, where y = the shift of the point in absorbance units and x=wavenumber. The slope, m, and intercept, b, in the equation can be calculated by the absorbance at 3990 and 2260 cm^{-1}. Any individual point on the uncorrected spectrum can be described by the equation: $A_1=A_0+y_n$, where A_1 is the observed observance at the wavenumber and A_0 is the "true" absorbance. Each point in the spectrum is then corrected by the equation $A_0=A_1-y_n$, for each wavenumber, x_n, resulting in a spectrum in which y=0 and a spectrum in which A=0 in nonabsorbing regions of the spectrum.

The first assumption in the process, that underlies all baseline corrections to absorbance spectra, is that A and y obey Beer's Law, i.e., exhibit linear behavior. The factors that affect the linearity of an infrared transmission system are numerous and complex, including detector, optical resolution, sample concentration, and scattering properties of the matrix. Although KBr is considered a nonabsorbing medium in the mid-infrared, for example, some attenuation of the energy always occurs through scattering.

The extent to which the combination of these factors obeys Beer's Law is probably beyond the scope of our work, although detector nonlinearity, for example, is well documented within the literature. It may be possible to investigate this effect in the Nexus instrument, at least partially. A second assumption is that the shifts in the baseline can be described by a straight line, as opposed to a more complex equation. Because of the broad absorbances within the spectra involved in this study, and the

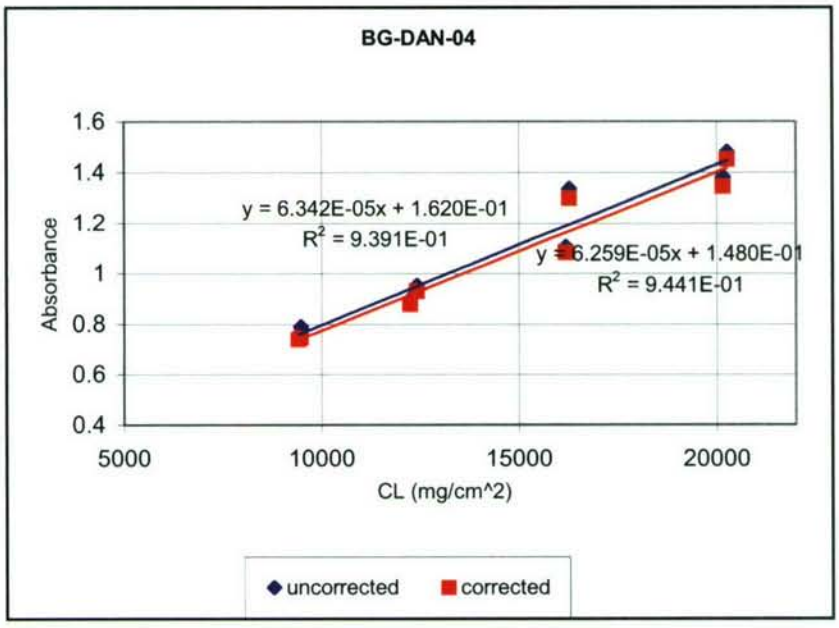

Figure 5. Effect of Baseline Correction on Linearity of Data in Beer's Law Plot of KBr Pellets from BG-DAN-04

relative lack of nonabsorbing spectral regions, it may not be possible to test the validity of this assumption using pellets prepared from BG spores.

We did, however, investigate the baseline correction routine in an indirect way using data from blank KBr pellets. The first single beam spectrum of a blank pellet was ratioed with the other single beam spectra of blank pellets analyzed on each day that data was collected to produce a total of 14 absorbance spectra. After the baseline correction routine was performed on the spectra, the mean absorbance and standard deviation were calculated in two regions: 550-2000 cm^{-1} and 2400-4000 cm^{-1}. The data showed a mean absorbance within the lower wavenumber region of –0.00388, with a standard deviation of 0.0063. The mean absorbances of the individual spectra within the region ranged from –0.004 to 0.021. For the higher wavenumber region, the corresponding mean and standard deviation were 0.00016 and 0.00085 respectively. Two caveats apply to this interpretation of the results. First, the spectra from the BG containing pellets were ratioed against the blank pellet that appeared to give the best results. This implies that the difference in the two methods of data handling may have skewed the above analysis to reflect a higher degree of baseline uncertainty than actually existed in the spectra of the BG containing pellets. Second, because of possible differences in particle sizes, refractive indices, and other scattering properties

of the BG spores, the variations in the spectra of the blank pellets may not accurately reflect those of the sample pellets. Neverthless, these numbers may reflect the best currently available quantitative measure of baseline uncertainty in these analyses.

In the absence of a complex set of experiments to attempt to identify and quantify the factors affecting the baseline in the KBr pellet experiments, perhaps the easiest test of the validity of the baseline correction is its effect on the linearity of the data. This can be seen in Figure 5, the Beer's Law plots at 1655 cm^{-1} of the eight pellets at the highest concentrations. Applying baseline corrections to the data improves the r^2 value of the least squares fit from 0.939 to 0.944. Although not investigated in a rigorously quantitative way, none of the data for either this set of BG spores, nor that of the previous data sets, appears to show any association between the concentration and the magnitude of the baseline shift. This implies that at any y value of baseline shift, the effect on the linearity of the data is greater as A approaches zero, i.e., weaker bands or lower concentrations. An additional implication is that any residual deviation from a "true" baseline will have a greater effect on the linearity of the data at lower concentrations or smaller absorbances. Assuming that this is correct, the inclusions of samples at the highest possible concentrations, without exceeding the linear range of the detector, should improve the fit of the data.

4. CALCULATION OF ABSORPTIVITY COEFFICIENTS

Absorptivity coefficients (alpha values) were calculated using run_analyze_vapor_absorption_coeff.m, a MatLab script file originally written by Dr. Avi Ben-David to do the calculations of the vapor-phase absorptivity coefficients. The script was modified in July 2004 to include a calculation of the intercept of each alpha value. In a well-behaved system in which $A=\alpha CL$, the measured absorbance is proportional to the concentration-pathlength product (CL) and the absorptivity coefficient (α). In order to determine the absorptivity coefficient, samples are measured at a range of concentration-pathlengths, and least squares calculations are performed wavelength by wavelength to solve for $\alpha=A/CL$. This equation assumes a zero intercept, i.e., a concentration-pathlength of zero results in an absorbance of zero. If a nonzero intercept is obtained during least squares fitting of the line to obtain the alpha value, this could imply a condition in which $A=\alpha CL+k$, but in a single component system such as that involved in the database work, such a case seems unlikely. The implication of a nonzero intercept in the equation in this case is more likely that there are problems with the sample preparation or analysis technique, the data points are scattered, making an accurate determination of the intercept difficult, or that data beyond the linear range of the detector has been included. This was the reason for requesting that Dr. Ben-David modify the algorithm to include calculations of the intercepts.

The script includes a user definable parameter (y_saturation) to specify the maximum absorbance (A_{max}) of data points that are used in calculating the absorptivity coefficient and standard deviation, with a default setting 1.0. Because a mercury-cadmium-telluride (MCT) detector, used in most of the experiments in our laboratory, has a smaller linear dynamic range than other slower detectors, determining an optimal

setting can be important. As A_{max} increases, more data points are included in the calculation of the alpha value, potentially decreasing the standard deviation but with the risk of including data beyond the detector linear range and resulting in a nonzero y-intercept. In the case of the vapor-phase work, with relatively well fitted data points, it is more apparent when this has occurred. With the scattering of the data from the KBr pellets, such a situation can be more difficult to ascertain.

5. EFFECTS OF CHANGES IN MAXIMUM ABSORBANCE

Absorptivity coefficients, standard deviations (2σ, 95% confidence), and intercepts were calculated for BG-DAN-04 with parameters that included first all data points with maximum absorbances (A_{max}) of 1.0 (default), and then repeated with maximum absorbances of 1.1, 1.2, and 1.3. Figures 6-9 are the calculated absorptivity coefficients (blue) and standard deviations (2σ in red).

For the most part, the inclusion of the higher absorbances produced only small changes in either the calculated absorptivity coefficients or the standard deviations. This is to be expected, since the increase in A_{max} incorporates data only from the centers of the two most intense bands at the four highest concentrations. An A_{max} of 1.0 results in a calculated absorptivity coefficient for the 1655 cm^{-1} band of 0.00007037 m^2/mg. With an A_{max} of 1.3, a coefficient of 0.00007093 is returned—an increase of 0.8%. The mean statistical uncertainty of the absorptivity coefficient spectrum as a whole decreases from $1.28X10^{-6}$ at A_{max}=1.0 to $1.22X10^{-6}$ at A_{max}=1.3. It is also worth noting that at A_{max}=1.3, the calculated absorptivity at 1655 cm^{-1}, including the uncertainty, is 0.000065-0.000077 m^2/mg, readily incorporating the data from all four iterations.

Most noticeable by visual inspection are small changes in the appearance of what appear to be poorly resolved narrow peaks along the shoulders of the two most intense bands in the absorptivity coefficients. These are most likely discontinuities that occur as a result of the small changes in the calculated absorptivity coefficients as data with increasingly greater absorbances are included within the bands. All of the spectra include data along the sides of the bands with absorbances less than the specified maximum value, and most of the spectra have only data<A_{max}. Therefore, even in the case of very intense peaks, at least some of the data along the shoulders of the bands will be included, increasing the number of data points that are rolled into the calculations along the shoulders of these peaks as A_{max} increases.

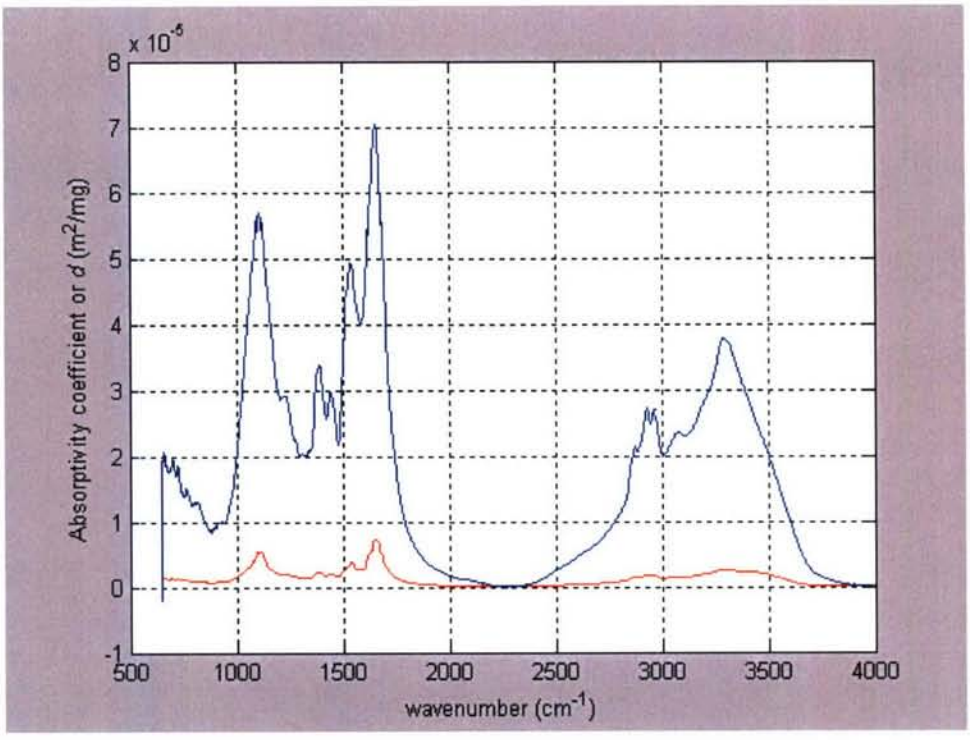

Figure 6. Absorptivity Coefficient (blue) and Standard Deviation (2σ) (red) at A_{max}=1.0

Figure 10 is a plot of the fractional uncertainty of the data for which α>0.00001 m²/g, incorporating nearly all of the absorption peaks within the spectrum. The uncertainty plot incorporates all data points with A_{max}=1.3. The data show an overall reduction in the standard deviation of approximately 75% versus figure 1. The new calculated uncertainties for BG-DAN-04 are, therefore, much more similar in magnitude to those observed for the previous two sets of spores, and these data are cited in the main body of the report.

In any case, it is worth noting that the major changes in the quality of the data occurred not because of increasing A_{max}, but rather as a result of incorporating additional data of higher quality. In fact, the data had previously included spectra with maximum absorbances of approximately 0.9, close to the default setting for y_saturation. The poor statistical fits occurred primarily because the older data points at the higher concentrations were scattered. Although including new data at higher concentrations had a positive statistical effect, this was probably not the only cause of the improvement.

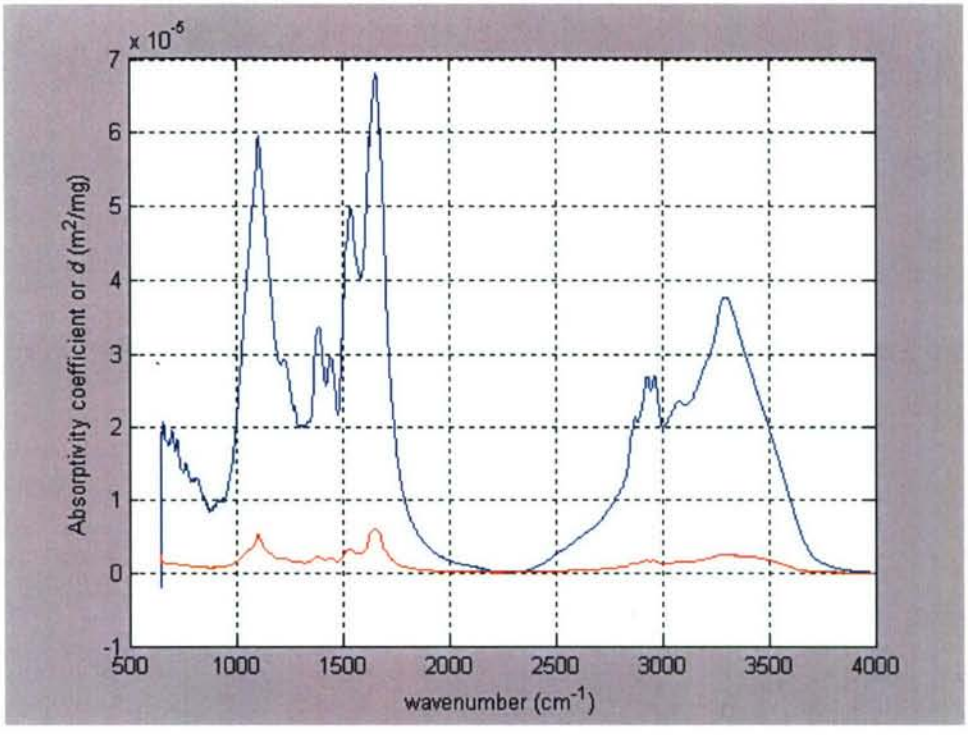

Figure 7. Absorptivity Coefficient (blue) and Standard Deviation (2σ) (red) at A_{max}=1.1 from BG-DAN-04

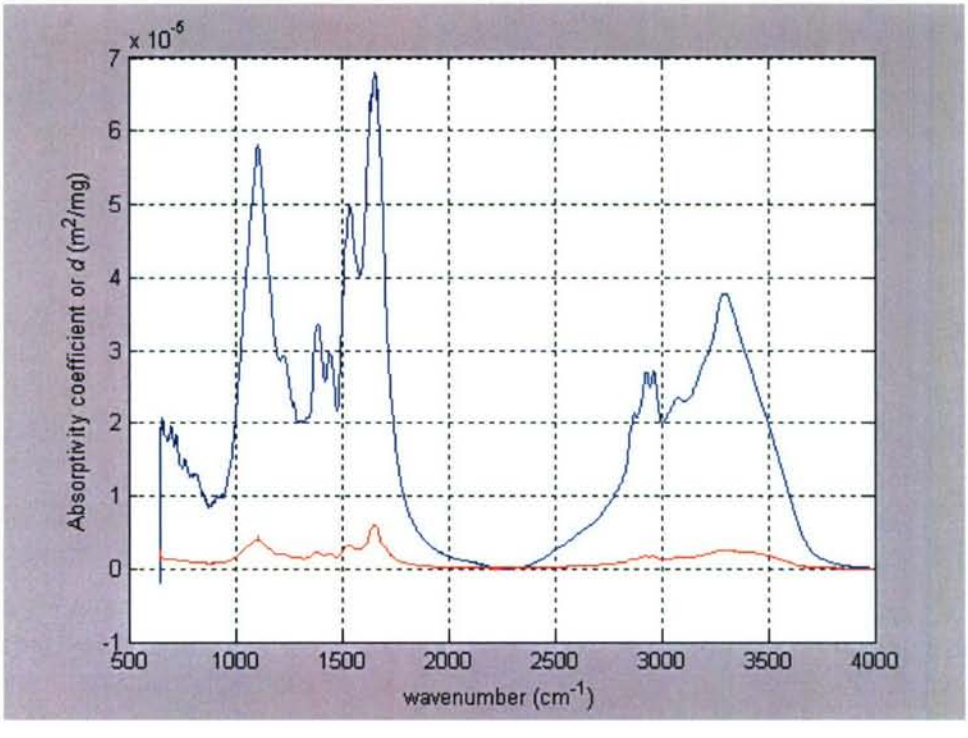

Figure 8. Absorptivity Coefficient (blue) and Standard Deviation (2σ) (red) at A_{max}=1.2 from BG-DAN-04

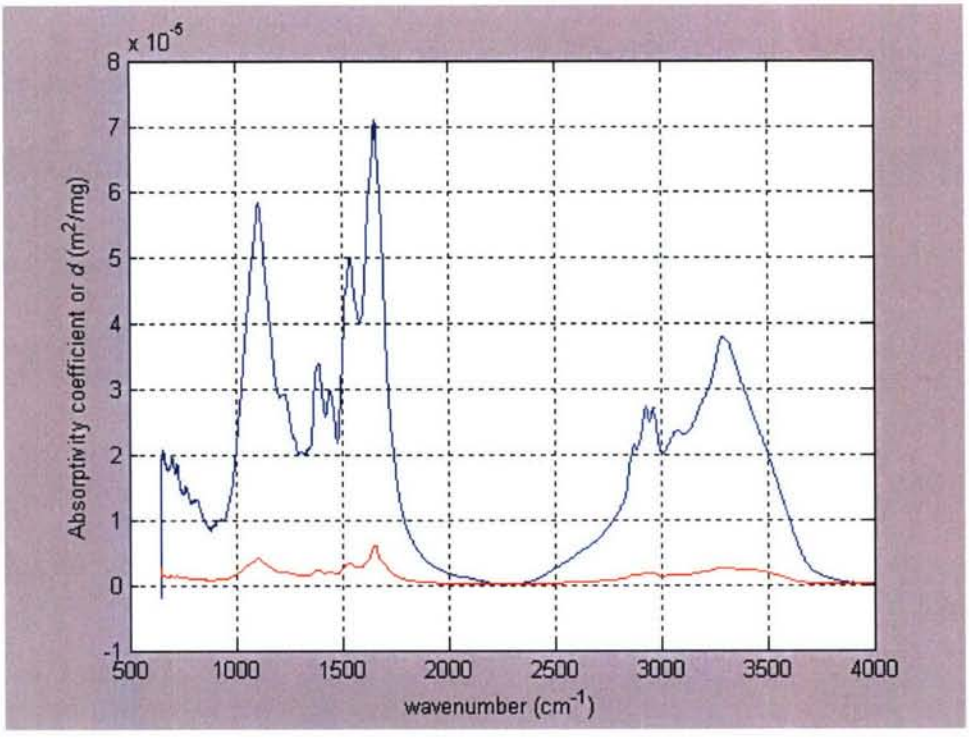

Figure 9. Absorptivity Coefficient (blue) and Standard Deviation (2σ) (red) at A_{max}=1.3 from BG-DAN-04

An analysis of the changes in the y-intercepts of the calculated absorptivity coefficients after incorporating the newer data was also made. Because of the previously noted negative effect of incorporating data taken at absorbances greater than 1, the mean y-intercepts were computed at each incremental increase in A_{max} from 1.0 to 1.3. The increase in the parameter did not result in a significant deterioration of the data and appeared to have improved it slightly. At A_{max}=1.0 the mean was equal to 0.00467, and at A_{max}=1.3, the mean was 0.00463. In comparison to a mean y-intercept for the old data of 0.0107, the additional spectra incorporated into the most recent data set would appear to have improved this statistical measure significantly as well. It is not necessarily clear, however, that such an assertion would be valid. At least part of the reason for the reduction in the intercept resulted from an apparent negative shift in the region below 2000 cm^{-1}, as a result of which, regions with absorptivities less than approximately 0.00002 m^2/mg show intercepts centered around 0.005. Nevertheless, the relative size of the area under this region does appear to have been reduced as a result of incorporating the new data. The region above 2000 cm^{-1} was affected much less.

Because the baseline correction of the raw spectra is performed with points incorporating only the region above 2000 cm^{-1}, the difference in results within the two regions is not necessarily surprising and may reflect the fact that the assumption of a straight line function in the baseline shift within the spectra may not reflect the actual behavior of the data.

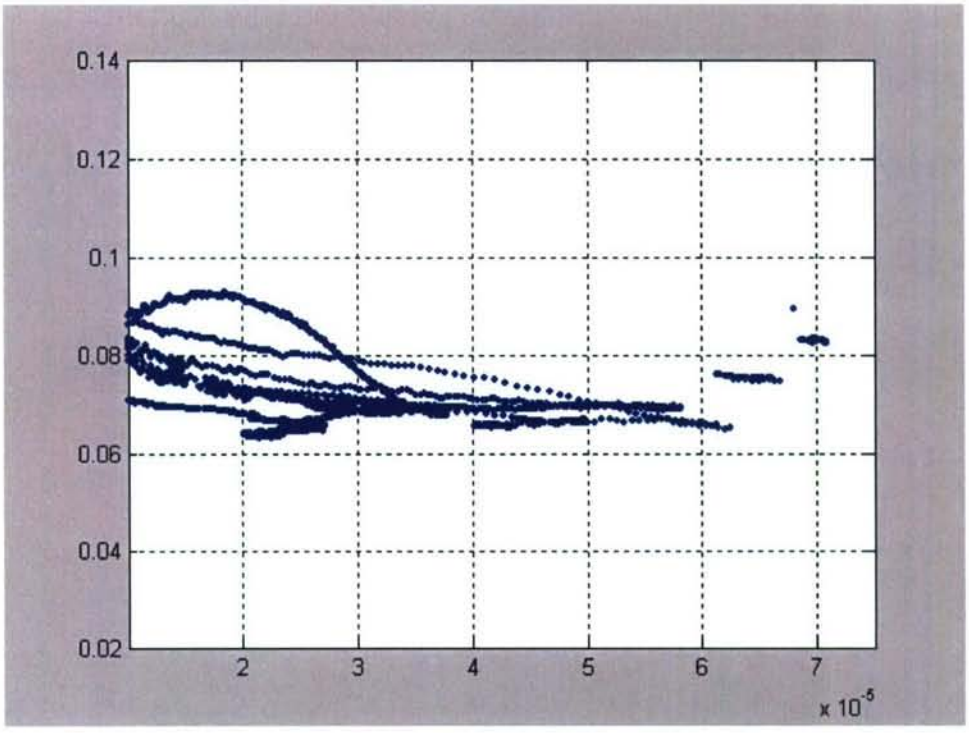

Figure 10. Fractional Uncertainties (2δ) of the Absorptivity Coefficient (A_{max}=1.3) from BG-DAN-04

An additional interesting observation is that the calculations from two of three sets of spores thus far do, in fact, demonstrate clear positive y-intercepts, although the remaining set is somewhat ambiguous. This occurs even in the very broad band within the region above 3000 cm^{-1} where the baseline corrections should be most effective. It is possibly useful to consider this phenomenon in conjunction with other apparent anomalies. The y-intercepts in the C-H stretching region in the vicinity of 2900 cm^{-1} are actually quite small, relative to the size of their absorptivities as compared to the region above 3000 cm^{-1}. Near 1650 cm^{-1}, the absorptivity coefficient and standard deviation show discontinuities, and the y-intercepts in this region actually demonstrate what appears to be a derivative-type feature on the low wavelength side of the strong absorption feature. The regions involved include the areas of the spectrum with absorption bands that would result from adsorbed water, and this may account for at least part of the anomalies. Plots of the y-intercepts derived from the older data are in Figure 11, with the more recent analysis in Figure 12.

Another possible explanation for persistent presence of nonzero y-intercepts in the data plots may be the presence of Christiansen effect in the spectra. This effect, which can decrease transmission within absorption bands, accompanied by increased transmission in the spectral regions adjacent to the absorption bands, should be studied in a more theoretical way. This explanation is especially intriguing because of the possibility that it could account for the derivative-like y-intercepts adjacent to absorption features.

It may be possible, at least partially, to estimate the type B uncertainty contributed by baseline effects by acquiring data from a series of blank KBr pellets, converting to absorbance spectra, performing baseline corrections, and determining residuals. In the case of the additional type B uncertainty arising from the y-intercepts, it may be possible to gain a sense of the contribution by adding an additional calculation to the MatLab algorithm to perform the standard mathematical procedure to calculate the statistical uncertainty of that parameter.

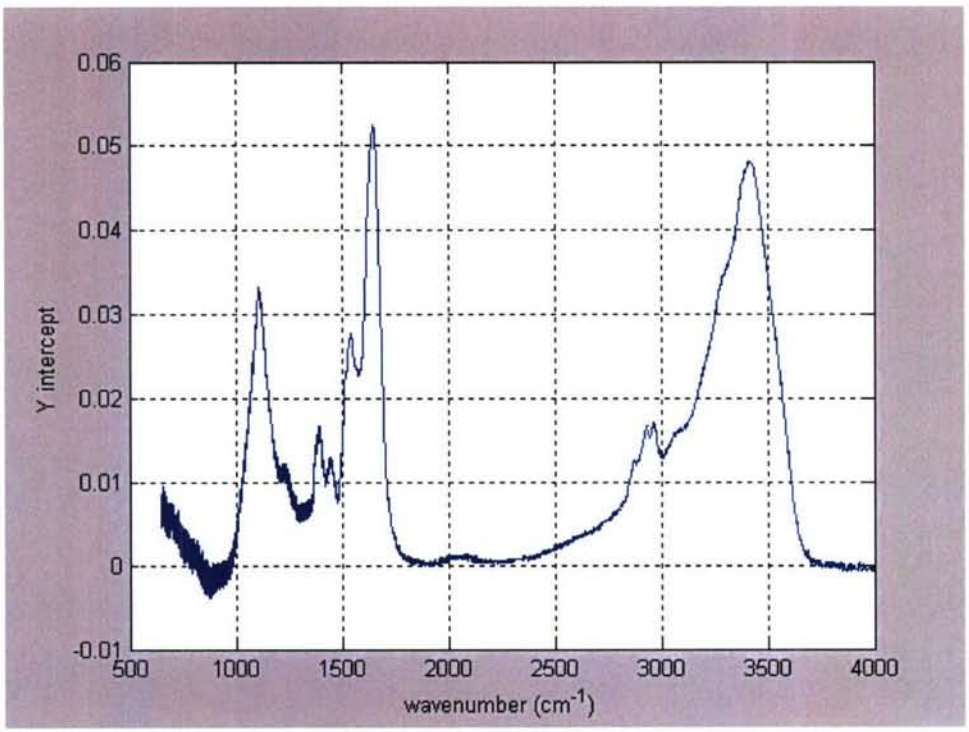

Figure 11. Y-intercepts of Absorptivity Coefficients from Early Data (BG-DAN-04)

Table 1 is a tabulation of the statistical data. A summary of data used to calculate the concentration-pathlengths for BG-DAN-04 is presented in Table 2.

6. Mass uncertainty

We investigated the possibility that errors in the serial dilution technique used to prepare the powdered samples from which the pellets were made contributed in a significant way to the scattering of the data when plotted and the presence of outliers. This potential problem is most easily visualized using artificial data.

Figure 12 combines plots derived from the data in Table 3. All plots assume that the FTIR is free from measurement errors, i.e., the measured absorbance is an accurate representation of the ratio of the transmitted energy. These plots further assume that the sample does not scatter. The absorptivity coefficient at the measured wavelength is 0.032 in arbitrary units.

6.1 Plot of "True" Data

The plot in black is based upon the "true" concentration-pathlengths—again in arbitrary units and (column 2 of Table 3). In such an ideal case, of course, the statistical fit is perfect and the y-intercept is essentially 0. (The very small deviation from 0 that is displayed is presumably within the finite precision of the computer software.)

The discussion of the remaining two plots is by necessity considerably more complex.

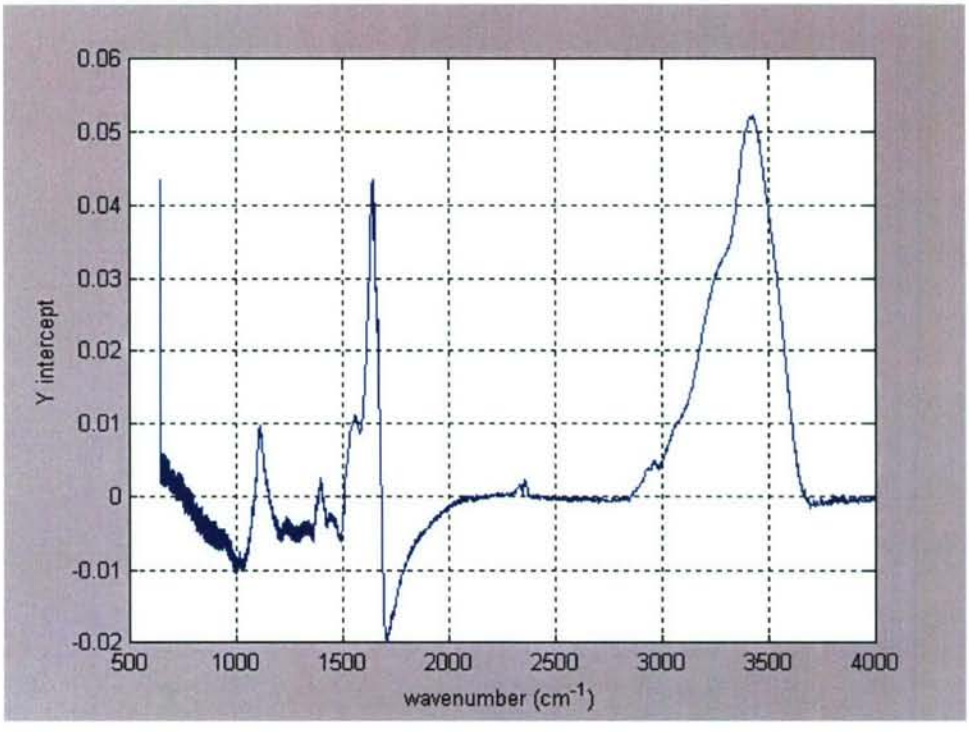

Figure 12. Y-intercepts of Absorptivity Coefficients from BG-DAN-04 After Incorporating Newer Data

Table 1. Summary of Statistical Data Obtained as a Result of Calculations of Absorptivity Coefficients from KBr Pellets of BG-DAN-04

A_{max}	α at 1655 cm^{-1} (m^2/mg)**	Mean Std Dev (2σ)	Mean Y-intercept
"old"*	0.0000607(±0.0000171)+0.052	0.00000386	0.0107
1.0	0.0000704(±0.0000072)+0.036	0.00000128	0.0047
1.1	0.0000680(±0.0000061)+0.042	0.00000125	0.0047
1.2	0.0000680(±0.0000061)+0.042	0.00000124	0.0047
1.3	0.0000709(±0.0000060)+0.034	0.00000123	0.0046

*All data points in earlier data set of BG-DAN-04 had absorbances <1
**In the form of m(±2σ)+b

6.2 Plot of Data Incorporating Bias in Mass Measurements

The plot in blue (column 1 of Table 3) was assumed to have been based upon samples prepared from a single stock solution using serial dilutions, with two pellets having been prepared at each dilution level. The samples were assumed to be homogeneous. An additional assumption was made that during the weighing of the aliquots of analyte (BG) and KBr, the balance was biased to display masses in the range of the analyte that were less that the actual mass and that this bias was greater at lower masses. This could occur, for example, if the analytical balance had a nonzero intercept in its response and an additional bias arising from a nonlinear response. Table 4 illustrates the result of such an error, which will be explained below.

Similar to most measurement instruments, a simplified description of the response of a balance can be obtained with a graph of true versus measured values.* Although manufacturers like to achieve a one-for-one response from a product (i.e., perfect accuracy), this is, of course, never obtained. A desirable compromise is to achieve a product in which the response can be fitted to a line in which y=mx+b, where y is the true value, and x is the measured response for the quantity (and m approaches 1, with b approaching 0). In such a case, as errors accumulate over time and m and b deviate from 1 and 0 respectively, adjustments can be made during calibration to improve the accuracy of the instrument. This is the principle behind the "zero" and "span" on many gas mass flowmeters. The "zero" button or screw serves to adjust the "b" or zero intercept, and the "span" is used to adjust "m" (the slope). Autocalibration features on many electronic analytical balances function similarly, using a standard mass that can be swung into position beneath the balance pan to establish a response slope. In practice, even such a compromise is rarely obtained and instrument response typically follows a more complex polynomial. This is the basis of the inclusion of a

* Although a more complete mathematical description normally also encompasses precision (repeatability), it is useful for this discussion to ignore that issue.

linearity parameter in the accuracy specifications of much analytical equipment. It is also, at least in part, the basis of the higher accuracies of the 5850S Series gas mass flow controllers that we have recently obtained from Brooks. During calibration, which must be done by computer software, the response of the flow controller is fitted to a second order polynomial of type $y=ax^2+bx+c$.

Column 1 of Table 3 and column 2 of Table 4 illustrate the effect on the measured mass (and concentration-pathlength) of measurements made with an analytical balance with a slightly nonlinear response and a zero intercept less than zero ($b<0$). The effect also produces a positive intercept when the resulting spectra are used to calculate absorptivity coefficients, as shown by the blue line in Figure 13. Mass measurements made with a balance having a positive y intercept in its response will produce a negative intercept when used to measure absorptivity coefficients by the pellet method. Also illustrated in the plot is the effect of nonlinearity in the mass measurements, resulting in clusters of data points that do not fit well with a straight line function but show little scattering relative to each other.

Table 2. Physical Measurements of KBr Pellets Prepared from BG-DAN-04 and File Names

Pellet ID NB 02-0049	Omnic file	Grams file	MatLab file	Average Mass (g)	BG (mg)	Radius (cm)	Average Thickness (cm)	Volume (m^3)	CL (mg/m^2)	Density (g/cm^3)
P27B Rep 1	04101301.spa	04101301.spc	bgdan04_42659em2_1	0.22911	0.0562	0.6475	0.0674	8.883E-08	426.59	2.58
Rep 2	04101302.spa	04101302.spc	bgdan04_41837em2_1	0.22470	0.0551	0.6475	0.0677	8.912E-08	418.37	2.52
Rep 3	04101303.spa	04101303.spc	bgdan04_4156em1_1	0.22321	0.0547	0.6475	0.0707	9.317E-08	415.60	2.40
P27C Rep 1	04101304.spa	04101304.spc	bgdan04_82053em2_1	0.21837	0.1081	0.6475	0.0662	8.714E-08	820.53	2.51
Rep 2	04101305.spa	04101305.spc	bgdan04_86458em2_1	0.23009	0.1139	0.6475	0.0700	9.223E-08	864.58	2.49
Rep 3	04101306.spa	04101306.spc	bgdan04_8427em1_1	0.22427	0.1110	0.6475	0.0682	8.988E-08	842.70	2.50
P27D Rep 1	04101307.spa	04101307.spc	bgdan04_1604em0_1	0.21716	0.2113	0.6475	0.0675	8.891E-08	1604.02	2.44
Rep 2	04101308.spa	04101308.spc	bgdan04_166897em2_1	0.22595	0.2198	0.6475	0.0693	9.125E-08	1668.97	2.48
Rep 3	04101309.spa	04101309.spc	bgdan04_16735em1_1	0.22656	0.2204	0.6475	0.0676	8.904E-08	1673.47	2.54
P27E Rep 1	04101310.spa	04101310.spc	bgdan04_33608em1_1	0.22505	0.4427	0.6475	0.0682	8.985E-08	3360.76	2.50
Rep 2	04101311.spa	04101311.spc	bgdan04_35113em1_1	0.23480	0.4618	0.6475	0.0710	9.354E-08	3511.33	2.51
Rep 3	04101312.spa	04101312.spc	not used	0.18832	0.3704	0.6475	0.0563	7.413E-08	2812.21	2.54
P27F Rep 1	04101313.spa	04101313.spc	not used	0.23065	0.9041	0.6475	0.0688	9.067E-08	6864.18	2.54
Rep 2	04101314.spa	04101314.spc	not used	0.23264	0.9119	0.6475	0.0704	9.267E-08	6923.30	2.51
Rep 3	04101315.spa	04101315.spc	not used	0.22906	0.8979	0.6475	0.0681	8.972E-08	6816.76	2.55
P31A Rep 1	04122101.spa	04122101.spc	bgdan04_94175em1_1	0.22461	1.2404	0.6475	0.0642	8.453E-08	9417.53	2.66
Rep 2	04122102.spa	04122102.spc	bgdan04_94750em1_1	0.22598	1.2480	0.6475	0.0653	8.601E-08	9474.97	2.63
P31B Rep 1	04122103.spa	04122103.spc	bgdan04_20264em0_1	0.22777	2.6690	0.6475	0.0687	9.051E-08	20263.91	2.52
Rep 2	04122104.spa	04122104.spc	bgdan04_20159em0_1	0.22659	2.6552	0.6475	0.0690	9.086E-08	20158.94	2.49
P31C Rep 1	04122105.spa	04122105.spc	bgdan04_12421em0_1	0.22577	1.6360	0.6475	0.0710	9.354E-08	12420.85	2.41
Rep 2	04122106.spa	04122106.spc	bgdan04_12252em0_1	0.22270	1.6137	0.6475	0.0651	8.575E-08	12251.59	2.60
P32D Rep 1	04122201.spa	04122201.spc	bgdan04_16276em0_1	0.22811	2.1438	0.6475	0.0674	8.877E-08	16276.42	2.57
Rep 2	04122202.spa	04122202.spc	bgdan04_16190em0_1	0.22690	2.1325	0.6475	0.0690	9.088E-08	16190.32	2.50

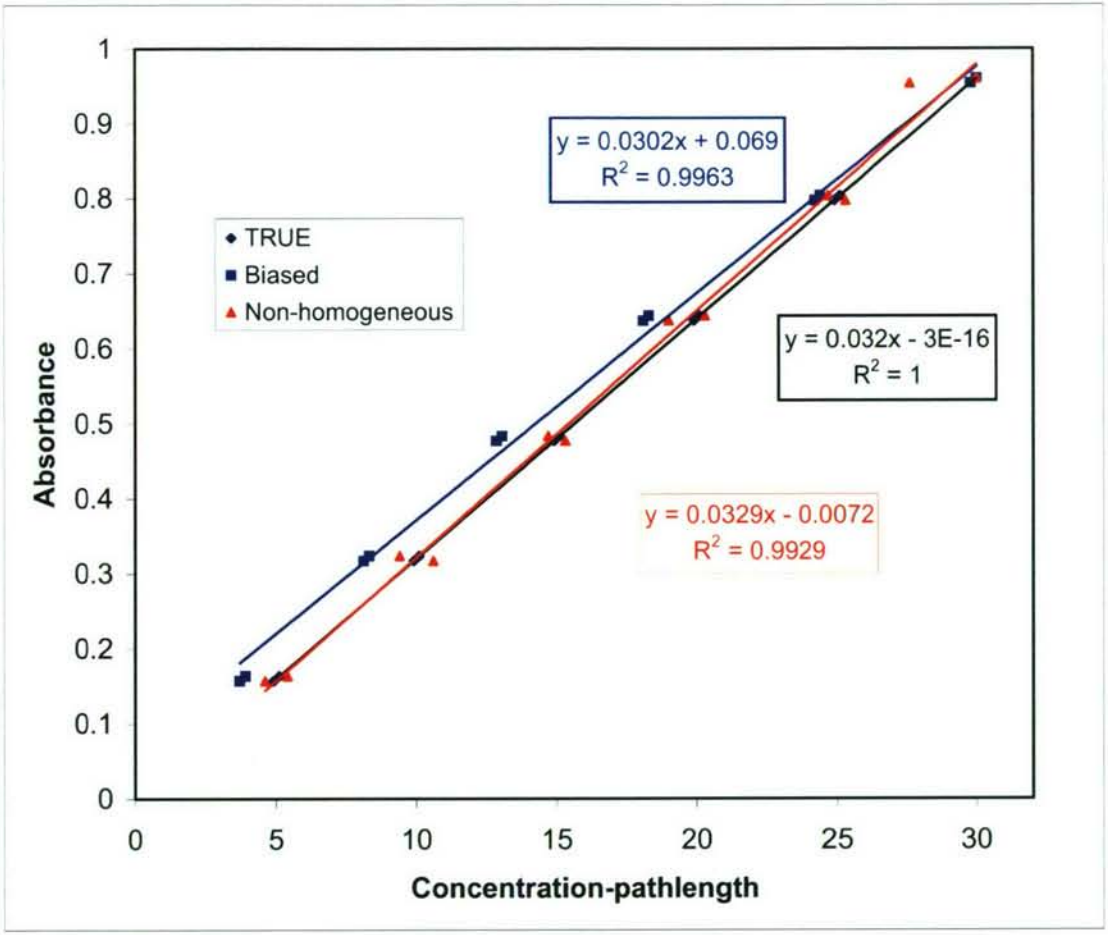

Figure 13. Effects on Response of Bias in Mass Determination During Serial Dilution and Non-homogeneity in Pellets (artificial data)

Table 3. Artificial Data Used to Obtain Plots in Figure 13

Concentration-pathlength			
Biased	True	Non-homogeneous	Absorbance
3.7	4.9	4.6	0.1568
3.9	5.1	5.4	0.1632
8.1	9.9	10.6	0.3168
8.3	10.1	9.4	0.3232
12.85	14.9	15.3	0.4768
13.05	15.1	14.7	0.4832
18.1	19.9	19	0.6368
18.3	20.1	20.3	0.6432
24.2	24.9	25.3	0.7968
24.4	25.1	24.7	0.8032
29.8	29.8	27.6	0.9536
30	30	30	0.96

Table 4. Effect of Nonzero Intercept and Nonlinearity in an Analytical Balance

Actual mass	Measured mass
10	9.20
5	4.10
1	0.09

Two counter-arguments must first be considered before mass measurement issues can be presumed to be responsible for the presence of scattering and outliers in the KBr pellet data. The first, and perhaps most persuasive, in most of the cases three, and never fewer than two pellets have been made from the final diluent. Because, assuming homogeneity, these samples have the same concentration, the plot of the data should tend to form a straight line with a y-intercept approaching zero. This has not been the case with the real world data so far, which clearly has demonstrated a randomly scattered aspect.

The second factor arguing against a serious problem with the measurement of masses from which the samples are made is that the accuracy of the Sartorius balance used in the majority of measurements is better than 1% at the mass ranges in the experiments.[1] The balance is registered in the U.S. Army calibration system and calibrated on-site by the local TMDE unit annually. Additionally, we verify the performance of the instrument with NIST-traceable standard weights at weekly intervals when experiments are ongoing in the laboratory. (Because the Sartorius was temporarily not available at the time, the final set of eight pellets from BG-DAN-04 was prepared using a Mettler Model AT261, although its specifications and procedures are similar to those of the Sartorius.) The stock solution for serial dilutions for the series of the first fifteen pellets was NB 02-0049-27A, using the Sartorius balance, which was used in a single serial dilution step to prepare all of the additional 5 solutions (3 pellets from each solution). This was made by combining 2.02056 g of KBr and 0.00999 g of BG spores. The performance of the balance was verified at several masses <10 g within one day of preparation of the solutions and found to be $\leq \pm 0.00006$ g (2σ). The worst case will be assumed here. The lowest concentration of solution (also the worst case) from which pellets were prepared for BG-DAN-04 was NB 02-0049-27B. This was prepared by diluting 0.05626 g of 27A in 1.07240 g of KBr. The measured mass of pellet NB 02-0049-27B1 was 0.22911 g. Relative combined uncertainty of the mass for the latter solution can be calculated using standard procedures:

$$\text{Unc}=[(0.00006/0.00999)^2+(0.00006/2.02056)^2+(0.00006/0.05626)^2+(0.00006/1.07240)^2 + (0.00006/0.22911)^2]^{1/2} = 0.006$$

It is clear from this example that the initial mass of BG from which 27A was prepared is the dominant factor in the uncertainty calculation. Because this stock solution was used

for the entire initial series of 15 pellets from this variant, the estimated uncertainty for all 15 pellets is essentially the relative uncertainty of the initial mass of the BG, or 0.006.

6.3 Plot of Data Showing Sample Non-Homogeneity

The previous discussion assumed sample homogeneity. A non-homogeneous sample, on the other hand, will have the effect of producing both scattering of data points and a poor statistical fit in the data. The red plot in Figure 13 demonstrates such an effect. This is much more similar to the situation that has been observed in the real world data thus far, and a possible explanation may be found in the following statement: "Since it is extremely difficult to prepare a pellet that exhibits complete homogeneity and has an equal density across, a small beam focus may record the spectrum for a nonrepresentative region of the pellet. In such instances, it is highly recommended that a pellet size that is smaller than the standard 13-mm pellet diameter be used in order to appropriately match the beam size and acquire the spectrum of the whole pellet."[2]

In the absence of detailed engineering specifications for the Thermo-Nicolet 670 spectrometer, an effort was made to estimate the diameter of the collimated beam at the location of the sample. The first method used a card that responds to infrared energy by showing a color change. Several seconds after placing the card in the beam, the size of the spot within the IR sensitive portion of the card was measured with a ruler at approximately 5-mm. An additional estimate was made using measurements of the optical beam path with a ruler. The instrumental parameters during acquisition of data for the KBr pellets specified a diameter for the Jacquinot stop at the source of 2-mm. An assumption was made that at an aperture of 10.7-mm, the maximum setting available, the instrument was designed such that the diameter of the collimated beam would not exceed the 20-mm diameter of the detector window. Based upon a beam divergence from 10.7-mm at the maximum aperture to 20-mm at the detector, a total optical path of 87-cm from the aperture to the detector, and 26-cm from the sample to the detector, the diameter of the beam at the sample could be as wide as 18-mm. This is obviously larger than the standard 13-mm KBr pellet in the experiments. Nevertheless, the ratio of 2:8-mm would indicate a beam diameter of approximately 4 to 5-mm at the smaller aperture setting, consistent with the rough approximation obtained with the card. Regardless of whether either of the above approaches represents a rigorous method of measuring the collimated beam impacting upon the sample, the key point to note is that the diameter was probably not greater than 5-mm and may very well be smaller. Even at 5-mm, the area seen by the infrared energy would represent only 15% of the total area of the pellet.

Increasing the diameter of the aperture is technically possible, thus permitting more of the pellet to be impacted by the IR beam, although this will limit the spectral resolution. A modest reduction in spectral resolution, given the broad bands observed thus far in the materials under study, may not cause a significant degradation in the quality of the spectra. An additional concern for quantitative data is photometric accuracy. Nonlinearities in MCT detectors, used to acquire the data in these experiments, are well known, however, and one method of reducing the problem is with a smaller aperture.[3,4]

It has been proposed to continue the KBr pellet work using a smaller diameter in order to conserve the limited amount of biological materials available. Such an approach may also represent at least a partial solution to the problem observed with scattering and outliers in the data. The disadvantages of this approach are the higher relative inaccuracy when weighing pellets with smaller weights and the fact that as the pellet is reduced in size, it may be possible that the pellet will be smaller than the collimated beam potentially causing problems with energy that is not transmitted through the sample.

Some direct physical evidence of non-homogeneity in the pellets was indicated by non-uniformities that appeared to be cracks, internal channels, or striations in the crystalline structure that were visible to the naked eye in some cases. Photomicrographs of several pellets were obtained in an attempt to ascertain whether these were clusters of BG spores, although this was not ascertained at the magnification available. A photo of a pellet taken under visible light can be seen in Figure 14. It was also apparent, as can be seen, that the features did not extend to the surface of the pellets. An attempt to examine pellets under ultraviolet fluorescence was also not productive. We believe the available magnification may have been too low to observe the spores directly. The failure to see spore clusters may, however, also indicate that they were at least reasonably well dispersed within the pellets. Because the UV microscopy was performed with pellets from BG-DAN-04, less affected by the gross non-uniformities observed in the pellets from the earlier two variants, it may be that they were not representative of the earlier problems.

Figure 14. Photomicrograph of BG Pellet Prepared from BG-BF-01

Perhaps the best evidence of non-homogeneities in the pellets was obtained through the measurements of their physical cross sections. As noted in the main body of the report, each pellet was measured at 5 points with a Mitutoyo digital comparator. The Mitutoyo instrument has a specified accuracy of 1% at the cross sections studied (usually 600-700 μm). For BG-DAN-01 and BG-BF-01, acquired mostly under conditions of high relative humidity and prior to installation of some equipment that has subsequently limited the negative effects of such environmental conditions, relative standard deviations for the 5 measurements for most of the pellets exceeded 4-5% and were as high as 11%. For BG-DAN-04, relative standard deviations of 14 were in the range of 0.5-2.0%, and none of the remaining 5 exceeded 9%. Despite the improvement, an RSD of 2% still represents an expanded uncertainty, in order to encompass a 95% confidence band, of 4% of the measured thickness. Indeed, it is possible that the measurements of the thickness of the pellets may represent the best quantitative estimate of non-homogeneity, which should perhaps be stated in the future as a Type B uncertainty represented as variability in the physical cross sections.

We investigated the possibility that because the collimated beam from the infrared source sees only a portion of the center of the pellet, the micrometer reading at the center of the pellet would provide a better statistical fit to the data than the average. An analysis of data from BG-BF-01 using only the thickness at the center of the pellet compared to the data obtained from using the average of five measurements showed that this was not the case (Figures 16 and 17). The average of the five points apparently still represented a better estimate of the physical cross section within the area viewed by the spectrometer.

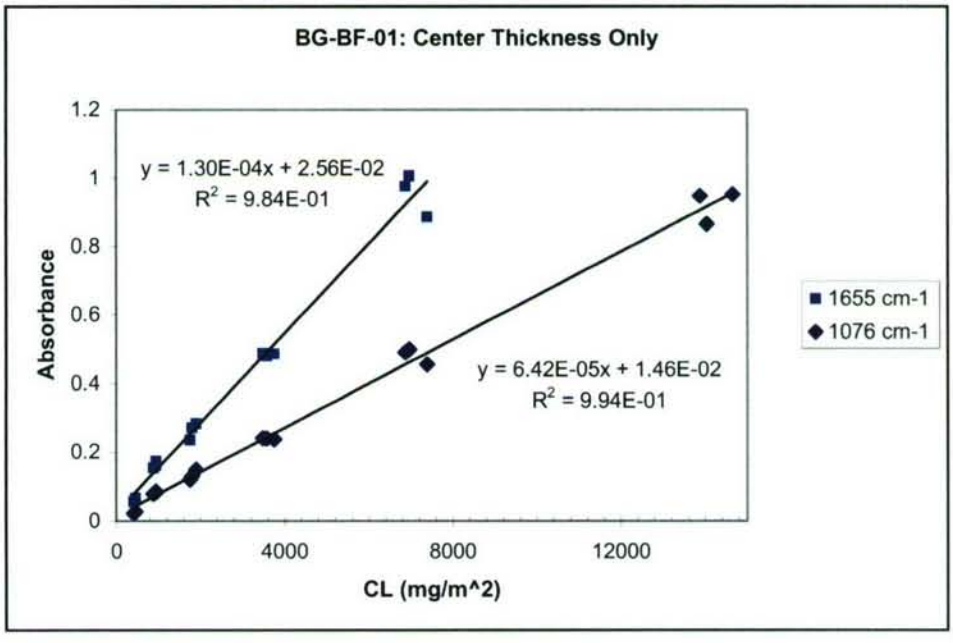

Figure 15. Beer's Law Plot of Data from BG-BF-01 Using only the Thickness of the Pellet at the Center

In the gross statistical sense, our data are similar to at least one other study involving the use of salt pellets to determine mineral composition, providing further evidence of the difficulty of using this technique to prepare homogeneous samples for infrared work.[5]

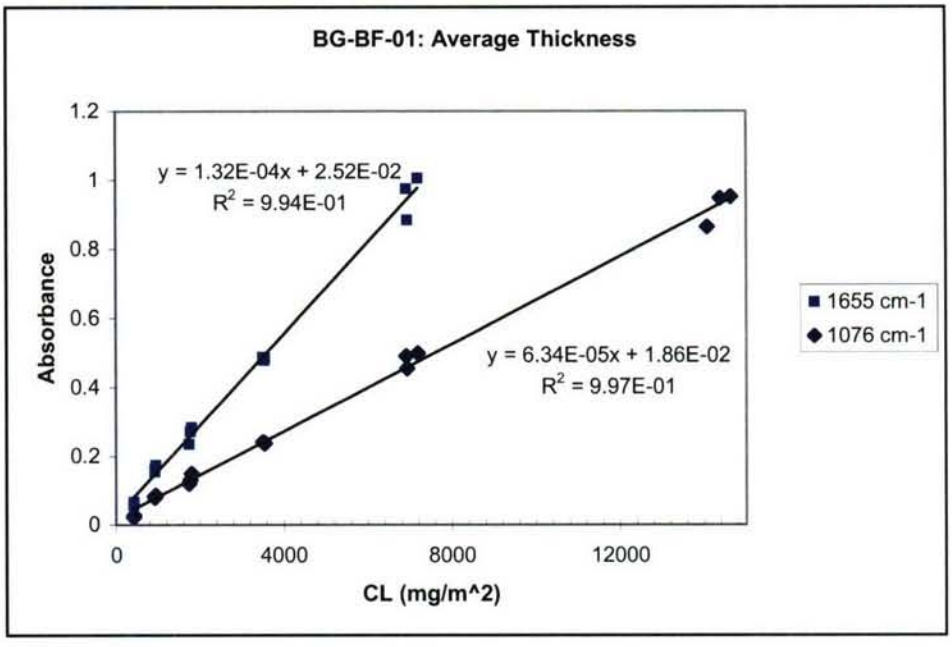

Figure 16. Plot of Data from BG-BF-01 Using the Average of Physical Cross Sections at Five Points

7. CONCLUSIONS

Although only a preliminary statistical analysis of the data from the three variants of BG studied, we believe that we have provided evidence of the major sources of errors, as well as identifying a possible systematic approach toward quantifying the uncertainties, necessary for reference quality data.

Evidence from the most recent set of spectra obtained from BG-DAN-04 appears to indicate that refinements in equipment and technique have improved the quality of the data further.

8. REFERENCES

1. Sartorius BasicplusElectronic Semi-micro-, Analytical and Precision Balances Installation and Operating Instructions.

2. Patricia B. Coleman, Ed. *Practical Sampling Techniques for Infrared Analysis,* CRC Press, Boca Raton, FL, 1993.

3. R.L. Richardson, H. Yang, P.R. Griffiths. *Applied Spectroscopy*, 52(4), 572-578.

4. R.O. Carter, N.E. Lindsay, D. Beduhn. *Applied Spectroscopy*, 44(7), 1147-1151.

5. Mewbourne School of Petroleum and Geological Engineering, http://ic3db.ou.edu/ic3/ic3/ftir.htm.

Blank

APPENDIX C

SUPPORTING DOCUMENTATION

Table 1. Concentration-Pathlength Calculations of KBr Pellets Prepared from BG Variant BG-DAN-01

Mass (g)	Average	BG (mg)	Radius (cm)	Thickness (cm)	Average	Volume m^3	CL mg/m^2	Density g/cm^3
0.22609	0.22602	0.1197	0.6475	0.0622	0.0660	8.693E-08	908.5533	2.60
0.22598				0.0607				
0.22600				0.0697				
0.22602				0.0704				
				0.0670				
0.22973	0.22964	0.1216	0.6475	0.0626	0.0667	8.785E-08	923.0947	2.61
0.22960				0.0642				
0.22961				0.0718				
0.22962				0.0678				
				0.0671				
0.22351	0.22347	0.1183	0.6475	0.0625	0.0638	8.403E-08	898.3029	2.66
0.22349				0.0531				
0.22345				0.0645				
0.22344				0.0733				
				0.0656				
0.22290	0.22276	0.2341	0.6475	0.0649	0.0649	8.546E-08	1777.675	2.61
0.22274				0.0643				
0.22271				0.0642				
0.22270				0.0658				
				0.0652				
0.22885	0.22873	0.2404	0.6475	0.0644	0.0673	8.870E-08	1825.256	2.58
0.22868				0.0718				
0.22868				0.0702				
0.22869				0.0628				
				0.0675				
0.22009	0.21999	0.2312	0.6475	0.0606	0.0633	8.337E-08	1755.53	2.64
0.21997				0.0658				
0.21995				0.0660				
0.21994				0.0603				
				0.0638				
0.25287	0.25274	0.5345	0.6475	0.0734	0.0733	9.657E-08	4058.275	2.62
0.25269				0.0677				
0.25270				0.0718				
0.25271				0.0797				
				0.0740				
0.22805	0.22801	0.4822	0.6475	0.0607	0.0656	8.643E-08	3661.106	2.64
0.22798				0.0656				
0.22801				0.0710				
0.22799				0.0639				

Mass (g)	Average	BG (mg)	Radius (cm)	Thickness (cm)	Average	Volume m^3	CL mg/m^2	Density g/cm^3
				0.0669				
0.22261	0.22255	0.4707	0.6475	0.0652	0.0676	8.906E-08	3573.395	2.50
0.22255				0.0635				
0.22250				0.0699				
0.22252				0.0714				
				0.0681				
0.22255	0.22236	0.9292	0.6475	0.0647	0.0666	8.772E-08	7054.683	2.54
0.22228				0.0666				
0.22231				0.0675				
0.22230				0.0666				
				0.0676				
0.22073	0.22072	0.9223	0.6475	0.0622	0.0677	8.917E-08	7002.652	2.48
0.22075				0.0678				
0.22068				0.0723				
0.22072				0.0675				
				0.0687				
0.22119	0.22112	0.9240	0.6475	0.0621	0.0643	8.469E-08	7015.422	2.61
0.22111				0.0718				
0.22110				0.0641				
0.22109				0.0587				
				0.0648				
0.22118	0.22116	1.8804	0.6475	0.0646	0.0642	8.453E-08	14276.62	2.62
0.22115				0.0661				
0.22115				0.0638				
0.22114				0.0619				
				0.0645				
0.21948	0.21949	1.8662	0.6475	0.0637	0.0644	8.477E-08	14168.81	2.59
0.21949				0.0656				
0.21948				0.0654				
0.21949				0.0630				
				0.0641				
0.22226	0.22228	1.8900	0.6475	0.0609	0.0675	8.893E-08	14349.24	2.50
0.22230				0.0641				
0.22228				0.0727				
0.22228				0.0717				
				0.0682				

APPENDIX C

Table 2. Concentration-Pathlength Calculations of KBr Pellets Prepared from BG Variant BG-BF-01

Mass (g)	Average	BG (mg)	Radius (cm)	Thickness (cm)	Average	Volume m^3	CL mg/m^2	Density g/cm^3
0.21850	0.22018	1.8545	0.6475	0.0626	0.0671	8.83796E-08	14079.7	2.47
0.22076				0.0641				
0.22071				0.0709				
0.22074				0.0710				
				0.0669				
0.22488	0.22495	1.8947	0.6475	0.0662	0.0663	8.738E-08	14384.9	2.57
0.22501				0.0717				
0.22494				0.0685				
0.22497				0.0613				
				0.0640				
0.22867	0.22888	1.9278	0.6475	0.0671	0.0691	9.101E-08	14636.1	2.51
0.22887				0.0687				
0.22897				0.0707				
0.22900				0.0698				
				0.0692				
0.22138	0.22150	0.9136	0.6475	0.0738	0.0800	1.054E-07	6936.03	2.10
0.22153				0.0723				
0.22158				0.0880				
0.22151				0.0808				
				0.0853				
0.22088	0.22073	0.9104	0.6475	0.0682	0.0671	8.833E-08	6912	2.50
0.22069				0.0674				
0.22077				0.0668				
0.22059				0.0662				
				0.0667				
0.22962	0.22965	0.9472	0.6475	0.0793	0.0811	1.068E-07	7191.16	2.15
0.22961				0.0920				
0.22972				0.0836				
0.22964				0.0721				
				0.0786				
0.22554	0.22543	0.4663	0.6475	0.0703	0.0772	1.016E-07	3540.47	2.22
0.22534				0.0772				
0.22544				0.0823				
0.22540				0.0742				
				0.0818				
0.22485	0.22453	0.4645	0.6475	0.0654	0.0701	9.230E-08	3526.38	2.44
0.22438				0.0692				
0.22447				0.0729				
0.22443				0.0718				
				0.0711				
0.22261	0.22255	0.4604	0.6475	0.0690	0.0674	8.877E-08	3495.16	2.51
0.22255				0.0645				
0.22250				0.0667				

Mass (g)	Average	BG (mg)	Radius (cm)	Thickness (cm)	Average	Volume m^3	CL mg/m^2	Density g/cm^3
0.22252				0.0696				
				0.0672				
0.22684	0.22683	0.2368	0.6475	0.0757	0.0742	9.776E-08	1797.67	2.32
0.22683				0.0702				
0.22683				0.0736				
0.22681				0.0733				
				0.0783				
0.22319	0.22319	0.2330	0.6475	0.0622	0.0677	8.917E-08	1768.87	2.50
0.22318				0.0678				
0.22322				0.0723				
0.22318				0.0675				
				0.0687				
0.21965	0.21959	0.2292	0.6475	0.0621	0.0643	8.469E-08	1740.32	2.59
0.21956				0.0718				
0.21956				0.0641				
0.21959				0.0587				
				0.0648				
0.22407	0.22440	0.1213	0.6475	0.0630	0.0669	8.817E-08	921.269	2.54
0.22452				0.0691				
0.22444				0.0726				
0.22457				0.0615				
				0.0685				
0.22467	0.22510	0.1217	0.6475	0.0692	0.0654	8.609E-08	924.153	2.61
0.22534				0.0698				
0.22524				0.0644				
0.22516				0.0607				
				0.0627				
0.22965	0.22964	0.1242	0.6475	0.0655	0.0668	8.804E-08	942.771	2.61
0.22967				0.0682				
0.22961				0.0687				
0.22962				0.0650				
				0.0668				
0.21711	0.21733	0.0566	0.6475	0.0703	0.0772	1.016E-07	429.442	2.14
0.21737				0.0772				
0.21738				0.0823				
0.21744				0.0742				
				0.0818				
0.23143	0.23169	0.0603	0.6475	0.0654	0.0701	9.230E-08	457.817	2.51
0.23174				0.0692				
0.23177				0.0729				
0.23180				0.0718				
				0.0711				

Mass (g)	Average	BG (mg)	Radius (cm)	Thickness (cm)	Average	Volume m^3	CL mg/m^2	Density g/cm^3
0.21271	0.21294	0.0554	0.6475	0.0690	0.0674	8.877E-08	420.772	2.40
0.21303				0.0645				
0.21297				0.0667				
0.21304				0.0696				
				0.0672				

Table 3. Concentration-Pathlength Calculations of KBr Pellets Prepared from BG Variant BG-DAN-04

Mass (g)	Average	BG (mg)	Radius (cm)	Thickness (cm)	Average	Volume m^3	CL mg/m^2	Density g/cm^3
0.22919	0.22911	0.0562	0.6475	0.0679	0.0674	8.883E-08	426.59	2.58
0.22908				0.0677				
0.22907				0.0680				
				0.0675				
				0.0661				
0.22472	0.22470	0.0551	0.6475	0.0668	0.0677	8.912E-08	418.37	2.52
0.22471				0.0674				
0.22467				0.0684				
				0.0682				
				0.0675				
0.22322	0.22321	0.0547	0.6475	0.0711	0.0707	9.317E-08	415.60	2.40
0.22321				0.0712				
0.22321				0.0707				
				0.0702				
				0.0705				
0.21837	0.21837	0.1081	0.6475	0.0650	0.0662	8.714E-08	820.53	2.51
0.21837				0.0655				
0.21836				0.0672				
				0.0666				
				0.0665				
0.23013	0.23009	0.1139	0.6475	0.0685	0.06682	9.223E-08	864.58	2.49
0.23005				0.0670				
0.23009				0.0686				
				0.0685				
				0.0686				
0.22427	0.22427	0.1110	0.6475	0.0685	0.0682	8.988E-08	842.70	2.50
0.22425				0.0670				
0.22428				0.0686				
				0.0685				
				0.0686				
0.21719	0.21716	0.2113	0.6475	0.0697	0.0675	8.891E-08	1604.02	2.44
0.21715				0.0580				
0.21713				0.0673				
				0.0746				
				0.0679				

Mass (g)	Average	BG (mg)	Radius (cm)	Thickness (cm)	Average	Volume m^3	CL mg/m^2	Density g/cm^3
0.22594	0.22595	0.2198	0.6475	0.0699	0.0693	9.125E-08	1668.97	2.48
0.22597				0.0700				
0.22594				0.0698				
				0.0684				
				0.0683				
0.22656	0.22656	0.2204	0.6475	0.0669	0.0676	8.904E-08	1673.47	2.54
0.22657				0.06683				
0.22655				0.0697				
				0.0670				
				0.0661				
0.22506	0.22505	0.4427	0.6475	0.0669	0.0682	8.985E-08	3360.76	2.50
0.22506				0.0689				
0.22504				0.0700				
				0.0668				
				0.0685				
0.23513	0.23514	0.4618	0.6475	0.0722	0.0710	9.354E-08	3511.33	2.51
0.23515				0.0710				
0.23513				0.0712				
				0.0698				
				0.0709				
0.18833	0.18832	0.3704	0.6475	0.0533	0.0563	7.413E-08	2812.21	2.54
0.18833				0.0535				
0.18830				0.0584				
				0.0614				
				0.0548				
0.23066	0.23065	0.9041	0.6475	0.0697	0.0688	9.067E-08	6864.18	2.54
0.23065				0.0684				
0.23065				0.0676				
				0.0694				
				0.0691				
0.23266	0.23264	0.9119	0.6475	0.0709	0.0704	9.267E-08	6923.30	2.51
0.23261				0.0695				
0.23265				0.0712				
				0.0699				
				0.0703				
0.22904	0.22906	0.8979	0.6475	0.0670	0.0681	8.972E-08	6816.76	2.55
0.22908				0.0702				
0.22906				0.0683				
				0.0662				
				0.0689				
0.22450	0.22461	1.2404	0.6475	0.0639	0.0642	8.453E-08	9417.53	2.66
0.22471				0.0646				
0.22461				0.0653				
				0.0645				
				0.0626				
0.22614	0.22598	1.2480	0.6475	0.0647	0.0653	8.601E-08	9474.97	2.63

Mass (g)	Average	BG (mg)	Radius (cm)	Thickness (cm)	Average	Volume m^3	CL mg/m^2	Density g/cm^3
0.22591				0.0616				
0.22588				0.0687				
				0.0689				
				0.0626				
0.22781	0.22777	2.6990	0.6475	0.0685	0.0687	9.051E-08	20263.91	2.52
0.22777				0.0696				
0.22774				0.0684				
				0.0677				
				0.0694				
0.22662	0.22659	2.6552	0.6475	0.0676	0.0690	9.086E-08	20158.94	2.49
0.22657				0.0673				
0.22659				0.0693				
				0.0708				
				0.0699				
0.22575	0.22577	1.6360	0.6475	0.0703	0.0710	9.354E-08	12420.85	2.41
0.22580				0.0707				
0.22577				0.0729				
				0.0701				
				0.0711				
0.22287	0.22270	1.6137	0.6475	0.0642	0.0651	8.575E-08	12251.59	2.60
0.22259				0.0646				
0.22263				0.0666				
				0.0660				
				0.0641				
0.22811	0.22811	2.1438	0.6475	0.0661	0.0674	8.877E-08	16276.42	2.57
0.22812				0.0645				
0.22810				0.0685				
				0.0704				
				0.0675				
0.22688	0.22690	2.1325	0.6475	0.0662	0.0674	9.088E-08	16190.32	2.50
0.22690				0.0618				
0.22693				0.0738				
				0.0745				
				0.0675				

Table 4. Masses and Physical Cross Sections of Pellets Prepared from BG Variant BG-DAN-01

0.053% BG				
BG-DPG-07	Rep 1	Rep 2	Rep 3	
12 o'clock	0.622	0.626	0.625	
3 o'clock	0.607	0.642	0.531	
6 o'clock	0.697	0.718	0.645	
9 o'clock	0.704	0.678	0.733	
Center	0.670	0.671	0.656	
Average	0.660	0.667	0.638	0.655
STDev	0.0438	0.0355	0.0725	0.0507
%RSD	6.63%	5.32%	11.36%	7.74%
Day 1 Weight	0.22609	0.22973	0.22351	
Weight 1	0.22598	0.22960	0.22349	
Weight 2	0.22600	0.22961	0.22345	
Weight 3	0.22602	0.22962	0.22344	
Average	0.22602	0.22964	0.22347	0.22638
STDev	0.000048	0.000061	0.000033	0.002643
%RSD	0.02%	0.03%	0.01%	1.17%

0.105% BG				
BG-DPG-08	Rep 1	Rep 2	Rep 3	
12 o'clock	0.649	0.644	0.606	
3 o'clock	0.643	0.718	0.658	
6 o'clock	0.642	0.702	0.660	
9 o'clock	0.658	0.628	0.603	
Center	0.652	0.675	0.638	
Average	0.649	0.673	0.633	0.652
STDev	0.0066	0.0379	0.0274	0.0305
%RSD	1.02%	5.62%	4.33%	4.69%
Day 1 Weight	0.22290	0.22885	0.22009	
Weight 1	0.22274	0.22868	0.21997	
Weight 2	0.22271	0.22868	0.21995	
Weight 3	0.22270	0.22869	0.21994	
Average	0.22276	0.22873	0.21999	0.22383
STDev	0.000093	0.000083	0.000069	0.003808
%RSD	0.04%	0.04%	0.03%	1.70%

0.21% BG				
BG-DPG-06	Rep 1	Rep 2	Rep 3	
12 o'clock	0.734	0.607	0.652	
3 o'clock	0.677	0.656	0.635	
6 o'clock	0.718	0.710	0.699	
9 o'clock	0.797	0.639	0.714	
Center	0.740	0.669	0.681	
Average	0.733	0.656	0.676	0.689
STDev	0.0433	0.0380	0.0326	0.0489
%RSD	5.91%	5.79%	4.82%	7.10%
Day 1 Weight	0.25287	0.22805	0.22261	
Weight 1	0.25269	0.22798	0.22255	
Weight 2	0.25270	0.22801	0.22250	
Weight 3	0.25271	0.22799	0.22252	
Average	0.25274	0.22801	0.22255	0.23443
STDev	0.000085	0.000031	0.000048	0.013723
%RSD	0.03%	0.01%	0.02%	5.85%

0.417% BG				
BG-DPG-09	Rep 1	Rep 2	Rep 3	
12 o'clock	0.647	0.622	0.621	
3 o'clock	0.666	0.678	0.718	
6 o'clock	0.675	0.723	0.641	
9 o'clock	0.666	0.675	0.587	
Center	0.676	0.687	0.648	
Average	0.666	0.677	0.643	0.662
STDev	0.0116	0.0362	0.0482	0.0359
%RSD	1.75%	5.35%	7.49%	5.43%
Day 1 Weight	0.22255	0.22073	0.22119	
Weight 1	0.22228	0.22075	0.22111	
Weight 2	0.22231	0.22068	0.22110	
Weight 3	0.22230	0.22072	0.22109	
Average	0.22236	0.22072	0.22112	0.22140
STDev	0.000127	0.000029	0.000046	0.000732
%RSD	0.06%	0.01%	0.02%	0.33%

0.848% BG				
BG-DPG-10	Rep 1	Rep 2	Rep 3	
12 o'clock	0.646	0.637	0.609	
3 o'clock	0.661	0.656	0.641	
6 o'clock	0.638	0.654	0.727	
9 o'clock	0.619	0.630	0.717	
Center	0.645	0.641	0.682	
Average	0.642	0.644	0.675	0.654
STDev	0.0153	0.0111	0.0501	0.0327
%RSD	2.38%	1.73%	7.42%	5.01%
Day 1 Weight	0.22118	0.21948	0.22226	
Weight 1	0.22115	0.21949	0.22230	
Weight 2	0.22115	0.21948	0.22228	
Weight 3	0.22114	0.21949	0.22228	
Average	0.22116	0.21949	0.22228	0.22097
STDev	0.000017	0.000006	0.000016	0.001199
%RSD	0.01%	0.00%	0.01%	0.54%

8.48 mg/g nb138p97a	Rep 1	Rep 2	Rep 3	
12 o'clock	0.626	0.662	0.671	
3 o'clock	0.641	0.717	0.687	
6 o'clock	0.709	0.685	0.707	
9 o'clock	0.710	0.613	0.698	
Center	0.669	0.640	0.692	
Average	0.671	0.663	0.691	0.675
STDev	0.0384	0.0401	0.0134	0.0328
%RSD	5.72%	6.04%	1.94%	4.86%
Day 1 Weight	0.21850	0.22488	0.22867	
Weight 1	0.22076	0.22501	0.22887	
Weight 2	0.22071	0.22494	0.22897	
Weight 3	0.22074	0.22497	0.22900	
Average	0.22018	0.22495	0.22888	0.22467
STDev	0.001119	0.000055	0.000149	0.003762
%RSD	0.51%	0.02%	0.07%	1.67%

4.12 mg/g nb138p97b	Rep 1	Rep 2	Rep 3	
12 o'clock	0.738		0.793	
3 o'clock	0.723		0.920	
6 o'clock	0.880		0.836	
9 o'clock	0.808	0.662	0.721	
Center	0.853	0.667	0.786	
Average	0.800	0.671	0.811	0.761
STDev	0.0690	0.0077	0.0734	0.0854
%RSD	8.62%	1.14%	9.05%	11.22%
Day 1 Weight	0.22138	0.22088	0.22962	
Weight 1	0.22153	0.22069	0.22961	
Weight 2	0.22158	0.22077	0.22972	
Weight 3	0.22151	0.22059	0.22964	
Average	0.22150	0.22073	0.22965	0.22396
STDev	0.000085	0.000123	0.000050	0.004214
%RSD	0.04%	0.06%	0.02%	1.88%

2.07 mg/g nb138p97c	Rep 1	Rep 2	Rep 3	
12 o'clock	0.703	0.654	0.690	
3 o'clock	0.772	0.692	0.645	
6 o'clock	0.823	0.729	0.667	
9 o'clock	0.742	0.718	0.696	
Center	0.818	0.711	0.672	
Average	0.772	0.701	0.674	0.715
STDev	0.0509	0.0294	0.0202	0.0541
%RSD	6.60%	4.20%	3.00%	7.55%
Day 1 Weight	0.22554	0.21987	0.22485	
Weight 1	0.22534	0.21977	0.22438	
Weight 2	0.22544	0.21963	0.22447	
Weight 3	0.22540	0.21968	0.22443	
Average	0.22543	0.21974	0.22453	0.22323
STDev	0.000084	0.000106	0.000215	0.002613
%RSD	0.04%	0.05%	0.10%	1.17%

1.04 mg/g nb138p97d	Rep 1	Rep 2	Rep 3	
12 o'clock	0.757	0.622	0.621	
3 o'clock	0.702	0.678	0.718	
6 o'clock	0.736	0.723	0.641	
9 o'clock	0.733	0.675	0.587	
Center	0.783	0.687	0.648	
Average	0.742	0.677	0.643	0.687
STDev	0.0301	0.0362	0.0482	0.0558
%RSD	4.05%	5.35%	7.49%	8.11%
Day 1 Weight	0.22684	0.22319	0.21965	
Weight 1	0.22683	0.22318	0.21956	
Weight 2	0.22683	0.22322	0.21956	
Weight 3	0.22681	0.22318	0.21959	
Average	0.22683	0.22319	0.21959	0.22320
STDev	0.000013	0.000019	0.000042	0.003086
%RSD	0.01%	0.01%	0.02%	1.38%

0.541 mg/g nb138p97e	Rep 1	Rep 2	Rep 3	
12 o'clock	0.630	0.692	0.655	
3 o'clock	0.691	0.698	0.682	
6 o'clock	0.726	0.644	0.687	
9 o'clock	0.615	0.607	0.650	
Center	0.685	0.627	0.668	
Average	0.669	0.654	0.668	0.664
STDev	0.0459	0.0401	0.0162	0.0345
%RSD	6.86%	6.13%	2.42%	5.20%
Day 1 Weight	0.22407	0.22467	0.22965	
Weight 1	0.22452	0.22534	0.22967	
Weight 2	0.22444	0.22524	0.22961	
Weight 3	0.22457	0.22516	0.22962	
Average	0.22440	0.22510	0.22964	0.22638
STDev	0.000226	0.000298	0.000028	0.002432
%RSD	0.10%	0.13%	0.01%	1.07%

0.260 mg/g nb138p98a	Rep 1	Rep 2	Rep 3	
12 o'clock	0.722	0.712	0.601	
3 o'clock	0.712	0.707	0.629	
6 o'clock	0.702	0.708	0.650	
9 o'clock	0.690	0.697	0.603	
Center	0.715	0.695	0.602	
Average	0.708	0.704	0.617	0.676
STDev	0.0125	0.0074	0.0219	0.0457
%RSD	1.76%	1.05%	3.54%	6.75%
Day 1 Weight	0.21711	0.23143	0.21271	
Weight 1	0.21737	0.23174	0.21303	
Weight 2	0.21738	0.23177	0.21297	
Weight 3	0.21744	0.23180	0.21304	
Average	0.21733	0.23169	0.21294	0.22065
STDev	0.000147	0.000172	0.000155	0.008364
%RSD	0.07%	0.07%	0.07%	3.79%

0.0244% BG				
NB 02-0049 P27B	Rep 1	Rep 2	Rep 3	
12 o'clock	0.679	0.668	0.711	
3 o'clock	0.677	0.674	0.712	
6 o'clock	0.680	0.684	0.707	
9 o'clock	0.675	0.682	0.702	
Center	0.661	0.675	0.705	
Average	0.674	0.677	0.707	0.686
STDev	0.0077	0.0065	0.0042	0.0166
%RSD	1.15%	0.96%	0.59%	2.43%
Weight 1	0.22919	0.22472	0.22322	
Weight 2	0.22908	0.22471	0.22321	
Weight 3	0.22907	0.22467	0.22321	
Average	0.22911	0.22470	0.22321	0.22568
STDev	0.000067	0.000026	0.000006	0.002658
%RSD	0.03%	0.01%	0.00%	1.18%

0.049% BG				
NB 02-0049 P27C	Rep 1	Rep 2	Rep 3	
12 o'clock	0.650	0.700	0.685	
3 o'clock	0.655	0.683	0.670	
6 o'clock	0.672	0.710	0.686	
9 o'clock	0.666	0.716	0.685	
Center	0.665	0.692	0.686	
Average	0.662	0.700	0.682	0.681
STDev	0.0089	0.0133	0.0069	0.0188
%RSD	1.35%	1.90%	1.02%	2.76%
Weight 1	0.21837	0.23013	0.22427	
Weight 2	0.21837	0.23005	0.22425	
Weight 3	0.21836	0.23009	0.22428	
Average	0.21837	0.23009	0.22427	0.22424
STDev	0.000006	0.000040	0.000015	0.005076
%RSD	0.00%	0.02%	0.01%	2.26%

0.097% BG				
NB 02-0049 P27D	Rep 1	Rep 2	Rep 3	
12 o'clock	0.697	0.699	0.669	
3 o'clock	0.580	0.700	0.683	
6 o'clock	0.673	0.698	0.697	
9 o'clock	0.746	0.684	0.670	
Center	0.679	0.683	0.661	
Average	0.675	0.693	0.676	0.681
STDev	0.0604	0.0085	0.0141	0.0345
%RSD	8.94%	1.23%	2.09%	5.06%
Weight 1	0.21719	0.22594	0.22656	
Weight 2	0.21715	0.22597	0.22657	
Weight 3	0.21713	0.22594	0.22655	
Average	0.21716	0.22595	0.22656	0.22322
STDev	0.000031	0.000017	0.000010	0.004557
%RSD	0.01%	0.01%	0.00%	2.04%

0.196% BG				
NB 02-0049 P27E	Rep 1	Rep 2	Rep 3	
12 o'clock	0.669	0.722	0.533	
3 o'clock	0.689	0.710	0.535	
6 o'clock	0.700	0.712	0.584	
9 o'clock	0.668	0.698	0.614	
Center	0.685	0.709	0.548	
Average	0.682	0.710	0.563	0.652
STDev	0.0137	0.0086	0.0352	0.0693
%RSD	2.00%	1.20%	6.25%	10.64%
Weight 1	0.22506	0.23513	0.18833	
Weight 2	0.22506	0.23515	0.18833	
Weight 3	0.22504	0.23513	0.18830	
Average	0.22505	0.23514	0.18832	0.21617
STDev	0.000012	0.000012	0.000017	0.021339
%RSD	0.01%	0.00%	0.01%	9.87%

0.390% BG				
NB 02-0049 P27F	Rep 1	Rep 2	Rep 3	
12 o'clock	0.697	0.709	0.670	
3 o'clock	0.684	0.695	0.702	
6 o'clock	0.676	0.712	0.683	
9 o'clock	0.694	0.699	0.662	
Center	0.691	0.703	0.689	
Average	0.688	0.704	0.681	0.691
STDev	0.0084	0.0070	0.0157	0.0141
%RSD	1.23%	0.99%	2.31%	2.04%
Weight 1	0.23066	0.23266	0.22904	
Weight 2	0.23065	0.23261	0.22908	
Weight 3	0.23065	0.23265	0.22906	
Average	0.23065	0.23264	0.22906	0.23078
STDev	0.000006	0.000026	0.000020	0.001553
%RSD	0.00%	0.01%	0.01%	0.67%

0.552% BG			
NB 02-0049 P31A	Rep 1	Rep 2	
12 o'clock	0.639	0.647	
3 o'clock	0.646	0.616	
6 o'clock	0.653	0.687	
9 o'clock	0.645	0.689	
Center	0.626	0.626	
Average	0.642	0.653	0.647
STDev	0.0101	0.0339	0.0243
%RSD	1.58%	5.19%	3.75%
Weight 1	0.22450	0.22614	
Weight 2	0.22471	0.22591	
Weight 3	0.22461	0.22588	
Average	0.22461	0.22598	0.22529
STDev	0.000105	0.000142	0.000759
%RSD	0.05%	0.06%	0.34%

1.17% BG				0.72% BG				0.94% BG			
NB 02-0049 P31B	Rep 1	Rep 2		NB 02-0049 P31C	Rep 1	Rep 2		NB 02-0049 P32D	Rep 1	Rep 2	
12 o'clock	0.685	0.676		12 o'clock	0.703	0.642		12 o'clock	0.661	0.662	
3 o'clock	0.696	0.673		3 o'clock	0.707	0.646		3 o'clock	0.645	0.618	
6 o'clock	0.684	0.693		6 o'clock	0.729	0.666		6 o'clock	0.685	0.738	
9 o'clock	0.677	0.708		9 o'clock	0.701	0.660		9 o'clock	0.704	0.745	
Center	0.694	0.699		Center	0.711	0.641		Center	0.675	0.687	
Average	0.687	0.690	0.689	Average	0.710	0.651	0.681	Average	0.674	0.690	0.682
STDev	0.0078	0.0150	0.0113	STDev	0.0112	0.0113	0.0330	STDev	0.0225	0.0532	0.0394
%RSD	1.13%	2.17%	1.65%	%RSD	1.58%	1.74%	4.84%	%RSD	3.34%	7.71%	5.78%
Weight 1	0.22781	0.22662		Weight 1	0.22575	0.22287		Weight 1	0.22811	0.22688	
Weight 2	0.22777	0.22657		Weight 2	0.22580	0.22259		Weight 2	0.22812	0.22690	
Weight 3	0.22774	0.22659		Weight 3	0.22577	0.22263		Weight 3	0.22810	0.22693	
Average	0.22777	0.22659	0.22718	Average	0.22577	0.22270	0.22424	Average	0.22811	0.22690	0.22751
STDev	0.000035	0.000025	0.000647	STDev	0.000025	0.000151	0.001688	STDev	0.000010	0.000025	0.000661
%RSD	0.02%	0.01%	0.28%	%RSD	0.01%	0.07%	0.75%	%RSD	0.00%	0.01%	0.29%

Blank

GLOSSARY

A	absorbance
α	alpha, absorptivity coefficient
BG	*bacillus atrophaeus* (formerly known as *bacillus globigii*)
BSL	biosafety level
CL	concentration-pathlength
CW	chemical warfare, chemical weapons
CWT	Chemical Weapons Treaty
DR	diffuse reflectance
DMMP	dimethyl methylphosphonate (CAS RN 756-79-6)
DTGS	deuterated triglycine sulfide
ECBC	Edgewood Chemical Biological Center
EMPA	ethyl methylphosphonate (CAS 1832-53-7)
FTIR	Fourier transform infrared
GC	gas chromatograph, gas chromatography
HITRAN	high resolution transmission
MCT	mercury-cadmium-telluride
MFC	mass flow controller
μL	microliter
μmol/mol	micromole per mole
NIST	National Institute of Standards and Technology
PTFE	poly(tetrafluoro) ethylene
PNNL	Pacific Northwest National Laboratory

ppm	part per million
PSI	pounds per square inch
sccm	standard cubic centimeters per minute
SLPM	standard liters per minute
SOP	standard operating procedures
SPIE	International Society for Optical Engineering
TOF	time of flight
VLE	vapor-liquid equilibrium
VX	O-ethyl-S-(2-diisopropylamino)ethyl methylphosphonothioate (CAS RN 50782-69-0)